# 3D Oxygen Microfluidic Platform for *In Vitro* Hypoxic Studies

BY

Gerardo Mauleon Ramos
B.S., University of Illinois at Chicago, Chicago, 2009
M.S., University of Illinois at Chicago, Chicago, 2011

THESIS

Submitted as partial fulfillment of the requirements
for the degree of Doctor of Philosophy in Bioengineering
in the Graduate College of the
University of Illinois at Chicago, 2016

Chicago, Illinois

Defense Committee:
Dr. David Eddington, Chair and Advisor
Dr. Richard Magin
Dr. Thomas Park, Biological Sciences
Dr. Jalees Rehman, Pharmacology
Dr. Jie Xu, Mechanical Engineering

*This thesis is dedicated to Jess, thank you for all your love and support through this process, you are my study buddy for life. To my parents, thank you for instilling in me the desire to continue learning and teaching me perseverance at a young age. To P and Jackson I hope my accomplishments will enable you to have a better life.*

## ACKNOWLEDGEMENTS

Thank you to David Eddington for being my research advisor and financially supporting me during all of my years in the lab. You taught me more than anyone else. Many thanks to Megan Rexius, Esther Shin, and Carlos Ng for their help with Matlab codes and figures used for this thesis. Thank you to Jess for all the hard work you did while editing my thesis. Thank you also to all of my labmates, past and present, for making the lab a great place to work.

Some of the sections shown on this dissertation have been previously published. Chapter 1 shows a published study for which I was the primary author and researcher. Joe Lo and Bethany Peterson provided assistanship to start the study. Chris Fall and David Eddington were the faculty in charge. Chapter 2 uses figures from 2 published studies. In both studies I performed the experiments that provided the data shown here.

## TABLE OF CONTENTS

**CHAPTER:**


**1. ENHANCED LOADING OF FURA-2/AM CALCIUM INDICATOR DYE IN ADULT RODENT BRAIN SLICES VIA A MICROFLUIDIC OXYGENATOR 1**

1.1 Introduction 1

1.1.1. Hypoxia Impacts Diverse Signaling Pathways in the Neuron 1

1.1.2. Brain Slice Preparation and Neonatal Specimens 4

1.1.3. Calcium Imaging 6

1.1.4. Previous Methods 7

1.1.5. Microfluidic Technology 8

1.1.6. Research Purpose 12

1.2 Materials and Methods 13

1.2.1. Design and Fabrication of Microfluidic Oxygenator 13

1.2.1.1. Design of Microfluidic Oxygenator 13

1.2.1.2. Fabrication of Microfluidic Gas Network 13

1.2.1.3. Fabrication of PDMS Membrane 15

1.2.1.4. Fabrication of PDMS Incubation Well 15

1.2.1.5. Assembly of PDMS Microfluidic Oxygenator 15

1.2.2. Animals and Experimental Groups 16

1.2.3. Brain Slice Preparation 16

1.2.4. Validation of Device Using Fiber Optic Oxygen Sensor 17

1.2.5. *In Vitro* Loading of Brain Slice with Fura-2/AM 18

1.2.6. Live/Dead Assay 19

1.2.7. Quantifying Calcium in Mice Under a Hypoxic Insult 20

1.2.8. Statistical Analysis 20

1.3 Results 22

1.3.1. Characterization of the Microfluidic Oxygenator 22

1.3.1.1. Media Oxygen Measurements 22

1.3.1.2. Brain Slice Oxygen Measurements 22

1.3.2. Live/Dead Assay 24

1.3.3. Fura-2 Loading 24

1.4 Discussion 29

1.5 Conclusion 32

1.6 Cited Literature 33

**2. 3D PRINTED MICROFLUIDIC OXYGEN MIXER [LARGE-SCALE OXYGEN GRADIENT GENERATION IN MICROFLUIDICS] 38**
2.1 Introduction 38
2.1.1. Oxygen 38
2.1.2. Oxygen Gradients 40
2.1.3. Current Oxygen Control Methods 41
2.1.4. Previous Microfluidic Methods 42
2.1.5. 3D Printing 44
2.1.6. Research Purpose 45
2.2 Materials and Methods 47
2.2.1. Design and Fabrication of Gradient Device 47
2.2.2. Validation of Devices Using Fiber Optic Oxygen Sensor 49
2.2.3. Design and Fabrication of 3D Printed Oxygen Mixer 49
2.2.4. Validation of 3D Printed Oxygen Mixer Using Fiber Optic Oxygen Sensor 52
2.2.5. Fabrication of PtOEPK 53
2.2.6. Validation of 3D Printed Oxygen Mixer Using PtOEPK Sensor 53
2.2.7. 3D Printed Oxygen Switchboard 54
2.2.8. Statistical analysis 54
2.3 Results 55
2.3.1 Source-Sink Design Oxygen Characterization 55
2.3.2 Inclined PDMS Membrane 56
2.3.3 Multiple Input Design Oxygen Characterization 57
2.3.4 Characterization of 3D Printed Oxygen Mixer 58
2.3.5 Characterization of 3D Printed Oxygen Mixer as an oxygen supply 58
2.3.6 3D Printed Oxygen Switchboard 62
2.4 Discussion 64
2.5 Conclusion 66
2.6 Cited Literature 67

**3. CHAPTER 3: 3D OXYGEN MICROFLUIDIC PLATFORM FOR *IN VITRO* HYPOXIC STUDIES 71**
3.1 Introduction 71
3.1.1 Angiogenesis 71
3.1.2 *In Vitro* Models for Angiogenesis 72
3.1.3 Microfluidic Models for Angiogenesis 74
3.1.4 Research Purpose 76
3.2 Materials and Methods 77
3.2.1 Design and Fabrication of 3D Oxygen Microfluidic Platform 77
3.2.1.1 Design of 3D Oxygen Microfluidic Platform 77
3.2.1.2. Fabrication of 3D Oxygen Microfluidic Platform 79
3.2.2 Validation of 3D Oxygen Microfluidic Platform –Fluid Control 82
3.2.3 Validation of 3D Oxygen Microfluidic Platform –Oxygen Control 82
3.2.4 Cell Culture 83
3.2.5 Oxygen Induced Sprouting Imaging 84
3.2.6 Statistical Analysis 84

3.3 Results 85
3.3.1 Validation of 3D Oxygen Microfluidic Platform –Fluid Control 85
3.3.2 Validation of 3D Oxygen Microfluidic Platform –Oxygen Control 85
3.3.3 Cell Culture 91
3.3.4 Oxygen Induced Sprouting Imaging 93
3.4 Discussion 100
3.5 Conclusion 104
3.6 Cited Literature 105
APPENDIX A 109
APPENDIX B 118
APPENDIX C 121
APPENDIX D 124
VITA 126

## LIST OF TABLES

**Table** **Page**

**CHAPTER 1:**

Table 1. Summary of microfluidic oxygenator advantages over standard method 19

## LIST OF FIGURES


**Figure** **Page**

**CHAPTER 1:**

Figure 1. Hypoxia and calcium relationship in the neuron 3

Figure 2. Photolithography 9

Figure 3. Replica molding 11

Figure 4. Standard method versus the microfluidic oxygenator 14

Figure 5. Validation of the microfluidic oxygenator with an oxygen sensor 23

Figure 6. Live dead assay results 25

Figure 7. Fura incubation results 28

**CHAPTER 2:**

Figure 1. Schematic of the microfluidic devices 48

Figure 2. 3D Printed Oxygen Mixer Version 1 51

Figure 3. 3D Printed Oxygen Mixer Version 2 52

Figure 4. Passive oxygen gradients 55

Figure 5. Inclined membrane oxygen validation 56

Figure 6. Active gradient devices 57

Figure 7. Oxygen mixer characterization version 1 59

Figure 8. 3D Printed Oxygen Mixer Version 2 60

Figure 9. 3D Printed Oxygen Mixer for microfluidic devices 61

Figure 10. 3D Printed Oxygen Mixer as a universal oxygen supply 63

**CHAPTER 3:**

Figure 1. Schematic of the 3D oxygen microfluidic platform 78

Figure 2. Fabrication process for the 3D oxygen microfluidic platform 81

Figure 3. Fluid control validation of the 3D oxygen microfluidic platform 87

Figure 4. Gas control validation of the 3D oxygen microfluidic platform 88

Figure 5. Hypoxia as a function of time 89

Figure 6. Long term hypoxic experiments 90

Figure 7. Vascularization of microfluidic channels 92

Figure 8. Hypoxic stimulus on endothelial cells 95

Figure 9. Network formation within the microchannels 96

Figure 10. Collagen invasion 97

Figure 11. Groups of invading cells 98

Figure 12. Invasion vs time 99

## LIST OF ABBREVIATIONS

| | |
|---|---|
| NMDA | N-methyl D aspartate |
| CA | Cornu Ammonis |
| 3D | Three dimensional |
| AM | Acetoxymethyl |
| nm | Nanometer |
| MCBL | Multicell Bolus Loading |
| UV | Ultraviolet |
| PDMS | Polydimethylsiloxane |
| P | Postnatal |
| µm | Micrometer |
| mm | Millimeter |
| °C | Degrees Celsius |
| min | Minutes |
| RPM | Revolutions Per Minute |
| sec | Seconds |
| cm | Centimeters |
| cc/min | Cubic Centimeters Per Minute |
| aCSF | Artificial Cerebral Spinal Fluid |
| $O_2$ | Oxygen |
| $N_2$ | Nitrogen |
| $CO_2$ | Carbon Dioxide |
| mM | Millimolar |

| | |
|---|---|
| mOsm | Milliosmol |
| DMSO | Dimethyl Sulfoxide |
| μM | Micromolar |
| PtOEPK | Platinum (II) Octaethylporphine Ketone |
| VEGF | Vascular Endothelial Growth Factor |
| mg | Microgram |
| FITC | Fluorescein Isothiocyanate |
| PBS | Phosphate Buffered Solution |

## SUMMARY

How cells and tissues respond at the microscale to a hypoxic insult is a fundamental question in angiogenesis as well as in stroke research. Oxygen is a critical modulator of cell physiological function; changes in the oxygen environment can lead to different biological responses ranging from angiogenesis, cell migration, and metabolism. Due to the importance of oxygen in the cell's viability and behavior, cell oxygen environment should be a critical factor in the experimental setting. Ironically, it is one of the most often overlooked components of cell culture experiments.

There is a pressing need to create an *in vitro* platform that can intimately recapitulate the oxygen environment experienced by cells *in vivo*. Physiologically relevant oxygen gradients are dynamic; a proper technique should provide temporal and spatial control over the oxygen environment. It should also provide a simple way to assess cell response to the hypoxic environment. Towards this end, three different techniques were developed to aid in the study of hypoxic research in cells and tissues.

In chapter 1, a microfluidic oxygenator is used to deliver constant oxygen to rodent brain slices, enabling the loading of the cell-permeant calcium indicator Fura-2/AM into cells of adult brain slices. When compared to traditional methods, our microfluidic oxygenator improves loading efficiency, measured by the number of loaded cells per unit area, for all tested age groups. Loading in slices from 1-year-old mice was achieved, which has not been possible with current bulk loading methods. This technique significantly expands the age range for which calcium studies are possible without cellular injection. This technique will facilitate opportunities for the study of calcium signaling of aging and long term stress related diseases. Moreover, it should be applicable to other membrane-

permeant physiological indicator varieties.

In chapter 2, a 3D microfluidic oxygen mixer was designed to output desired oxygen levels for ease of experiment use. The unit requires two inputs of gasses and will output twenty-two different gas concentrations. The gas-mixing network in the device was designed specifically for two gas inlets to mix at predetermined locations along the device generating a linear series of oxygen concentrations. The oxygen mixer was designed in AutoCad and printed using Fineline Prototyping on a stereolithographic 3D printer. The mixer is made of a nonpermeable photopolymer that prevents diffusion from affecting the mixing of the gas flows. Inlets and outlets were designed to allow easy connection to gas tanks and microfluidic devices. When compared to other existing techniques, our 3D oxygen mixer provides simplicity, accuracy, and low expense. The proposed model can be used in hypoxia research where the microenvironment must be greatly controlled due to the extreme sensitivity of cells to the oxygen levels.

In chapter 3, a three dimensional environment, oxygen control, and advanced microfabrication techniques are brought together to create a 3D oxygen microfluidic platform where *in vitro* angiogenic hypoxic studies can be performed. The design will improve upon previous methods by developing a hybrid collagen/PDMS platform that will mimic a 3D culture setting under hypoxic conditions. Using this oxygen platform, the separate effect that growth factors and hypoxia have on the angiogenic response will be studied. Using this platform, angiogenesis was observed with no chemical factors being used as the driving force; instead, a hypoxic insult was used as the angiogenic factor.

# 1. CHAPTER 1: ENHANCED LOADING OF FURA-2/AM CALCIUM INDICATOR DYE IN ADULT RODENT BRAIN SLICES VIA A MICROFLUIDIC OXYGENATOR

**Sections of this chapter have been previously published in:**

Mauleon, G. 2011, Stroke on a Chip: Spatial and Temporal Control of Oxygen for *in vitro* Brain Slices.

Mauleon, G., Lo, J.F., Peterson, B.L., Fall, C.P. & Eddington, D.T. 2013, "Enhanced loading of Fura-2/AM calcium indicator dye in adult rodent brain slices via a microfluidic oxygenator", *Journal of neuroscience methods,* vol. 216, no. 2, pp. 110-117.

## 1.1. Introduction

### 1.1.1. Hypoxia Impacts Diverse Signaling Pathways in the Neuron

Success in identifying pivotal signaling mechanisms of hypoxic damage in neuronal cells is greatly aided by the ability to monitor and measure the cascade of cellular processes triggered by the onset of a hypoxic insult. An increase of intracellular calcium within the cell is a principal component in this cascade (Small et al. 1997) and as such has garnered a great deal of interest from neuroscientists.

Calcium ions are a critical component of cellular communication pathways ranging from muscle contraction, cell division, and neuronal signal communication (Wu et al. 2008). During a hypoxic environment, several mechanisms work parallel to each other to alter the ionic concentration inside of the cell; some of the most important ionic fluctuations include sodium, hydrogen, and calcium (Xue et al. 2008, Bickler, Hansen 1994).

One of the first consequences of hypoxia in neurons is a marked decrease in production of ATP (Bickler, Hansen 1994). As cell fuel reserves are depleted, it depolarizes and

allows extracellular calcium to enter the cell through voltage-gated calcium channels (Tonkikh, Carlen 2009, Bickler, Kelleher 1992). Organelles inside the cell release their calcium contents, the largest reservoirs are the mitochondria and the endoplasmic reticulum (Bickler, Kelleher 1992, Tian, Looger 2008). However, the main influx of calcium is due to a substantial release of glutamate from the cells (Stork, Li 2009).

As seen in figure 1, during a hypoxic environment the presynaptic neuron will be depolarized. This event will start a chain reaction that will release the excitatory neurotransmitter glutamate. Glutamate will then bind to the N-methyl D aspartate (NMDA) receptor, which is a subclass of glutamate receptors, in the postsynaptic neuron (Stork, Li 2009). NMDA receptors act as the activation switch for cation channels that calcium ions are specially favored to use. If glutamate is able to find the receptor's binding site the channel will open allowing calcium into the cell. This effectively increases the intracellular calcium concentration (Stork, Li 2009).

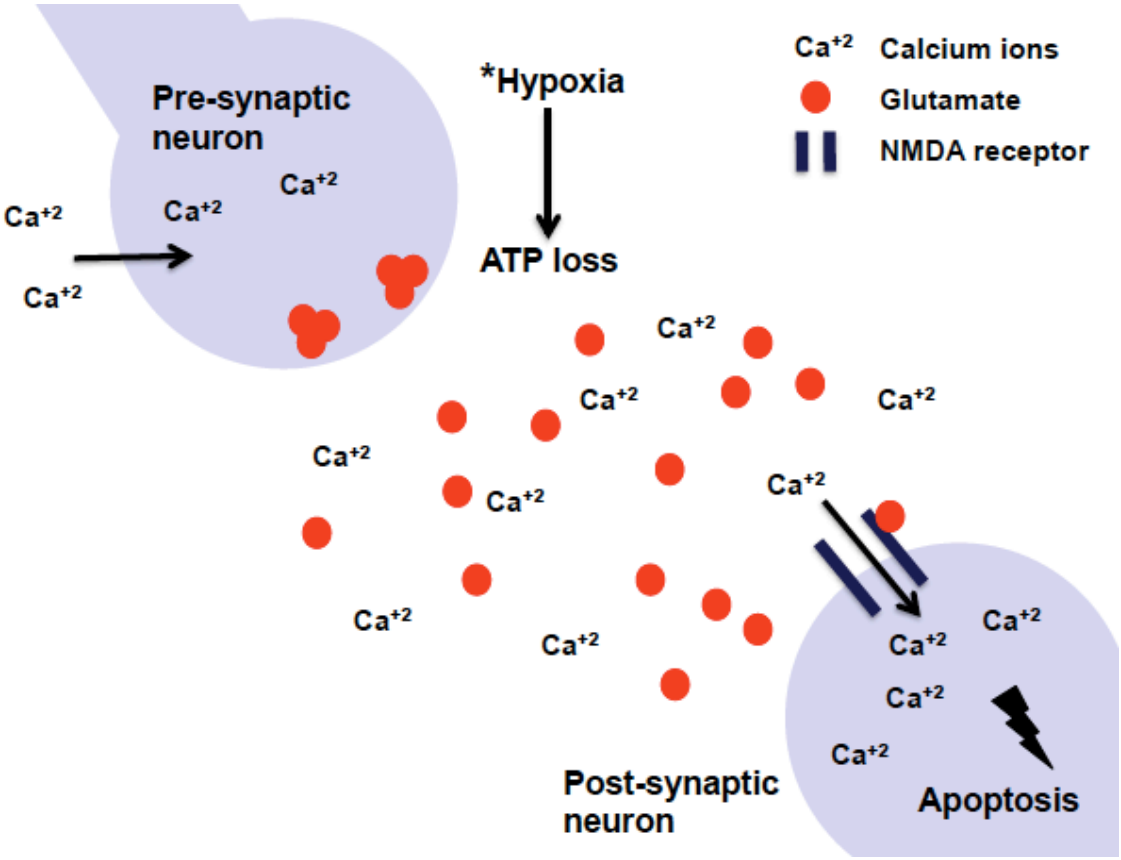


Figure 1. Hypoxia and calcium relationship in the neuron. During a hypoxic event, the cell loses its ability to regulate its metabolism. Glutamate is released into the synaptic cleft and eventually opens the NMDA receptors. A sudden calcium influx follows and can lead to cell death.

### 1.1.2. Brain Slice Preparation and Neonatal Specimens

Neuroscientists have developed several models that allow them to study the complexities of the brain in a controlled environment. Some recognized examples include: dissociated neuron models to study the protective effects of drugs (Wu et al. 2008) and organotypic brain slice cultures to study molecular and electrophysiological responses of neurons (Berdichevsky et al. 2009). Nonetheless, the acute brain slice preparation is still a preferred *in vitro* model of the brain. Close to half a century ago the acute brain slice preparation was introduced to the scientific community in order to provide an *in vitro* model (Cho, Wood & Bowlby 2007) that could offer a way to study the neuronal signaling while still retaining most of the local circuitry (Gahwiler et al. 1997).

Physiologically speaking, there are several reasons why the acute brain slice preparation is superior to other *in vitro* models. Unlike dissociated neurons, by maintaining the structural integrity, brain slices give researchers an idea of the *in vivo* brain cytoarchitecture, or arrangement of the cell bodies. Thus, researchers get an idea of the local anatomy and an inside look at the circuitry that the brain has developed (Queval et al. 2010). By remaining a solid piece of tissue, the slices provide a mechanical stability that allows long-term electrophysiological experiments. In addition to the mechanical stability, brain slices are able to provide experimental stability that cannot be obtained during *in vivo* experiments. Thanks to the absence of a heartbeat and pulmonary movement, which would cause pulsations; long-term electrophysiological experiments are possible (Reid et al. 1988). In short, all metabolic and vascular influences are mostly absent, which allows researchers to study the effect

of certain stimulants in isolation (Tang et al. 2011). Like all *in vitro* models, the local environment is easily controlled, so the researcher can manipulate the oxygen concentration, carbon dioxide, pH, temperature, and ion concentration (Gahwiler et al. 1997). Finally, one advantage of brain slices over *in vivo* models that cannot be undermined is the accessibility afforded by the slice. By doing *in vitro* experiments, the researcher can easily visualize the area of interest and can accurately place electrodes, apply chemicals, or move the tissue in any form that is needed to improve the success rate; in contrast to *in vivo* experiments where there is little access to the area of interest (Rambani et al. 2009).

Using the acute brain slice preparation specific components of the brain, such as the hippocampus can be dissected. The role of the hippocampus in memory formation and its sensitivity to oxygen level changes are well documented. The hippocampus is divided into several areas depending on cellular content: granular cells mainly populate the dentate gyrus while the 4 cornu ammonis (CA) areas have numerous pyramidal cells (Nitatori et al. 1995, Papazisis et al. 2008). The CA1 hippocampal area is the most vulnerable to hypoxic events, followed by the dentate gyrus (Papazisis et al. 2008).

The use of hippocampal acute brain slice preparation provides a three dimensional (3D) platform where the effect of oxygen deprivation on neuronal physiology can be studied in isolated detail. The ability to precisely control the spatiotemporal oxygen environment in a brain slice provides superior insight into the relationship between oxygen and neuronal function in the living brain.

### 1.1.3. Calcium Imaging

One of the main techniques used to relate hypoxia to intracellular calcium is fluorescent imaging, namely, calcium imaging (Chen et al. 2006). Using ratiometric molecules that bind to calcium ions, it is possible to indirectly measure the intracellular calcium concentrations (Rochefort, Jia & Konnerth 2008).

One of the most widely used calcium indicators is Fura-2/AM (acetoxymethyl) (Barreto-Chang, Dolmetsch 2009). The Fura-2 molecule, when combined with the acetoxymethyl ester group is able to penetrate the cell membrane of the neurons. Once inside the cell, it is de-esterafied by intracellular esterases, trapping the indicator in cytoplasm (Roe, Lemasters & Herman 1990). The Fura-2 molecule can then bind with the free calcium ions present in the vicinity (Nakamura, Nakai & Izumi 1996).

The Fura-2 molecule has the innate ability to change its excitation wavelength whenever a calcium ion binds to the molecule. Using ratiometric imaging, the calcium concentrations can be measured using the ratio of the 340nm over 380nm wavelengths (Peterlin et al. 2000a). Ratiometric imaging can negate several experimental errors, such as: instrument efficiency, the final concentration of the fluorescent dye, leakage present, and perhaps most importantly, photobleaching (Rochefort, Jia & Konnerth 2008).

During imaging, ratiometric signal will remain constant, dependent on a steady cell environment. However, when a hypoxic insult is applied and the calcium ions flow into the cell, the Fura-2 molecule will bind to the calcium ions; at this point, the molecule will shift its wavelength and the ratiometric change will be apparent. The increase in the signal signifies the influx of calcium ions.

Most studies that use calcium imaging to quantify hypoxic insults employ brain slices originating form neonatal subjects. Information from older subjects is severely lacking in research studies, this population is arguably more relevant to hypoxia diseases (Peterlin et al. 2000b).

### 1.1.4. Previous Methods

Prevalent techniques to load calcium indicator dyes into cells are microinjection and bulk loading (Regehr, Tank 1991). In microinjection, the user impales a single cell with an intracellular electrode to load it with the dye (Regehr, Tank 1991). This technique, while accurate and necessary for calibration of the intracellular calcium, can become cumbersome if a population of neuronal cells is the subject of the experiment. On the other hand, bulk loading methods allows several cells to be loaded with the dye in a simple step (Regehr, Tank 1991). The brain slices are incubated for a short amount of time in a membrane permeable ester form of the calcium indicator dye (Smetters, Majewska & Yuste 1999).

As previously mentioned, the Fura-2/AM is a very powerful calcium indicator used regularly in conjunction with the bulk loading technique. However, this method has limited loading success when brain slices utilized originate from adult mice (Peterlin et al. 2000b, Barreto-Chang, Dolmetsch 2009, Stosiek et al. 2003), for reasons though to be related to the development of the neuropil over time after birth.

Different techniques attempt to improve loading efficiency of calcium indicators in brain slices, especially in adult tissue with varying degrees of success. Various groups tried to increase the incubation periods (Lin et al. 2003, Kirischuk, Verkhratsky 1996); others would incubate the slices under atmospheric air (Beierlein et al. 2002), while others

would bubble carbogen gas in the incubation media (Yuste et al. 2011). Numerous studies have illustrated attempts to develop elaborate loading protocols ranging from a double incubation (Peterlin et al. 2000b) to a multicell bolus loading (MCBL) approach (Stosiek et al. 2003). Meanwhile, other researchers use genetically encoded calcium indicators (Lin et al. 2003).

While these techniques allow collection of quality data, they require specialized equipment (Stosiek et al. 2003, Lin et al. 2003) and time-consuming, intricate protocols (Peterlin et al. 2000b). Yet, remain limited in practice to samples originating from mice younger than 25 days old (Peterlin et al. 2000b, Lin et al. 2003, Beierlein et al. 2002).

### 1.1.5. Microfluidic Technology

Microfluidic technology provides neuroscientists with tools necessary to perform powerful brain slice experiments (Mauleon, Fall & Eddington 2012a). In order to create these microfluidic devices, photolithography and soft-lithography techniques have been perfected to accommodate the various needs of the biological community.

The entire process is shown in figures 2 and 3. Initially, a master is made using photolithography techniques. SU-8 (a photosensitive epoxy) is first poured over a silicone wafer. A predetermined mask design is then placed on top of the wafer and exposed to ultraviolet (UV) light. The UV light will polymerize the exposed epoxy areas and any unpolymerized epoxy will be washed off. Eventually, the master mold will have a raised design that will be a negative of the final design (Ng et al. 2002). In order to maximize the master mold's efficacy, a process called silanization can be applied. In this process, the vaporized form of chemical silane is deposited on top of the master for a period of two hours (Anderson et al. 2000).

a)

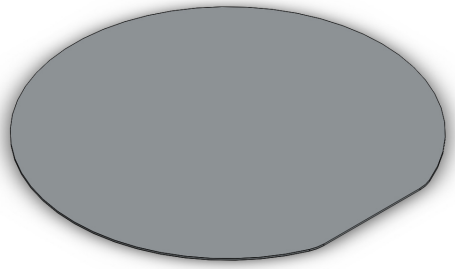

**Silicon wafer**

b)

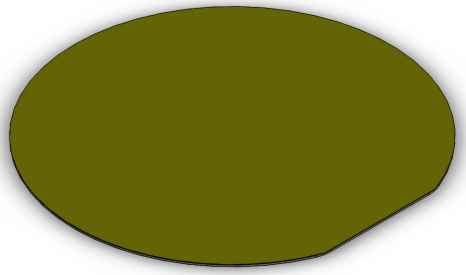

**SU-8 spin coated on top**

c)

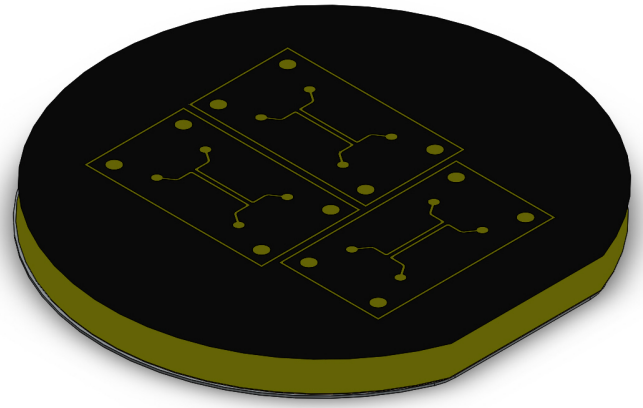

**UV light exposes photomask design on wafer**

d)

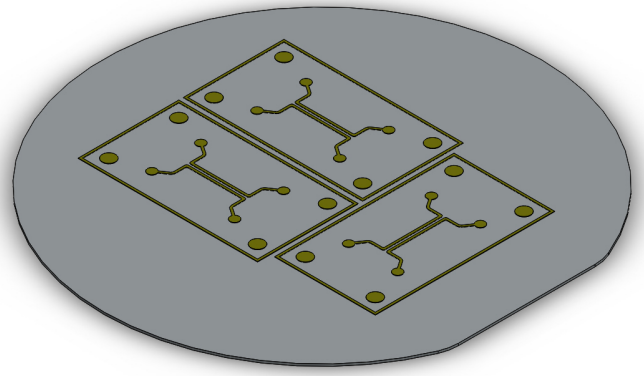

**Master mold**

Figure 2. Photolithography. A) A silicon wafer is cleaned thoroughly. B) SU-8 is spin coated onto the wafer. C) Selectively exposed to UV light through a photomask. D) Wafer is developed and silanized producing a reusable master.

From a SU-8 patterned silicon wafer, an elastomer chip is created which can be utilized numerous times (Berdichevsky et al. 2009). A principal component of this technique involves the use of elastomeric materials to create devices that display a patterned structure on their surfaces (Qin, Xia & Whitesides 2010), this is done via a technique called replica molding. In replica molding, the polymer mix (a combination of prepolymer and curing agent) is poured over the master and then heated. This causes the polymer mix to polymerize and solidify. The elastomer block can then be lifted up from the master. The final result is a device with a patterned structure and a master that can be reutilized (Ng et al. 2002).

The polydimethylsiloxane (PDMS) polymer is one of the main materials used to fabricate microfluidic devices. This polymer has several important properties that are beneficial to the biological community. For example, the PDMS components have a very low glass transition temperature, and as such, they are in the liquid state at room temperature and can be cross-linked with heat. Once it is polymerized, PDMS is relatively elastic depending on the curing agent and cross linker ratio used (Ng et al. 2002). PDMS makes an ideal platform for biological experiments because it is optically transparent and has a surface that is hydrophobic and chemically stable. Additionally, it is nontoxic and can be sterilized by many conventional methods (Blake et al. 2007, Oppegard et al. 2009). PDMS is also an optimal material for biological experiments due to its high oxygen diffusivity, which is in the same order as water, to nonpolar gasses, mainly oxygen (Mehta et al. 2007, Lam, Kim & Thorsen 2009). If the PDMS layers are small enough, it is safe to assume that the gasses will diffuse to fully oxygenate the biological tissue on the other side (Mehta et al. 2007).

a)

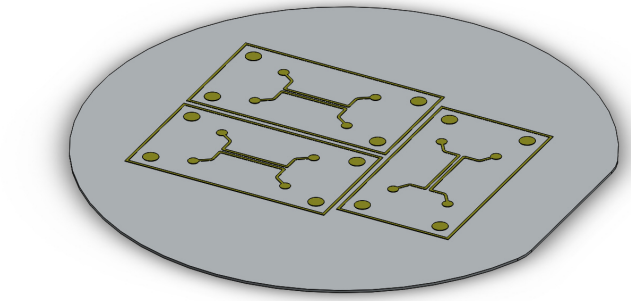

**Master mold**

b)

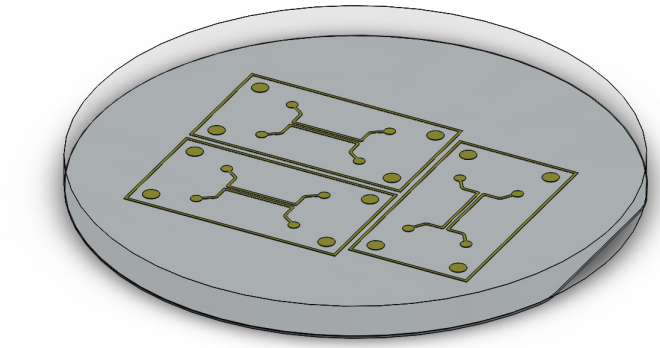

**PDMS poured over master**

c)

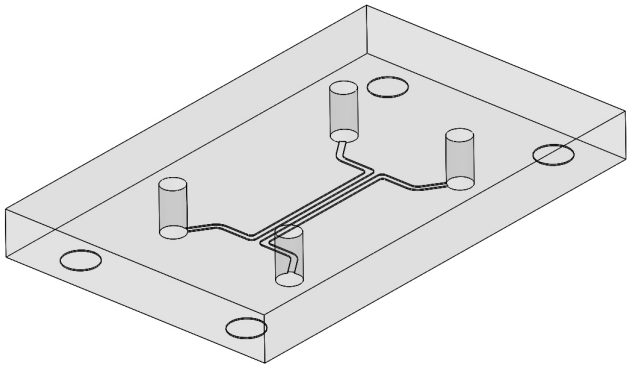

**PDMS parts can be cut from master**

Figure 3. Replica molding. A) The master should be silanized before use. B) PDMS is poured over the master and allowed to polymerize. C) The PDMS mold can then be peeled off from the master.

### 1.1.6. Research Purpose

Applying microfluidic technology, neuroscience researchers can improve on the current techniques available for calcium loading. A standard bulk loading method that requires the slices to rest in the incubation media for a short period of time (20 minutes for slices up to P20) (Peterson et al. 2012, Beierlein et al. 2002) has been successfully employed in this study as well as several others. This study will compare this standard method to a newly developed microfluidic protocol. Utilizing a modified version of an incubator for open-top cell culture oxygen incubation (Lo, Sinkala & Eddington 2010), brain slices were incubated in Fura-2/AM for longer periods of time than previously achievable. The microfluidic oxygenator uses gas microfluidic channels with a thin gas permeable membrane to diffuse oxygen to the brain slice and helps to maintain viability while improving calcium indicator loading. This microfluidic method is more efficient in oxygenating thin brain slices by eliminating boundary layers in bulk convective mass transfer. By utilizing this device the brain slice is in direct contact with the oxygen-permeable membrane substrate. This direct diffusion process allows for a more stable and uniform oxygen environment throughout the brain slice, thus keeping the tissue healthier. An improvement in calcium indicator loading at a wide range of brain tissue ages is demonstrated. Subjecting the slice of a mouse older than one year old to a period of hypoxia and measuring the calcium response demonstrate the functionality of the loading.

## 1.2. Materials and Methods

### 1.2.1 Design and Fabrication of Microfluidic Oxygenator

#### 1.2.1.1. Design of Microfluidic Oxygenator

A microfluidic oxygenator was developed to incubate brain slices during the Fura-2 loading protocol with constant, uninterrupted oxygen flow. As shown in figure 4, the microfluidic oxygenator is a multilayered PDMS device. The bottom layer consists of a microfluidic gas network that delivers the oxygen gas to the brain slice. The second layer of PDMS is a 100μm thick gas-permeable membrane that allows oxygen diffusion into the brain slice. The top layer of PDMS is 3cm thick with a 1cm diameter well. The well can hold 1 brain slice completely submerged by the incubation media. All 3 layers have aligned inlet and outlet ports that allow easy introduction of the oxygen gas to the gas network.

#### 1.2.1.2. Fabrication of Microfluidic Gas Network

The microfluidic gas network was fabricated using standard photolithography techniques. The photomask design was created in AutoCAD and printed onto high-resolution transparency film (Fineline Imaging). To fabricate the master mold, a 100mm silicon wafer was rinsed with acetone, isopropanol, and methanol and dried under nitrogen. Placed in a hotplate set to 125°C for 15 minutes, before being exposed to oxygen plasma. The treated wafer was then soft baked (65°C for 10 min, 95°C for 45 min), selectively exposed to UV light using the photomask, post-exposure baked (65°C for 5 min and 95°C for 14 min), and developed using SU-8 developer for 15 minutes. The developed master was then silanized with (Tridecafluoro 1, 2, 2-tetrahydroctyl)-1-trichlorosilane vapor in a desiccator overnight.

To fabricate the positive mold of the device, PDMS prepolymer was prepared (10:1 polymer base: curing agent), degassed, poured onto the master, and cured on a 75°C hot plate for 2 hours. PDMS was then removed from the master.

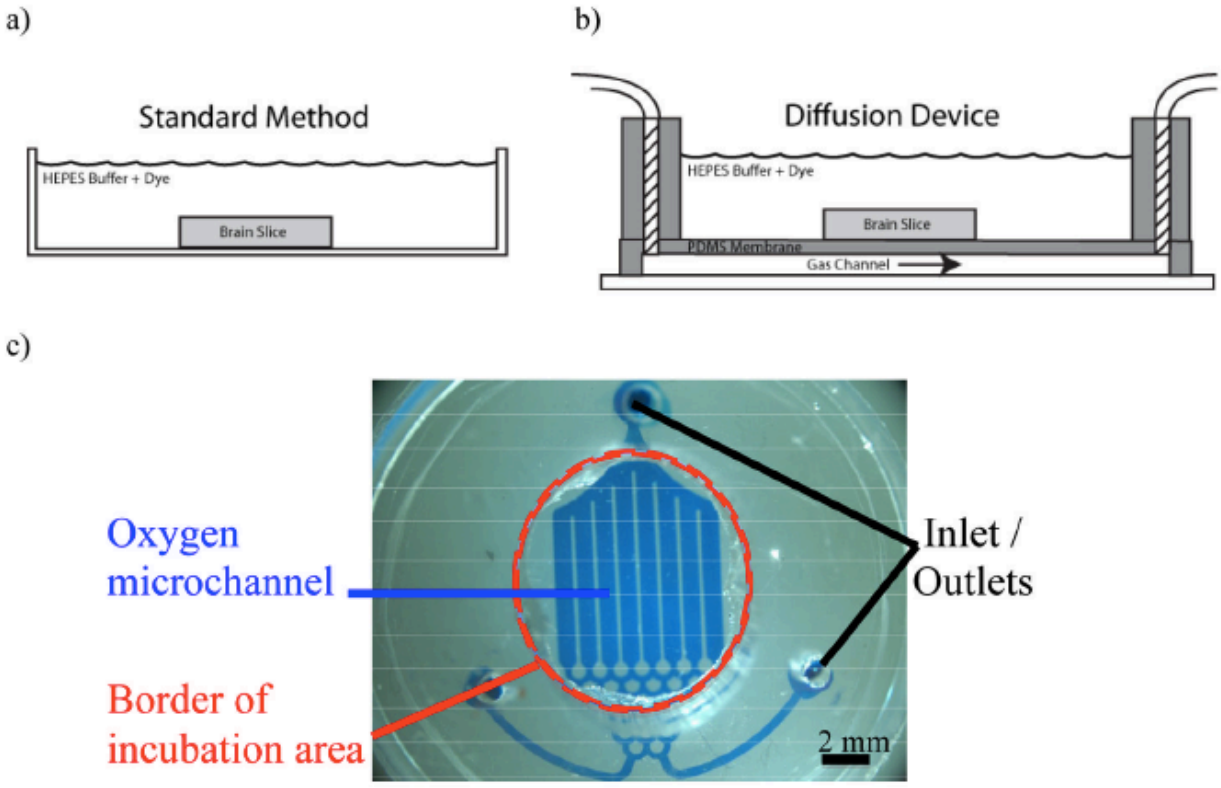


Figure 4. Standard method versus the microfluidic oxygenator. (A) Standard method of dye loading where the tissue is placed in a dish with the dye. (B) Schematic of the microfluidic oxygenator which consists of 3 independent parts: the microfluidic network, the gas-permeable membrane, and the incubation well. Gas flows beneath the membrane where the tissues sits and diffusion from the gas channel oxygenates the tissue via diffusion. (C) Photograph showing the features of the microfluidic oxygenator from above.

#### 1.2.1.3. Fabrication of PDMS Membrane

In order to make the gas-permeable membrane, a used silicon wafer was cleaned with isopropanol and acetone. 5 grams of PDMS was then mixed and spin coated onto the wafer to achieve a thickness of 100μm (500 RPM for 10 sec, 800 RPM for 30 sec) followed by curing for 2 hours at 75°C. After curing, a section that would fit the microfluidic network was removed from the wafer and placed on a transparency film. Following this step, using alignment marks, the inlet and outlet ports were made in the membrane using a blunted punch hole. Once the gas permeable membrane and the microfluidic network were ready, they were exposed to oxygen plasma and bonded together, ensuring that holes in the membrane would make contact with the inlet and outlet of the network device. The resulting product is a PDMS assembly consisting of the gas network irreversibly bonded to the membrane.

#### 1.2.1.4. Fabrication of PDMS Incubation Well

To fabricate the incubation well, pre-mixed PDMS was poured onto a 6-well plate until it reached a thickness of 3cm deep, and this was allowed to cure in a hot plate. The cured PDMS piece was removed from the 6-well plate and punched with a 1cm diameter hole-punch to remove the center of the object, effectively creating the incubation area of the device.

#### 1.2.1.5. Assembly of PDMS Microfluidic Oxygenator

Alignment marks were used to create inlet and outlet ports in the PDMS incubation well to allow oxygen to flow into and out of the microfluidic channel below the gas permeable PDMS membrane. Once the individual parts were aligned, they were irreversibly bonded using a plasma wand to complete the device.

Tygon tubing was attached to multiple incubation wells using plastic connectors where one gas line input could oxygenate all 6 incubation wells. The oxygen flow rate within the microfluidic gas channels is 40 cc/min, which is sufficient to maintain an infinite source for diffusion but low enough to prevent distending of the diffusion membrane. The incubation wells allow the slice to be completely submerged under the HEPES buffered aCSF solution while the PDMS membrane provides a mechanically stable surface for the tissue.

### 1.2.2 Animals and Experimental Groups

The Animal Care and Use Committee at the University of Illinois at Chicago approved all of the reported procedures. Experiments were performed on male and female BL7 mice (bred from stock obtained from Charles River Laboratories, Wilmington, MA). Experiments were conducted on postnatal mice [12-30 days old (P12-P30)] and adult mice [P50- 1yr old] housed under normoxic laboratory conditions.

### 1.2.3 Brain Slice Preparation

Mice were deeply anesthetized using Aerrane (isoflurane, USP) and decapitated. Brains were rapidly removed from the skull and placed in chilled (3-7°C) high-sucrose cutting solution. Then, the cerebellum was separated and disposed, while the rest of the brain tissue was glued to an agar block using cyanoacryl glue with the cerebral cortex facing down. While in high-sucrose cutting solution, 350μm thick hippocampal slices were cut with a tissue slicer (Vibratome Series 100 Classic) along the transverse plane. The slices were then placed in a custom-made holding chamber containing high sucrose cutting solution and incubated at 34°C for 35 min. Brain slices were transferred to another chamber containing artificial cerebral spinal fluid (aCSF) and incubated at the

same temperature for 25 minutes. Following the incubation period, the brain slices were kept at room temperature. 95% $O_2$/ 5% $CO_2$ gas was continually bubbled into all solutions containing brain slices.

The cutting solution contained (in mM): 82.70 NaCl, 23.81 $NaHCO_3$, 2.41 KCl, 2.65 $Na_2HPO_4$, 14.53 $MgCl_2$, 0.64 $CaCl_2$, 23.70 Glucose and 71.19 Sucrose. The aCSF solution used during slice incubation and experiments contained (in mM): 124.98 NaCl, 23.01 $NaHCO_3$, 2.50 KCl, 2.36 $Na_2HPO_4$, 0.43 $MgCl_2$, 0.26 $CaCl_2$, and 25 Glucose. The osmolarity of the solution was 300–310 mOsm, adjusted with sucrose. All experiments were performed at room temperature.

### 1.2.4 Validation of Device Using Fiber Optic Oxygen Sensor

A fiber optic oxygen sensor (Neofox, Ocean optics) was used to compare the microfluidic oxygenator versus the standard method. The tip of the oxygen probe has a diameter of 200μm and uses photoluminescence-quenching of a ruthenium compound to detect oxygen molecules. The sensor was calibrated according to manufacturer instructions. First, the probe is exposed to gas containing 0% $O_2$ (95% $N_2$/5% $CO_2$) for 30 seconds, followed by gas containing 95% $O_2$ (95% $O_2$/5% $CO_2$) for 30 seconds. The $CO_2$ is present as it can also alter the fluorescence of the probe. Once calibrated, the probe was lowered into the microfluidic oxygenator and the oxygen concentration in the HEPES buffered aCSF solution was recorded; the same procedure was repeated for the standard method.

The oxygen concentration inside the brain slice — the hippocampal CA1 area, P30 mice — was gathered while the slice was incubated for 90 minutes as shown in figure 5A. In figure 5B, the results obtained from a two-tailed, unpaired t-test (Excel) to compare the

oxygen concentration values obtained from the standard method and the microfluidic oxygenator at predetermined time periods (30, 60, and 90 minutes), are demonstrated.

In order to measure the oxygen concentrations inside the brain slice, the oxygen probe was attached to a piezoelectric micromanipulator that could maneuver the probe in the x, y, and z planes with a resolution of 0.1μm. For this study, the oxygen concentration at a height (measured from the bottom of the chamber) of 250μm was recorded within the brain slice.

### 1.2.5 *In Vitro* Loading of Brain Slice with Fura-2/AM

In order to determine the intracellular calcium response of the brain slice, Fura-2/AM (Biotium) was used. After finishing the aCSF incubation period, Fura-2/AM was dissolved in DMSO plus 20% Pluronic F-127 to yield a concentration of 5μM. Using a pipette, 1ml of HEPES buffered aCSF solution was deposited into the wells of the microfluidic incubation device, as well as on the chamber used for the standard method. Pairs of slices from the same mouse were then simultaneously placed into the wells filled with the HEPES buffered aCSF solution and the Fura-2/AM dye was puffed onto the brain slices focusing on the hippocampal area.

Incubation times were changed depending on the age of the tissue ranging from 20 minutes to 3 hours to maximize dye loading but minimize loading time. The microfluidic oxygenator was continuously perfused with 21% $O_2$/5% $CO_2$ while the standard method used only atmospheric air. After the allotted incubation time, the slices were placed back into the holding chamber containing aCSF.

### 1.2.6 Live/Dead Assay

Following the incubation period in the aCSF, the hippocampal brain slices were stained with the calcium indicator using the 2 methods previously outlined. The incubation period varied based on the age of the mice according to table 1. To assess for cell death after the incubation period in the different methods, the brain slices were subjected to a live/dead viability assay as per manufacturer's protocol. The slices were briefly incubated in 4μM of ethidium homodimer-1 (to highlight the dead cells) and 2μM of calcein acetoxymethyl ester (to highlight the live cells) in the dark for 30 minutes. Slices were washed in control aCSF at room temperature for 15 minutes; the number of live and dead cells was quantified in a given field of view using a 10X objective and fluorescence microscopy with the appropriate filters.

**Table 1. Summary of microfluidic oxygenator advantages over standard method**

| Age | Loading Time (min) | Viability Improvement (Fold) | Loading Improvement (Fold) |
|---|---|---|---|
| P12 | 20 | 1.0X | 1.1X |
| P20 | 30 | 1.0X | 1.5X |
| P30 | 90 | 1.2X | 2.0X |
| P50 | 120 | 2.0X | 3.0X |
| P70 | 150 | 2.2X | 11.0X |
| 1 yr old | 180 | 3.4X | 2.5X |

### 1.2.7 Quantifying Calcium in Mice Under a Hypoxic Insult

In order to create a hypoxic insult, which would allow close monitoring of the resulting intracellular calcium increase the procedure outlined in Mauleon et al (Mauleon, Fall & Eddington 2012b) was followed. A microfluidic device capable of manipulating the oxygen concentration inside the brain slice was utilized (more information about this microfluidic device can be found on appendix A). The brain slice was placed inside the oxygen delivery device. The chamber was filled with aCSF (no flow), and the oxygen concentration was control varied from 95% $O_2$ to 0% $O_2$. Images used to measure the calcium response were obtained from the CA1 area of the hippocampus by measuring the Fura-2 fluorescence emission at 510nm using a fluorescent inverted microscope (Olympus IX71). The ratiometric data was obtained by exciting the samples with 340/380 nm wavelengths using the image acquisition and analysis software MetaFluor Imaging System (Universal Imaging Corp.). For statistical analysis, the ratiometric data (340 nm intensity divided by 380 nm intensity) was converted to percent change in fluorescence by dividing the ratios obtained from each image by the average intensity ratio during the baseline-recording period (initial 5 minute period) and multiplying the result by 100; the pictures were acquired using the 10X objective.

### 1.2.8 Statistical Analysis

Experiments involving animal tissue were performed on a minimum of 3 brain slices obtained from 3 different animals for a total of 9 individual data sets, except slices from mice older than one year as only 1 animal was available in this group. Experiments not involving animal tissues were repeated a minimum of three times. Cell counting was performed using Image J. Graphs show the average value with the error bars

representing standard error. In addition, a two-tailed, unpaired t-test (Excel) to compare the data obtained from the incubation device and the standard method at the different mice ages was conducted.

## 1.3. Results

### 1.3.1 Characterization of the Microfluidic Oxygenator

#### 1.3.1.1 Media Oxygen Measurements

When the brain slices are loaded with Fura-2 using the standard method, they are incubated under normal atmospheric conditions; as such, the HEPES buffered aCSF solution contains an oxygen concentration of 21% (figure 5A). Using the microfluidic oxygenator, the HEPES solution contains the same oxygen concentration. The oxygen concentration does not fluctuate during the entire incubation period.

#### 1.3.1.2 Brain Slice Oxygen Measurements

In figure 5A, by measuring the oxygen concentration inside the brain slice at a height (starting from the bottom of the chamber) of 250μm, it is demonstrated that the microfluidic oxygenator is significantly better at oxygenating the brain slice than the standard method throughout the entire incubation period. Using the standard method, the inside of the brain slice receives an average of 3.7% $O_2$, while the microfluidic oxygenator provides the brain slice with an average concentration of 14.9% $O_2$ during a period of 90 minutes, $p<0.0001$, t-test. Figure 5B, shows static measurements taken at 30, 60, and 90 minutes during the incubation periods. The microfluidic oxygenator is superior at keeping brain slices oxygenated than the standard method and as such the slices are kept alive longer.

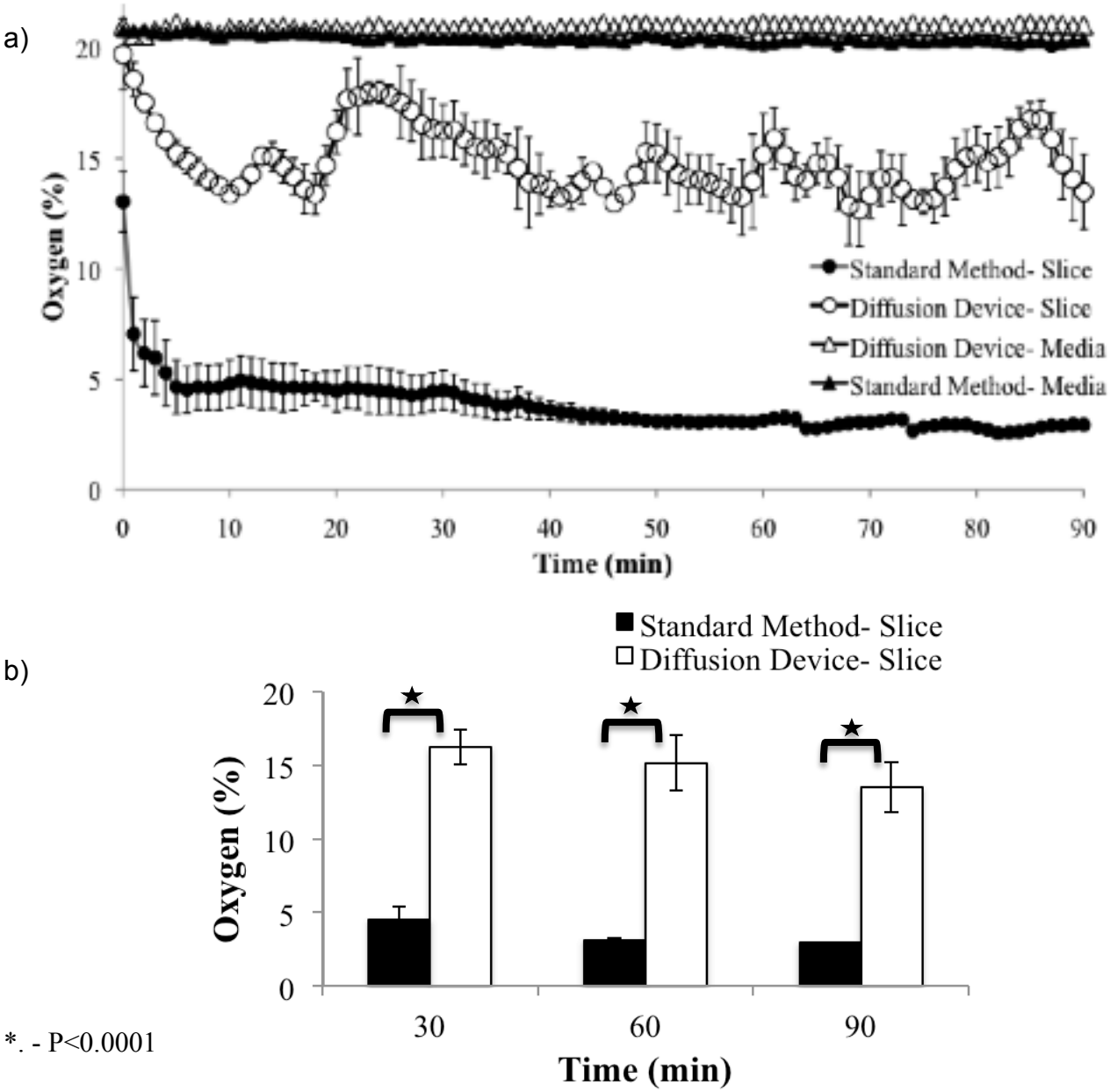


Figure 5. Validation of the microfluidic oxygenator with an oxygen sensor. (A) The oxygen concentration dissolved in the HEPES buffered aCSF solution was measured for the microfluidic oxygenator and the standard method. There is no difference in the oxygen concentration found in the HEPES buffered aCSF solution for these 2 methods. The oxygenation inside the brain slice at a height of 250μm was measured. The microfluidic oxygenator is able to continually oxygenate the brain slice with an average of 15% $O_2$. The standard method cannot oxygenate the brain slice in an efficient manner. During the 90 minutes incubation period, the average oxygen concentration inside the slice was less than 5%. (B) Summary data comparing the oxygen concentration values obtained from the standard method and the microfluidic oxygenator at predetermined time periods (30, 60, and 90 minutes).

### 1.3.2 Live/Dead Assay

Using a standard live/dead assay, the tissue viability of different age groups of mice was tested. With the P12 to 1-year-old mice as the age of the tissue increase, the viability of the cells decreases. This is shown by the live/dead assay using both methods (figure 6). However, the rate of decreased cell viability is considerably different from the two methods studied. The device and the standard method produce similar viability percentages up to age P20, as were expected considering the success rate of dye loading into neonate tissue. Starting with the P30 mice tissue, there is a small drop off in the viability from the standard method that is not seen with the microfluidic oxygenator. By P50 and on, the viability difference becomes statistically significant when compared to the microfluidic oxygenator method. Using the microfluidic oxygenator, brain slices from mice older than 1 year are kept viable during the incubation period.

### 1.3.3 Fura-2 Loading

There was no statistical difference between the P12 groups when incubated by either method (figure 7A). This is consistent with the common observation that neonatal brain tissue works well for bulk dye loading. However, as early as P20, we see an improved loading efficiency when using the microfluidic oxygenator. In a similar manner, the loading efficiency increases twofold at P30, while at P50 the efficiency increases by a factor of 3 with the device. At P70, a previously impossible age to load; we see a 10-fold increase in the number of cells loaded with the dye. Loading of brain slices from 1 year old mice was successfully done utilizing the microfluidic oxygenator and ratiometric imaging. The effectiveness of the loading procedure by means of calcium recording

from a hypoxic insult (figure 7B) is confirmed. Figure 7C shows representative images from the loaded neuronal cells from both methods at all age groups investigated.

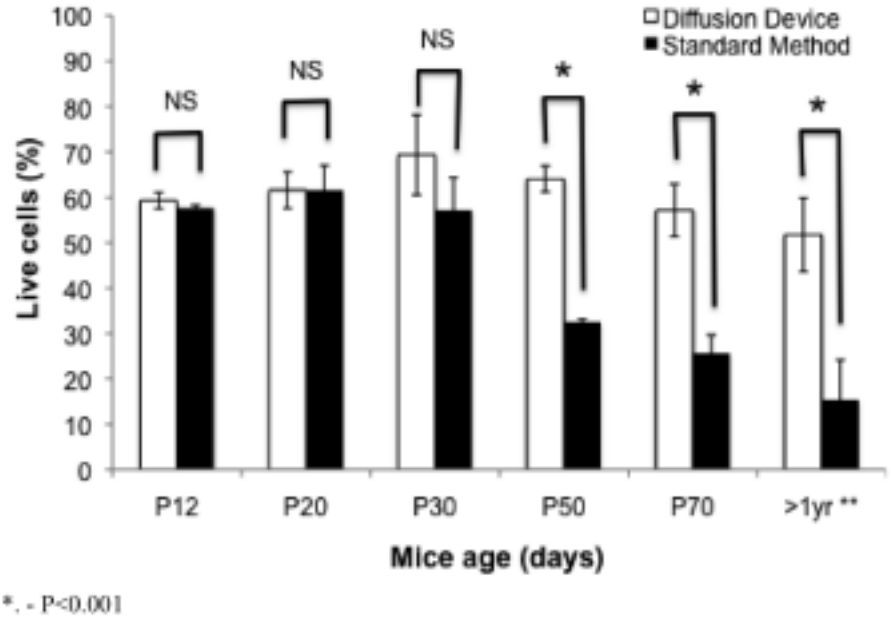


Figure 6. Live dead assay results. Quantification of the percent of cells left alive, as shown by the live/dead assay kit, after different incubation periods. P12-P30 showed no difference based on the different incubation protocols, however, starting with P50, there is a consistent drop off in cell viability in the standard method not experienced by the oxygenator method. The 1 year old mice data was obtained from only 1 mouse (due to lack of older mice), with 3 different slides stained with the live/dead assay kit. This means that the error bars represent 3 data points. All other age groups were obtained from 3 different mice for a total of 9 data points for each condition.

a)

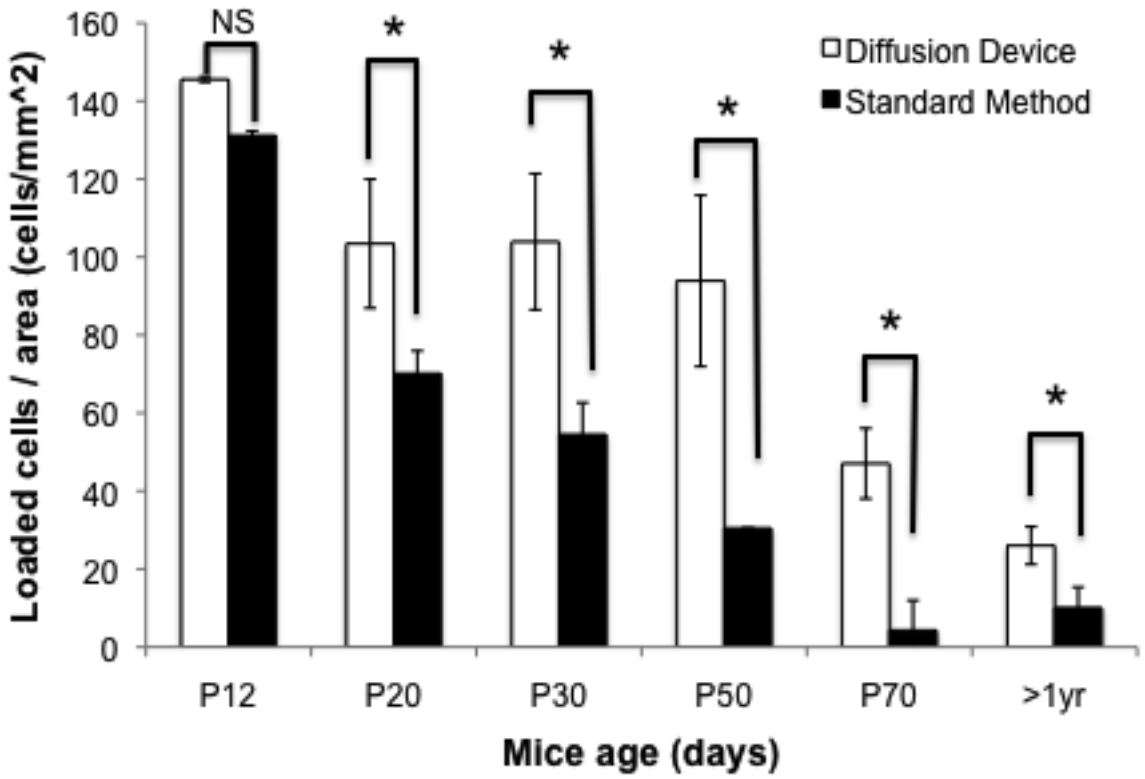
NS
*
*
*
*
*
Diffusion Device
Standard Method
Loaded cells / area (cells/mm^2)
160
140
120
100
80
60
40
20
0
P12
P20
P30
P50
P70
>1yr
Mice age (days)

*. - P<0.001

b)

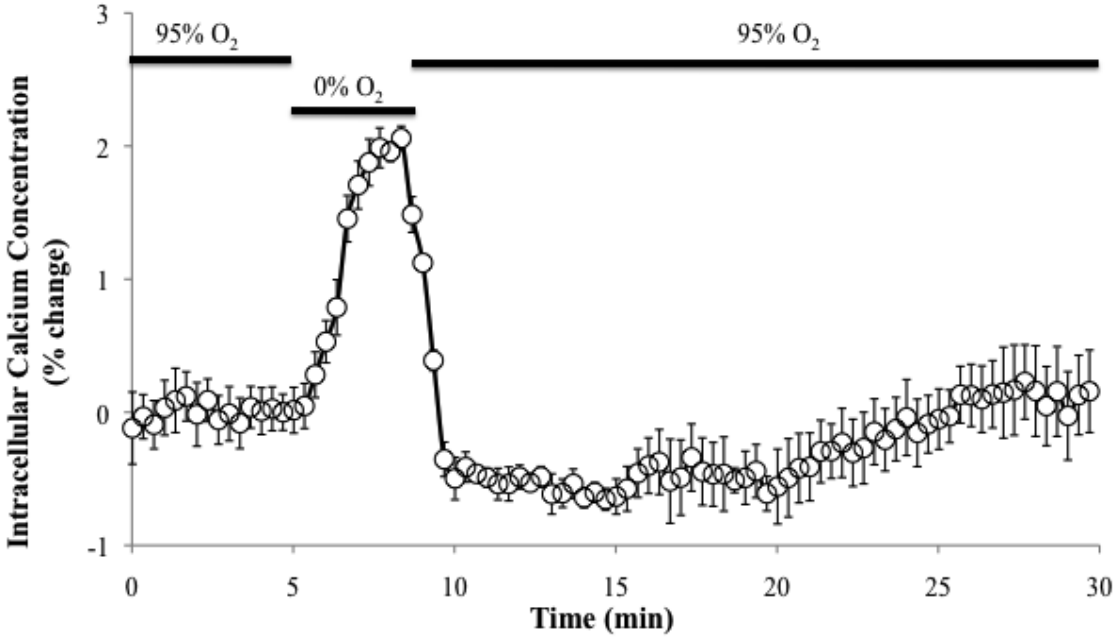
95% O2
0% O2
95% O2
Intracellular Calcium Concentration (% change)
3
2
1
0
-1
0
5
10
15
20
25
30
Time (min)

c)

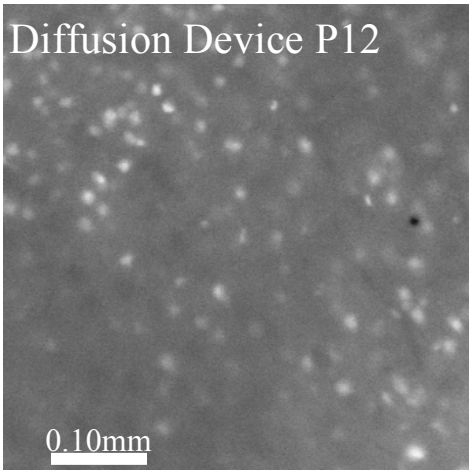
Diffusion Device P12
0.10mm

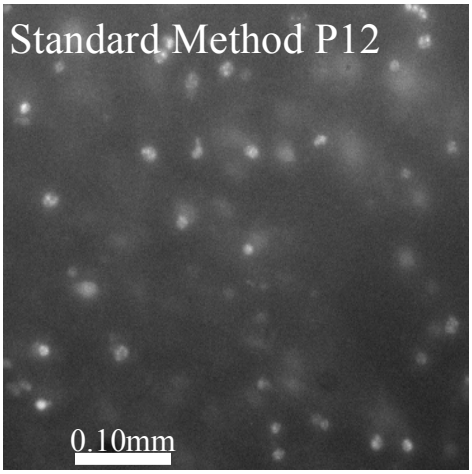
Standard Method P12
0.10mm

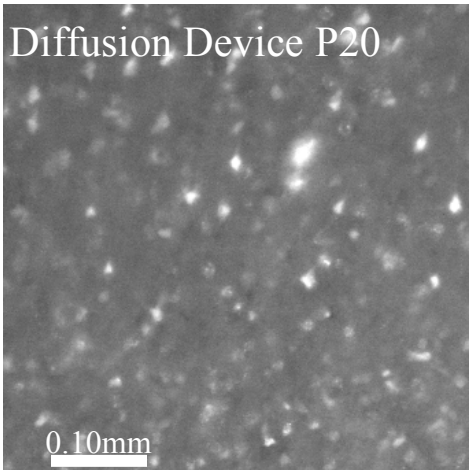
Diffusion Device P20
0.10mm

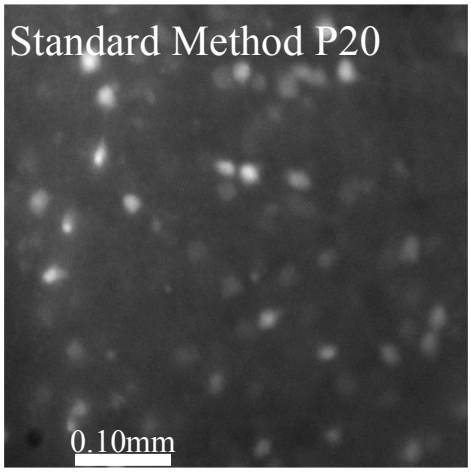
Standard Method P20
0.10mm

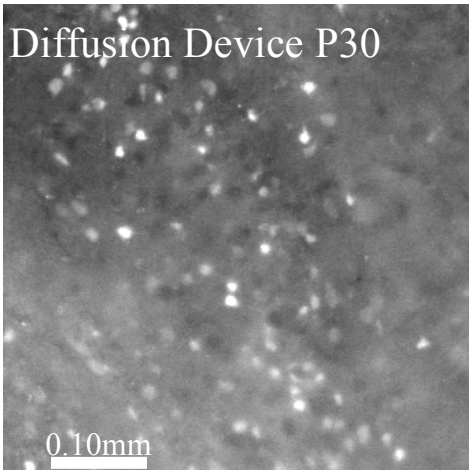
Diffusion Device P30
0.10mm

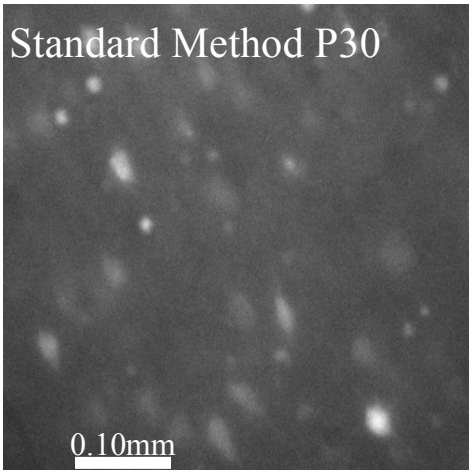
Standard Method P30
0.10mm

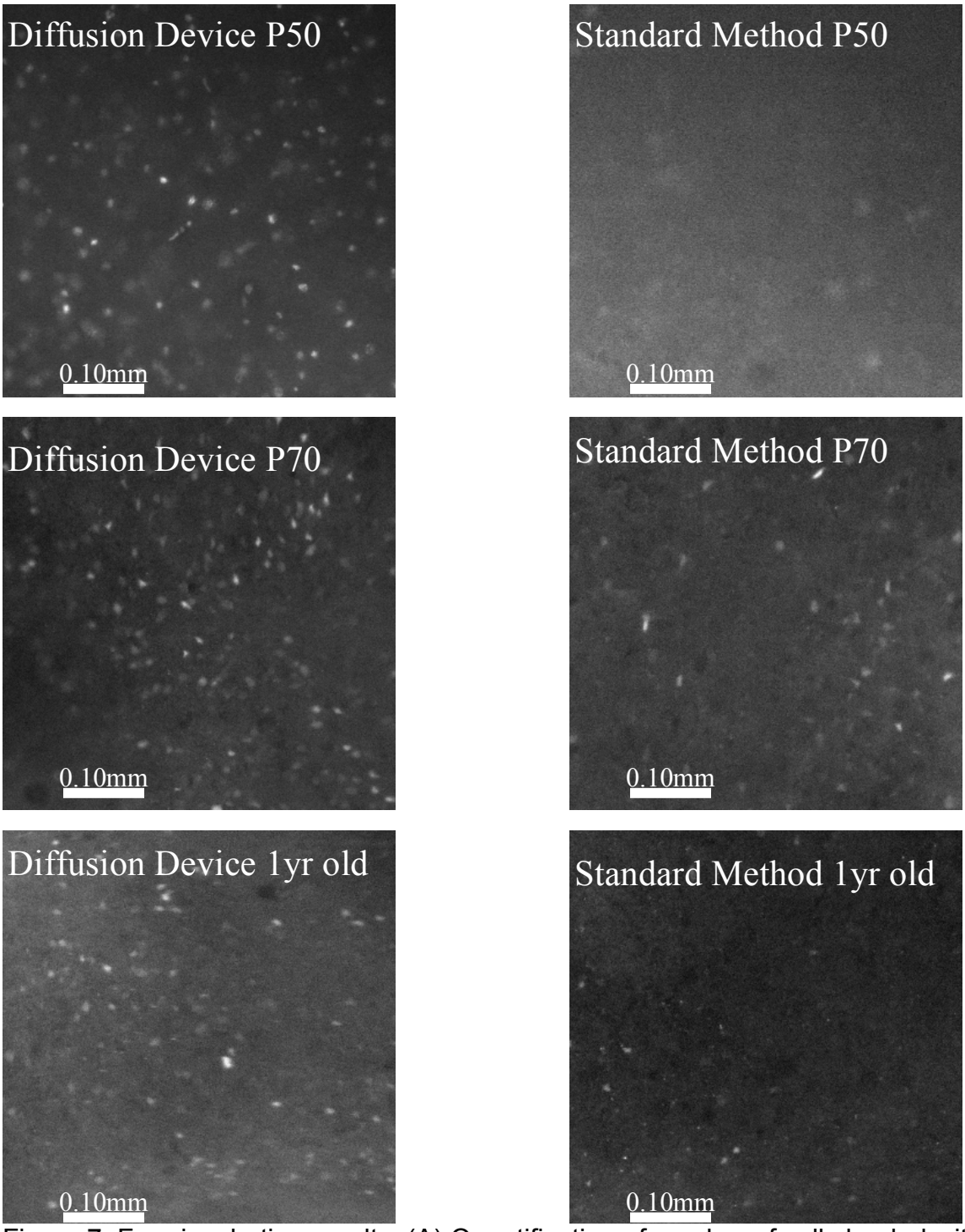


Figure 7. Fura incubation results. (A) Quantification of number of cells loaded with Fura-2 by two different methods. Using image J, the number of loaded cells per unit area in a given image were measured. The microfluidic oxygenator is able to better load the slices with the Fura-2 dye; even loading brain slices older than 50 days old. (B) During a hypoxic insult, the intracellular calcium increases as shown by the Fura-2 data. Brain slice originated from a mouse older than 1 year old. (C) Representative images from the different age groups

## 1.4. Discussion

Precise delivery of oxygen to the acute brain slice preparation using patterned microfluidic substrates has been examined (Mauleon, Fall & Eddington 2012b). This same technology now provides opportunity to improve on current dye loading protocols in order to obtain information from adult tissue. Conventional loading procedures were excellent when the brain slices came from neonates, however, even the most intricate protocols could not effectively load Fura-2 dye into mice older than P20 (Peterlin et al. 2000b). The microfluidic oxygenator developed can effectively oxygenate the brain slice for longer incubation periods. This study, investigates the optimal loading time necessary to effectively load the calcium indicator into the tissue. Unfortunately, the Fura-2/AM loading period for brain slices is not consistent from study to study (Lin et al. 2003, Kirischuk, Verkhratsky 1996), however, studies show that a longer incubation period would lead to improved dye loading. Results of this study indicate that standard method of dye loading causes oxygen within the brain slice to drop to an average of 3.8% $O_2$. Microfluidic oxygenator data demonstrates that oxygen concentration fluctuates, perhaps from cellular respiration, but still holding above 15% $O_2$ and reaching 19% $O_2$. Thus, the microfluidic oxygenator better oxygenates the slice for longer periods of time.

By adding constant oxygen delivery from the bottom of the slice, the slices are better oxygenated for longer periods of time and the lack of bubbles prevents stress experienced by the slices. It has been noted that standard method is able to load Fura-2 molecules into brain slices of neonates up to an age of 20 days old (Peterlin et al. 2000b). After this time period, however, the success rate decreases. This study

theorized that drop off in loading occurred due to loss of cell viability, as the oxygen decreases to 5% in 20 minutes. As demonstrated with a live/dead assay kit, the hypothesis was confirmed by testing different age groups of mice. Figure 6 shows that the microfluidic oxygenator allows the brain slices to stay viable with longer incubation periods than currently employed.

The microfluidic oxygenator, allowed for an increase in the dye loading times of the brain slices, this enabled increase loading times with an increase in age. This follows trends reported by other researchers, while ensuring the least amount of time possible. The ability to load brain slices with Fura-2 dye is an important goal, one that has inspired several studies (Peterlin et al. 2000b, Stosiek et al. 2003, Lin et al. 2003, Kirischuk, Verkhratsky 1996). This device has demonstrated to be superior compared to other protocols, it integrates the advantages from other protocols (increased loading times, constant oxygenation, simplicity), while avoiding the flaws (bubble stress, complexity, age limit) to achieve an optimized dye loading.

It is important to emphasize that the shortest incubation period possible was utilized while still obtaining optimal dye loading. One major concern facing the increase in loading time is the concomitant increase in background fluorescence (Kirischuk, Verkhratsky 1996), especially if the dye remains intercellular instead of inside viable cells. However, loading and viability were improved for all time durations tested, minimizing unusable background signals (figure 7B). Moreover, increases in intracellular calcium during hypoxic insults in 1 year old tissue demonstrates the microfluidic diffusion device dye loading method is still able to generate useable data. These calcium intensities are spatially correlated to labeled nuclei, demonstrating the expected

hypoxia response of functional neuronal cells, as shown in figure 7B and 7C. It is important to note that this technique could be generalized for loading dye into other tissue preparations.

## 1.5. Conclusion

This novel device design has many possible applications as a physiological tool for brain slice preparation in neuroscience and also any tissue requiring incubation preparations. While this study utilized only Fura-2/AM, it is possible to use this oxygenator for others dyes that take advantage of the membrane permeable esters for loading. Similarly, since the oxygen diffuses throughout the PDMS membrane, the gases do not disturb the slice mechanically, allowing sensitive tissues to be incubated for long periods of time. Applied technology has been examined to study neuronal tissues from species as different as naked mole rats and mice (Peterson et al. 2012). The ability to investigate tissue from older animals even up to 1 year of age may enable numerous studies in aging and long-term stress related diseases. Other tissues employing sensitive calcium imaging, such as pancreatic islets, heart tissue, liver sinusoids, and retina tissues can benefit from microfluidic oxygenator enhanced dye loading. In the wide spread application of calcium imaging for investigation of live tissues, the microfluidic oxygenator has the potential to be an important and indispensable scientific tool, that has the ability to change the future of cell studies.

## CITED LITERATURE


Anderson, J.R., Chiu, D.T., Jackman, R.J., Cherniavskaya, O., McDonald, J.C., Wu, H., Whitesides, S.H. & Whitesides, G.M. 2000, "Fabrication of topologically complex three-dimensional microfluidic systems in PDMS by rapid prototyping", *Analytical Chemistry,* vol. 72, no. 14, pp. 3158-3164.

Barreto-Chang, O.L. & Dolmetsch, R.E. 2009, "Calcium imaging of cortical neurons using Fura-2 AM", *Journal of visualized experiments : JoVE,* vol. (23). pii: 1067. doi, no. 23, pp. 10.3791/1067.

Beierlein, M., Fall, C.P., Rinzel, J. & Yuste, R. 2002, "Thalamocortical bursts trigger recurrent activity in neocortical networks: layer 4 as a frequency-dependent gate", *The Journal of neuroscience : the official journal of the Society for Neuroscience,* vol. 22, no. 22, pp. 9885-9894.

Berdichevsky, Y., Sabolek, H., Levine, J.B., Staley, K.J. & Yarmush, M.L. 2009, "Microfluidics and multielectrode array-compatible organotypic slice culture method", *Journal of neuroscience methods,* vol. 178, no. 1, pp. 59-64.

Bickler, P.E. & Hansen, B.M. 1994, "Causes of calcium accumulation in rat cortical brain slices during hypoxia and ischemia: role of ion channels and membrane damage", *Brain research,* vol. 665, no. 2, pp. 269-276.

Bickler, P.E. & Kelleher, J.A. 1992, "Fructose-1,6-bisphosphate stabilizes brain intracellular calcium during hypoxia in rats", *Stroke; a journal of cerebral circulation,* vol. 23, no. 11, pp. 1617-1622.

Blake, A.J., Pearce, T.M., Rao, N.S., Johnson, S.M. & Williams, J.C. 2007, "Multilayer PDMS microfluidic chamber for controlling brain slice microenvironment", *Lab on a chip,* vol. 7, no. 7, pp. 842-849.

Chen, T.W., Lin, B.J., Brunner, E. & Schild, D. 2006, "In situ background estimation in quantitative fluorescence imaging", *Biophysical journal,* vol. 90, no. 7, pp. 2534-2547.

Cho, S., Wood, A. & Bowlby, M.R. 2007, "Brain slices as models for neurodegenerative disease and screening platforms to identify novel therapeutics", *Current neuropharmacology,* vol. 5, no. 1, pp. 19-33.

Gahwiler, B.H., Capogna, M., Debanne, D., McKinney, R.A. & Thompson, S.M. 1997, "Organotypic slice cultures: a technique has come of age", *Trends in neurosciences,* vol. 20, no. 10, pp. 471-477.

Kirischuk, S. & Verkhratsky, A. 1996, "Ca2+]i recordings from neural cells in acutely isolated cerebellar slices employing differential loading of the membrane-permeant

form of the calcium indicator fura-2", *Pflugers Archiv : European journal of physiology,* vol. 431, no. 6, pp. 977-983.

Lam, R.H., Kim, M.C. & Thorsen, T. 2009, "Culturing aerobic and anaerobic bacteria and mammalian cells with a microfluidic differential oxygenator", *Analytical Chemistry,* vol. 81, no. 14, pp. 5918-5924.

Lin, X., Webster, P., Li, Q., Chen, S. & Ouyang, Y. 2003, "Optical recordings of Ca2+ signaling activities from identified inner ear cells in cochlear slices and hemicochleae", *Brain research.Brain research protocols,* vol. 11, no. 2, pp. 92-100.

Lo, J.F., Sinkala, E. & Eddington, D.T. 2010, "Oxygen gradients for open well cellular cultures via microfluidic substrates", *Lab on a chip,* vol. 10, no. 18, pp. 2394-2401.

Mauleon, G. 2011, *Stroke on a Chip: Spatial and Temporal Control of Oxygen for in vitro Brain Slices*.

Mauleon, G., Fall, C.P. & Eddington, D.T. 2012a, "Precise spatial and temporal control of oxygen within *in vitro* brain slices via microfluidic gas channels", *PloS one,* vol. 7, no. 8, pp. e43309.

Mauleon, G., Lo, J.F., Peterson, B.L., Fall, C.P. & Eddington, D.T. 2013, "Enhanced loading of Fura-2/AM calcium indicator dye in adult rodent brain slices via a microfluidic oxygenator", *Journal of neuroscience methods,* vol. 216, no. 2, pp. 110-117.

Mauleon, G., Fall, C.P. & Eddington, D.T. 2012b, "Precise Spatial and Temporal Control of Oxygen within *In Vitro* Brain Slices via Microfluidic Gas Channels", *PLoS ONE,* vol. 7, no. 8, pp. e43309.

Mehta, G., Mehta, K., Sud, D., Song, J.W., Bersano-Begey, T., Futai, N., Heo, Y.S., Mycek, M.A., Linderman, J.J. & Takayama, S. 2007, "Quantitative measurement and control of oxygen levels in microfluidic poly(dimethylsiloxane) bioreactors during cell culture", *Biomedical Microdevices,* vol. 9, no. 2, pp. 123-134.

Mulkey, D.K., Henderson, R.A.,3rd, Olson, J.E., Putnam, R.W. & Dean, J.B. 2001, "Oxygen measurements in brain stem slices exposed to normobaric hyperoxia and hyperbaric oxygen", *Journal of applied physiology (Bethesda, Md.: 1985),* vol. 90, no. 5, pp. 1887-1899.

Nakamura, I., Nakai, Y. & Izumi, H. 1996, "Use of fura-2/AM to measure intracellular free calcium in Selenomonas ruminantium", *The Tohoku journal of experimental medicine,* vol. 179, no. 4, pp. 291-294.

Ng, J.M., Gitlin, I., Stroock, A.D. & Whitesides, G.M. 2002, "Components for integrated poly(dimethylsiloxane) microfluidic systems", *Electrophoresis,* vol. 23, no. 20, pp. 3461-3473.

Nitatori, T., Sato, N., Waguri, S., Karasawa, Y., Araki, H., Shibanai, K., Kominami, E. & Uchiyama, Y. 1995, "Delayed neuronal death in the CA1 pyramidal cell layer of the gerbil hippocampus following transient ischemia is apoptosis", *The Journal of neuroscience : the official journal of the Society for Neuroscience,* vol. 15, no. 2, pp. 1001-1011.

Oppegard, S.C., Nam, K.H., Carr, J.R., Skaalure, S.C. & Eddington, D.T. 2009, "Modulating temporal and spatial oxygenation over adherent cellular cultures", *PloS one,* vol. 4, no. 9, pp. e6891.

Papazisis, G., Pourzitaki, C., Sardeli, C., Lallas, A., Amaniti, E. & Kouvelas, D. 2008, "Deferoxamine decreases the excitatory amino acid levels and improves the histological outcome in the hippocampus of neonatal rats after hypoxia-ischemia", *Pharmacological research,* vol. 57, no. 1, pp. 73-78.

Peterlin, Z.A., Kozloski, J., Mao, B.Q., Tsiola, A. & Yuste, R. 2000a, "Optical probing of neuronal circuits with calcium indicators", *Proceedings of the National Academy of Sciences of the United States of America,* vol. 97, no. 7, pp. 3619-3624.

Peterlin, Z.A., Kozloski, J., Mao, B.Q., Tsiola, A. & Yuste, R. 2000b, "Optical probing of neuronal circuits with calcium indicators", *Proceedings of the National Academy of Sciences of the United States of America,* vol. 97, no. 7, pp. 3619-3624.

Peterson, B.L., Larson, J., Buffenstein, R., Park, T.J. & Fall, C.P. 2012, "Blunted neuronal calcium response to hypoxia in naked mole-rat hippocampus", *PloS one,* vol. 7, no. 2, pp. e31568.

Qin, D., Xia, Y. & Whitesides, G.M. 2010, "Soft lithography for micro- and nanoscale patterning", *Nature protocols,* vol. 5, no. 3, pp. 491-502.

Queval, A., Ghattamaneni, N.R., Perrault, C.M., Gill, R., Mirzaei, M., McKinney, R.A. & Juncker, D. 2010, "Chamber and microfluidic probe for microperfusion of organotypic brain slices", *Lab on a chip,* vol. 10, no. 3, pp. 326-334.

Rambani, K., Vukasinovic, J., Glezer, A. & Potter, S.M. 2009, "Culturing thick brain slices: an interstitial 3D microperfusion system for enhanced viability", *Journal of neuroscience methods,* vol. 180, no. 2, pp. 243-254.

Regehr, W.G. & Tank, D.W. 1991, "Selective fura-2 loading of presynaptic terminals and nerve cell processes by local perfusion in mammalian brain slice", *Journal of neuroscience methods,* vol. 37, no. 2, pp. 111-119.

Reid, K.H., Edmonds, H.L.,Jr, Schurr, A., Tseng, M.T. & West, C.A. 1988, "Pitfalls in the use of brain slices", *Progress in neurobiology,* vol. 31, no. 1, pp. 1-18.

Rochefort, N.L., Jia, H. & Konnerth, A. 2008, "Calcium imaging in the living brain: prospects for molecular medicine", *Trends in molecular medicine,* vol. 14, no. 9, pp. 389-399.

Roe, M.W., Lemasters, J.J. & Herman, B. 1990, "Assessment of Fura-2 for measurements of cytosolic free calcium", *Cell calcium,* vol. 11, no. 2-3, pp. 63-73.

Small, D.L., Monette, R., Buchan, A.M. & Morley, P. 1997, "Identification of calcium channels involved in neuronal injury in rat hippocampal slices subjected to oxygen and glucose deprivation", *Brain research,* vol. 753, no. 2, pp. 209-218.

Smetters, D., Majewska, A. & Yuste, R. 1999, "Detecting action potentials in neuronal populations with calcium imaging", *Methods (San Diego, Calif.),* vol. 18, no. 2, pp. 215-221.

Stork, C.J. & Li, Y.V. 2009, "Rising zinc: a significant cause of ischemic neuronal death in the CA1 region of rat hippocampus", *Journal of cerebral blood flow and metabolism : official journal of the International Society of Cerebral Blood Flow and Metabolism,* vol. 29, no. 8, pp. 1399-1408.

Stosiek, C., Garaschuk, O., Holthoff, K. & Konnerth, A. 2003, "*In vivo* two-photon calcium imaging of neuronal networks", *Proceedings of the National Academy of Sciences of the United States of America,* vol. 100, no. 12, pp. 7319-7324.

Tang, Y.T., Kim, J., Lopez-Valdes, H.E., Brennan, K.C. & Ju, Y.S. 2011, "Development and characterization of a microfluidic chamber incorporating fluid ports with active suction for localized chemical stimulation of brain slices", *Lab on a chip,* vol. 11, no. 13, pp. 2247-2254.

Tian, L. & Looger, L.L. 2008, "Genetically encoded fluorescent sensors for studying healthy and diseased nervous systems", *Drug discovery today.Disease models,* vol. 5, no. 1, pp. 27-35.

Tonkikh, A.A. & Carlen, P.L. 2009, "Impaired presynaptic cytosolic and mitochondrial calcium dynamics in aged compared to young adult hippocampal CA1 synapses ameliorated by calcium chelation", *Neuroscience,* vol. 159, no. 4, pp. 1300-1308.

Wu, J.B., Song, N.N., Wei, X.B., Guan, H.S. & Zhang, X.M. 2008, "Protective effects of paeonol on cultured rat hippocampal neurons against oxygen-glucose deprivation-induced injury", *Journal of the neurological sciences,* vol. 264, no. 1-2, pp. 50-55.

Xue, J., Zhou, D., Yao, H. & Haddad, G.G. 2008, "Role of transporters and ion channels in neuronal injury under hypoxia", *American journal of physiology.Regulatory, integrative and comparative physiology,* vol. 294, no. 2, pp. R451-7.

Yuste, R., MacLean, J., Vogelstein, J. & Paninski, L. 2011, "Imaging action potentials with calcium indicators", *Cold Spring Harbor protocols,* vol. 2011, no. 8, pp. 985-989.

# 2. CHAPTER 2: 3D PRINTED MICROFLUIDIC OXYGEN MIXER

## [LARGE-SCALE OXYGEN GRADIENT GENERATION IN MICROFLUIDICS]

**Sections of this chapter have been previously published in:**

Khadka, S., Mauleon, G. & Eddington, D.T. 2014, "Fabrication of Oxygenation Microfluidic Devices for Cell Cultures", *Journal of Undergraduate Research,* vol. 7, no. 1, pp. 5-9.

Rexius-Hall, M.L., Mauleon, G., Malik, A.B., Rehman, J. & Eddington, D.T. 2014, "Microfluidic platform generates oxygen landscapes for localized hypoxic activation", *Lab on a chip,* vol. 14, no. 24, pp. 4688-4695.

## 2.1. Introduction

### 2.1.1. Oxygen

A global theme that will be discussed in these studies is spatial and temporal control of oxygen, specifically in cell microenvironment and its importance to the advancement of the scientific field. Oxygen is a critical modulator of cell physiological function; changes in the oxygen environment can lead to different biological responses. It is known that a change in the oxygen microenvironment plays a role in cell development, angiogenesis, cell migration, metabolism, apoptosis, and tumorigenesis (Cairns, Kalliomaki & Hill 2001, Dunwoodie 2009, Mohyeldin, Garzon-Muvdi & Quinones-Hinojosa 2010, Xiao et al. 2014b, Allen, Bhatia 2003, Allen et al. 2006). Due to the importance of oxygen in the cell's viability and behavior, cell oxygen environment should be a critical factor in the experimental setting. Ironically, it is one of the most often overlooked components of cell culture experiments (Sinkala, Eddington 2010).

Experiments presented thus far include 3 different oxygen regimens cells often experience. Hyperoxia refers to an environment where the oxygen concentration exceeds physiological levels. Normoxia is found when the oxygen concentration levels are in the same range as those observed in healthy cells; most of the normal metabolic pathways occur in this zone. Hypoxia is a condition in which the oxygen concentration is below physiological levels. Of the 3 oxygen regimens described, hypoxia is one of the most often studied. Several pathological events occur within the cell, under hypoxic condition, leading to anaerobic metabolism. If hypoxia is not resolved, it can potentially lead to apoptosis (Carmeliet et al. 1998, Cheran, Benvenuto & Thompson 2008, Paula-Lima et al. 2005). As previously stated in chapter 1, experiments utilized oxygen gas concentrations of 0%, 21%, and 95% $O_2$. While these experimental concentrations were used, they are not necessarily physiologically relevant.

Ambient air contains 21% $O_2$, however, the oxygen concentration experienced by the cells *in vivo* is much lower than this value and it varies across the body with values ranging from 1- 11% $O_2$. For example, the oxygen concentration around the bone marrow is somewhere between 4-7% $O_2$ (Kofoed et al. 1985), venous blood carries 4-6% $O_2$, while arterial blood carries 9-13% $O_2$ (Xiao et al. 2014a). The oxygen environment experienced by cells during *in vitro* experiments should be cell specific, but historically, the majority of cell culture work has been done under atmospheric oxygen concentrations (21% $O_2$) (Park et al. 2006). Not only is most cell culture work done at a physiologically irrelevant oxygen concentration, but it is also done under static conditions, that is, with cells experiencing only one oxygen concentration, when in reality the cells are exposed to a dynamic oxygen environment.

### 2.1.2. Oxygen Gradients

Overall, the body's oxygen concentration is in a constant state of flux that generates dynamic oxygen gradients. Oxygen gradient levels on a specific tissue are caused by oxygen delivery, oxygen consumption by neighboring cells, as well as diffusion limitations within the tissue (Park et al. 2006, Tsai et al. 1998). Within these gradients, the cells are exposed to different microenvironments, which can lead to different cellular responses. For example, cells that have proper oxygen supply are more sensitive to several drugs when compared to hypoxic cells, it has been noted that this can influence the effect of anticancer medication during clinical trials (Wang et al. 2015). Dynamic oxygen gradients are also known to have a direct influence on tumor growth, stem cell migration, stem cell angiogenesis and vascular remodeling (Park et al. 2006, Allen, Bhatia 2003). Natural oxygen microgradients can be formed within individual tissue. For example, there is an oxygen gradient formed naturally in the animal intestine; this gradient allows anaerobic microbes to inhabit certain areas of the gut and aid in digestion (Espey 2013). Oxygen gradients are formed in the liver where synthesis, metabolism, biotransformation are regulated by the dynamic gradient formed by the liver sinusoids (Allen et al. 2006).

All of these naturally occurring oxygen gradients should be studied in further depth (Allen, Bhatia 2003). Yet, the microenvironment spatially and temporally controls physiologically relevant oxygen gradients, making it difficult to replicate in an experimental setting with currently available techniques.

### 2.1.3. Current Oxygen Control Methods

The gold standard for *in vitro* hypoxic studies is the hypoxic chamber, which allows researchers to introduce a low oxygen mixture (usually 0% $O_2$) into the cellular environment and study the cellular response (Oppegard et al. 2009). However, this chamber only allows one oxygen environment at a time, giving no spatial control. The chamber also has no temporal control as it takes a long time, 30 minutes to 1 hour depending on the desired concentration, to equilibrate (Oppegard et al. 2009).

Hypoxic workstations offer another possibility for low oxygen experiments. As the name implies, the hypoxic workstation is completely designed to facilitate hypoxic studies. The workstation incorporates a sealed safety hood with an incubator, microscopes, and necessary equipment for the experiments. The required gas floods the hood and creates a controlled hypoxic environment. While this station provides a better alternative compared to the hypoxic chamber, due to its size, expense increases significantly. Similar to the hypoxic chamber, one oxygen condition can be studied at a time; this prevents a physiologically relevant environment to be simulated (Byrne et al. 2014).

Another option for hypoxic studies is the use of perfusion chambers. Perfusion chambers use oxygenated or deoxygenated liquids to control the oxygen environment. Several types of chambers have been designed over the years, however, most of them can be classified into two groups: interface- and submerged-type chambers. In interface-type chambers, a nylon mesh is placed in the chamber in such a way that the tissue is slightly elevated from the bottom of the chamber. This allows the perfusate to deliver nutrients and oxygen to the bottom of the tissue while the top face is exposed to a humidified gas (Hajos, Mody 2009). This type of chamber has proven highly reliable

and is a staple of numerous neurophysiology studies (Hajos et al. 2009). In submerged-type chambers, the tissue is completely covered by the perfusate, which creates several advantages. These chambers offer the capacity of improved imaging techniques and allow drugs dissolved in the liquid to take effect faster than in other types of perfusion chambers (Hajos et al. 2009). However, like previously described, only one oxygen environment can be studied with these methods, causing temporal control of the hypoxic condition to be potentially delayed.

Mentioned techniques rely on the use of bulky gas canisters to provide the oxygen concentration of interest for the specific experiment. However, physiological oxygen concentrations vary among different tissues. Using a single gas canister for necessary oxygen concentrations can quickly become tedious and cumbersome. Additionally, commercially available gas mixers can become prohibitively expensive for the lab setting. Other studies have attempted to create digitally controlled gas mixers (Lo et al. 2013), while these mixers provide efficient oxygen control, computer requirements to run mixing software creates a hindrance that is not easy to overcome.

There is a pressing need to create an *in vitro* platform that can intimately recapitulate the oxygen gradients experienced by cells *in vivo*. Physiologically relevant oxygen gradients are dynamic; a proper technique should provide temporal and spatial control over the oxygen environment. It should also provide a simple way to assess cell response to the hypoxic environment.

### 2.1.4. Previous Microfluidic Methods

As was the case in the previous chapter, microfluidic technology can provide an elegant way to create a hypoxic gradient with a controlled spatial and temporal control.

One of the easiest ways to provide dynamic control over the oxygen environment experienced by the cells is to seed cells into PDMS membranes with oxygen channels running under the membrane. The PDMS membrane device model, with its high transparency, nontoxic properties, low price, and high oxygen permeability, provides a great model for oxygen control studies (Mauleon, Fall & Eddington 2012).

Some of the first published papers using microfluidic devices to create different oxygen environments used on-chip gas mixers to grow cells and bacteria on separate chambers; each chamber had different constant oxygen environments (Lam, Kim & Thorsen 2009, Polinkovsky et al. 2009). In a similar manner, spatial control can be achieved using gas channels flanking the main culture chamber and allowing diffusion to equilibrate the gradient (Funamoto et al. 2012, Grist et al. 2015, Acosta et al. 2014). Increasingly complicated devices can be utilized in a setting where computer controlled mixers are able to provide the appropriate gas concentration (Adler et al. 2012). At times, simple design geometry can provide the oxygen concentration desired (Lo, Sinkala & Eddington 2010). Similarly, spatial gradients can be achieved with chemical control (Skolimowski et al. 2010, Chen et al. 2011, Wang et al. 2013, Thomas, Raghavan & Forry 2011). Oxygen consumption can also create the oxygen gradient as shown in previous devices (Allen, Bhatia 2003, Mehta et al. 2007).

Most of these techniques employ active methods to create the gradient, however, some studies have attempted to use sink-source diffusive mixing methods to create passive oxygen gradients (Oppegard et al. 2009, Mauleon, Fall & Eddington 2012, Lo, Sinkala & Eddington 2010, Rexius-Hall et al. 2014). While all of these results provide results on

certain aspects of hypoxia none provide an oxygen gradient with the ability to provide physiological conditions in real time.

While microfluidic technology has relied on photolithography and soft lithography methods in its infancy, new techniques are slowly coming to the foreground that can provide microfluidics with the techniques necessary to take the next step in its evolution.

### 2.1.5. 3D Printing

While 3D printing technology has been used in industrial settings for several years now, it is not until recently that it found its way into the microfluidic field. Several different techniques can be used to create microfluidic channels such as selective laser sintering, inkjet printing, fused deposition modeling, laminated object manufacturing, and stereolithography (Gross et al. 2014, Au et al. 2016). However, for the purposes of this study, we will focus on stereolithography.

Stereolithography is one of many techniques that rely on additive manufacturing. In this technique, a computer generated 3D model is broken down into different layers and the coordinates are directed to a computer controlled UV laser. Using a movable bath containing a photocurable liquid resin, the laser cures the resin according to the 3D model design. The 3D model is produced layer by layer until design completion occurs. In order to create microfluidic channels, the walls defining the channels are cured completely and when the design is complete, uncured resin is drained from the device (Gross et al. 2014, Au et al. 2016).

Fabrication techniques such as soft-lithography and replica molding are a staple in microfluidic laboratories, yet they have several identified deficits. One of the main disadvantages is the difficulty of device replication, particularly in different laboratories.

Microfluidic fabrication techniques often contain: unstandardized methods, training requirement of specialized skill, and are labor intensive. 3D printing techniques, conversely, utilize a computer design model, which is typically sent to a third-party company for manufacturing. The 3D fabrication process is uncomplicated and often more economical. Due to the simple fabrication process, some features, which cannot be designed using soft-lithography, can be done with 3D printing, such as pipes-within pipes (Brennan, Rexius-Hall & Eddington 2015) luer fittings and hose barbs (Au et al. 2015).

By combining newer fabrication techniques such as 3D printing, with older techniques such as lithography and replica molding, we can create novel microfluidic devices that will give us superior microfluidic control.

### 2.1.6. Research Purpose

Several oxygen platforms have been created to determine the distinct effect that varying oxygen levels have on cells. However, these devices require several bulky gas canisters to provide the required oxygen mixture, which makes them impractical for research. A 3D microfluidic oxygen mixer was designed to output desired oxygen levels for ease of experiment use. The unit requires two inputs of gasses and will output twenty-two different gas concentrations.

The gas-mixing network in the device was designed specifically for two gas inlets to mix at predetermined locations along the device generating a linear series of oxygen concentrations. The oxygen mixer was designed in AutoCad and printed using Fineline Prototyping on a stereolithographic 3D printer. The mixer is made of a nonpermeable photopolymer that prevents diffusion from affecting the mixing of the gas flows. Inlets

and outlets were designed to allow easy connection to gas tanks and microfluidic devices. When compared to other existing techniques, our 3D oxygen mixer provides simplicity, accuracy, and low expense. The proposed model can be used in hypoxia research where the microenvironment must be greatly controlled due to the extreme sensitivity of cells to the oxygen levels.

## 2.2. Materials and Methods

### 2.2.1. Design and Fabrication of Gradient Device

5 microfluidic devices were designed to generate oxygen gradients across a large surface area using passive and active methods. As shown in figure 1, the microfluidic constructs are multilayered PDMS devices consisting of a glass slide at the bottom, a PDMS gas network, a PDMS membrane, and a PDMS chamber.

Standard microfabrication techniques, described in chapter 1, were utilized for the creation of the SU-8 master as well as the PDMS channel network making up the bottom layer.

The gas permeable membrane, similarly to the one described in chapter 1, was fabricated by spin coating PDMS on a 100mm diameter silicon wafer to obtain a constant 100μm thick membrane. However, an alternative design protocol was used for one of the experiments, where a membrane of varying thickness (inclined membrane) was fabricated. For this protocol, stacked adhesive tape was utilized to fabricate the inclined membrane. Four pairs of adhesive tape with varying thickness were distributed uniformly across a 100mm diameter silicon wafer; the thickness of the adhesive tapes was measured to be 100μm, 200μm, 300μm, and 400μm, respectively. PDMS was then poured onto the wafer and covered with a transparency film. A weight was placed on top to provide pressure and the wafer was baked at 65°C for 60 minutes. Independent of the method used, after curing, the PDMS membrane was irreversibly bonded to the channel network layer using oxygen plasma.

The media chamber was cut into a rectangular shape of PDMS to match the channel network. Within the PDMS block a second rectangular cut was made in the open chamber. The chamber was then bond on top of the PDMS membrane.

The final assembly was punched with inlet/outlet ports, and then bonded on a 75mm X 50mm glass slide.

a)

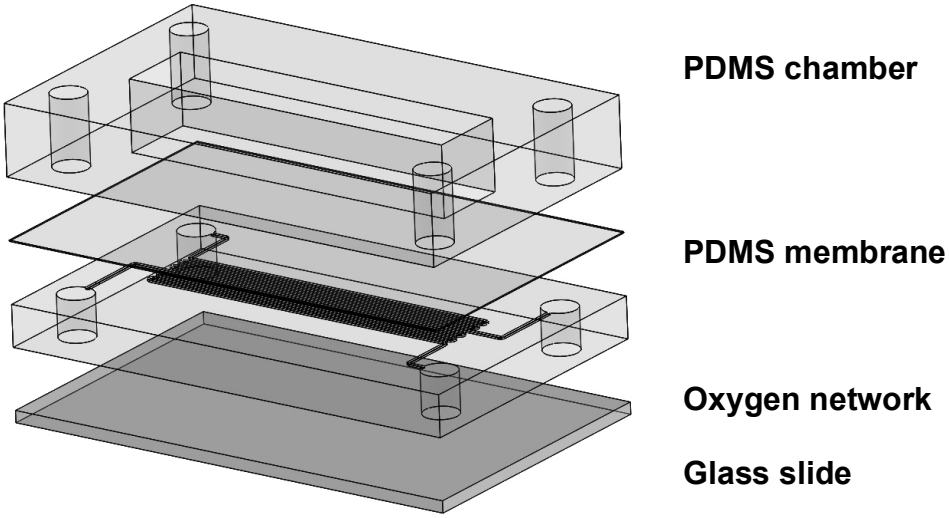


b)

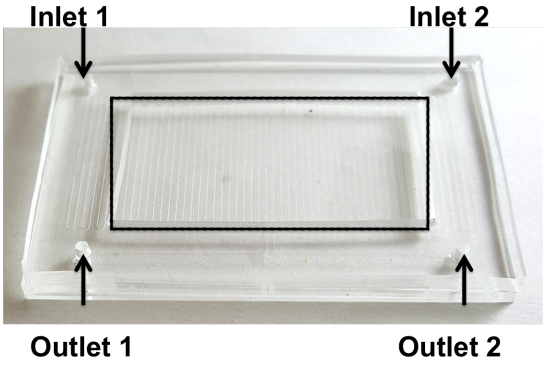


Figure 1. Schematic of the microfluidic devices. A) Exploded view of the microfluidic constructs, which consists of 4 independent parts: the PDMS chamber, the gas permeable PDMS membrane, the PDMS oxygen network, and a glass slide for support. B) Photograph showing a top view of the device. Depending on the device, the PDMS gas oxygen network will be different. In this case, 2 inlets and 2 outlets are shown.

### 2.2.2. Validation of Devices Using Fiber Optic Oxygen Sensor

Initial experimental microfluidic devices relied on the use of passive diffusive methods to generate oxygen gradients. Experiments were carried out using 95% $N_2$, 5% $CO_2$ as the first inut and 21% $O_2$, 5% $CO_2$ as the second input. A fiber optic oxygen sensor was utilized to measure the oxygen concentration gradient at predetermined locations across the entire chamber. The sensor was calibrated as previously discussed in chapter 1. In order to precisely measure the oxygen concentrations, the oxygen probe was attached to a piezoelectric micromanipulator that could maneuver the probe in the x, y, and z planes with a resolution of 0.1μm. For the purposes of this study, the oxygen concentration at a height (measured from the bottom of the chamber) of 0μm was recorded.

### 2.2.3. Design and Fabrication of 3D Printed Oxygen Mixer

3D models were designed in AutoCAD and Blender. They were printed via stereolithography in Watershed XC (Fineline Prototyping). Inlets and outlets were designed to allow easy connection to gas tanks and microfluidic devices. In both models, experiments were carried out using 95% $N_2$, 5% $CO_2$ and 21% $O_2$, 5% $CO_2$ mixtures, which resulted in 22 different concentrations.

Throughout the course of this project, 2 different designs were fabricated in order to find the best geometry that would result in a complete oxygen gradient.

The first 3D printed mixer contains a gas-mixing network designed specifically to mix 2 different gases at predetermined device locations, this generated a linear series of oxygen concentrations. With this design, 2 different inputs deliver 22 different gas concentrations. The mixing points of the device can be calculated based on the

following assumptions: 1) volumetric and mass flow rate are conserved 2) equal input flow rates are used 3) no gas mixing due to diffusion 4) equal channel dimensions. Under these assumptions, the channel lengths can be calculated as follows:

$$Eq.1 \qquad [X_{out}] = \left[{}^{n}/_{N}\right][X_1]$$

$$Eq.2 \qquad [L_1] = [k][U_2][N-n]$$

Where [X] is the mass concentration, n is the channel number, N is the total number of channels, L is the channel length, U is the viscosity, and k is an equivalency constant. Figure 2 shows the finalized mixing network with the 22 mixing locations.

The second iteration of 3D printed mixer relies on flow-based diffusive mixing along a dilution tree. As shown in figure 3, 2 different gases will mix along 22 steps until 22 different gas concentrations are achieved. The channels have a width of 500μm and a depth of 500μm.

a)

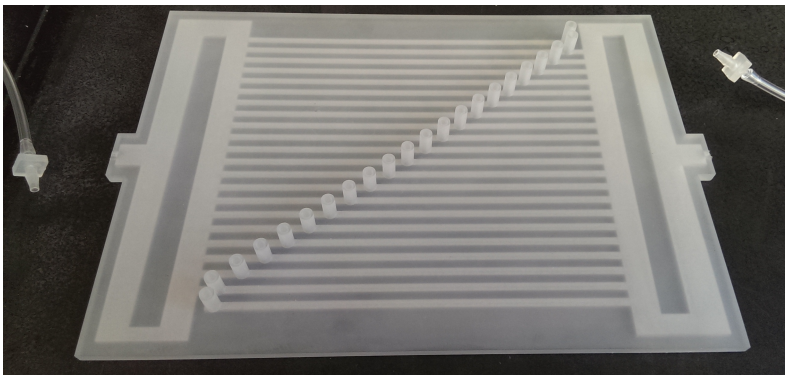

b)

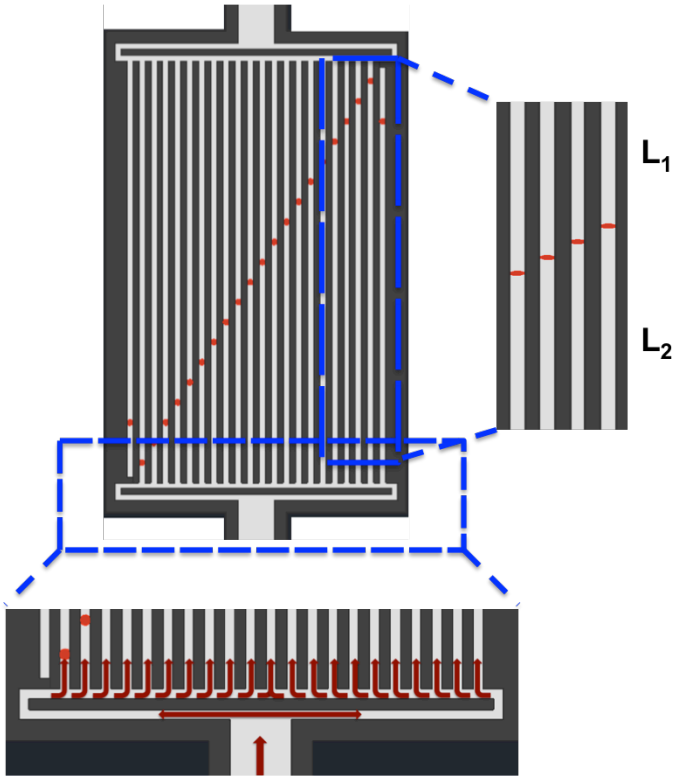


Figure 2. 3D Printed Oxygen Mixer Version 1. A) Photograph shows how the oxygen mixer can take two different oxygen concentrations as the inputs and deliver 22 different oxygen concentrations as the outputs. B) Diagram shows the location of the 22 different outlets; $L_1$ and $L_2$ can be used to locate the precise location where the 2 inputs will mix and provide the required oxygen concentration.

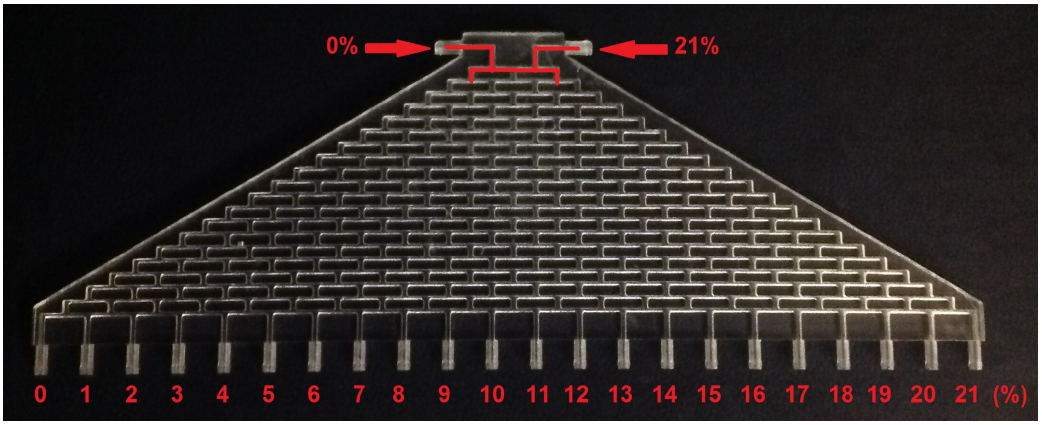


Figure 3. 3D Printed Oxygen Mixer Version 2. Photograph showing how the oxygen mixer can take two different oxygen concentrations as the inputs and deliver 22 different oxygen concentrations as the outputs. Image shows how for this design, the mixer works similar to a diffusion tree; each step diffuses the gas flowing through the channels until the end product consists of 22 gases ranging from 0% to 21% $O_2$.

### 2.2.4. Validation of 3D Printed Oxygen Mixer Using Fiber Optic Oxygen Sensor

3D printed oxygen mixer inlets were connected to a 95% $N_2$, 5% $CO_2$ and 21% $O_2$, 5% $CO_2$ gas tanks, flow rates were measured using a flow meter (FL-5311; Omega). A 5-minute equilibration period was completed before a fiber optic oxygen sensor measured the oxygen concentration at each of the 22 different outlets. The entire procedure was repeated three independent times on each of the 2 designs used.

Error graphs created after the measurements were taken, correlate the theoretical oxygen gas concentration to the experimental value obtained from the fiber optic measurements, this was evaluated at each gas channel.

### 2.2.5. Fabrication of PtOEPK

In order to measure the oxygen concentration gradient created by the 3D mixer in a microfluidic device, the fluorophore PtOEPK (platinum (II) octaethylporphine ketone) was employed. To fabricate the sensors, a mixture of 35% (w/w) polystyrene/toluene was made by mixing the two on a shaker for 24 hours. PtOEPK powder was then added to the mixture at a 1mg/ml concentration and mixed in the shaker for 24 hours. The PtOEPK mixture is then spin coated on top of a 100μm PDMS membrane, which can be utilized as a planar sensor on microfluidic devices. The fluorescence of PtOEPK is quenched in the presence of oxygen, as such, calibration of the sensor can be done using 5% $CO_2$, balanced nitrogen and 5% $CO_2$, balanced air prior to the experiment. Additional information about the PtOEPK oxygen sensor can be found in appendix 2.

### 2.2.6. Validation of 3D Printed Oxygen Mixer Using PtOEPK Sensor

In order to validate the oxygen gradient created by the 3D printed oxygen mixer, a microfluidic device containing 22 adjacent channels was fabricated. Once the device was finalized, a thin film of PDMS-containing PtOEPK sensor was placed in contact with the PDMS membrane of the device in such a way that it covered the entire length of the chamber. Outlet ports of the 3D printed oxygen mixer were then connected to the inlets of the microfluidic device. Using a fluorescent inverted microscope (Olympus IX71), computer-controlled fluorescent scanning images were taken across the entire PtOEPK sensor. By solving the Stern-Volmer equation, a relationship between PtOEPK intensity and oxygen concentration is identified.

### 2.2.7. 3D Printed Oxygen Switchboard

The 3D printed oxygen mixer can be utilized as a switchboard, where specific outlets can provide an oxygen mixture to a microfluidic device. In this study, several different landscapes were created using different PDMS oxygen microfluidic networks. The 3D printed oxygen mixer was utilized to create an oscillating and linear oxygen profile. These profiles can be utilized with a combination of only 2 gas tanks.

### 2.2.8. Statistical analysis

Experiments were performed a minimum of three independent times, and data was expressed as the average ± standard deviation. A matlab code was used to solve the Stern-Volmer equation. Graphs were created in Excel. Additional information about the code and the PtOEPK sensor can be found in appendix B.

## 2.3. Results

### 2.3.1. Source-Sink Design Oxygen Characterization

A source-sink configuration was used in 2 different designs to create a linear oxygen gradient. A hand-held oxygen sensor placed at the top of the PDMS membrane measured the oxygen gradient generated. Results were plotted as a function of the position in the x-direction. As shown in figure 4, both designs produced landscapes containing both a linear gradient and a plateau. However, neither design produced a stable linear gradient across the entire device.

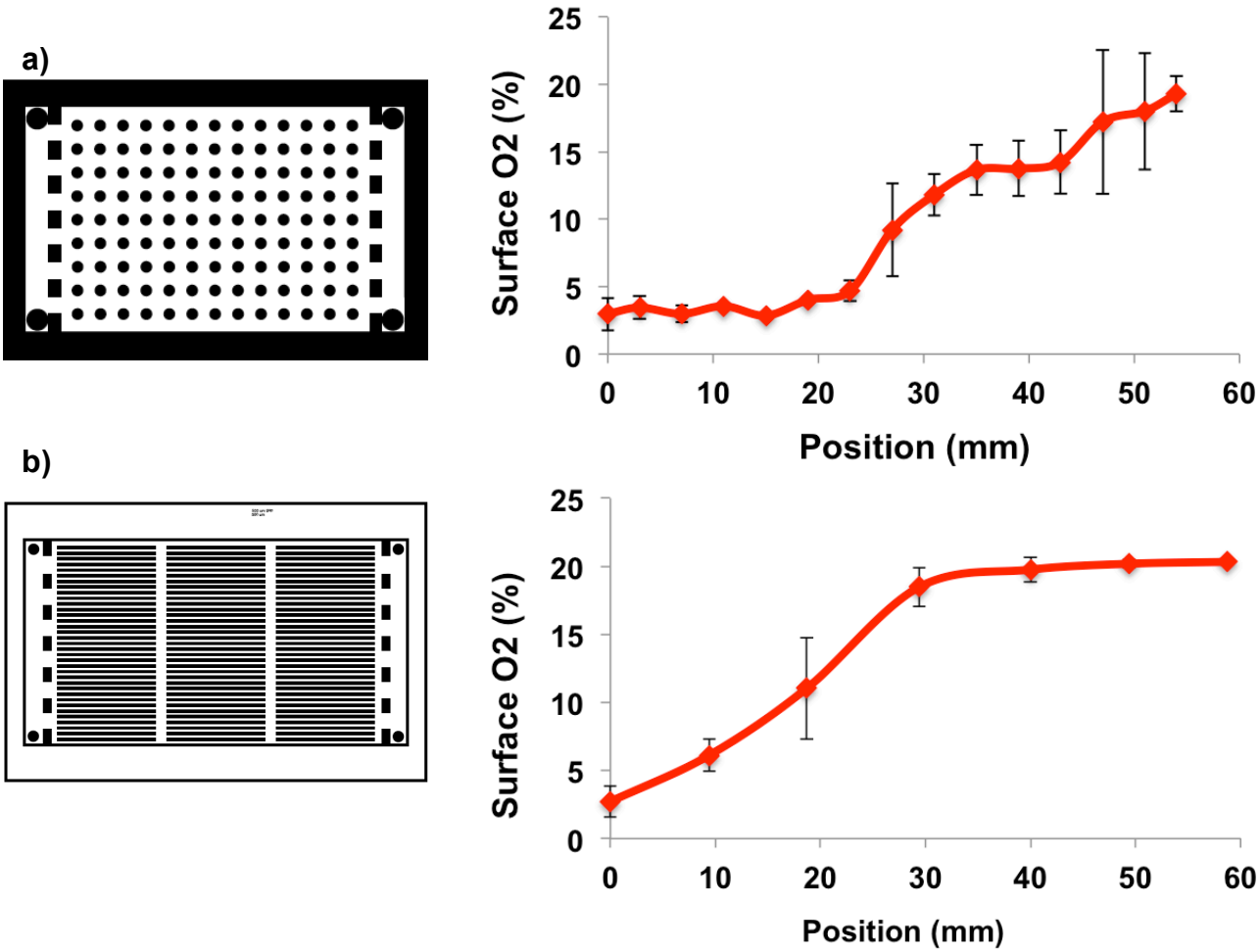


Figure 4. Passive oxygen gradients. The photomask design as well as the corresponding oxygen gradient generated by two different diffusion based PDMS devices are shown. Figures A and B show linear sections in conjunction to plateaus.

### 2.3.2. Inclined PDMS Membrane

An alternative design consisting of 1 oxygen network bonded to an inclined PDMS membrane was fabricated. Membrane thickness increased linearly from 100μm to 400μm as shown in figure 5B. A hand-held oxygen sensor placed at the top of the PDMS membrane measured the oxygen gradient generated while 95% $N_2$/5% $CO_2$ was injected into the device. As shown in figure 5C, the highest oxygen percentage measured was 4.5% $O_2$ while the lowest was 0.5% $O_2$.

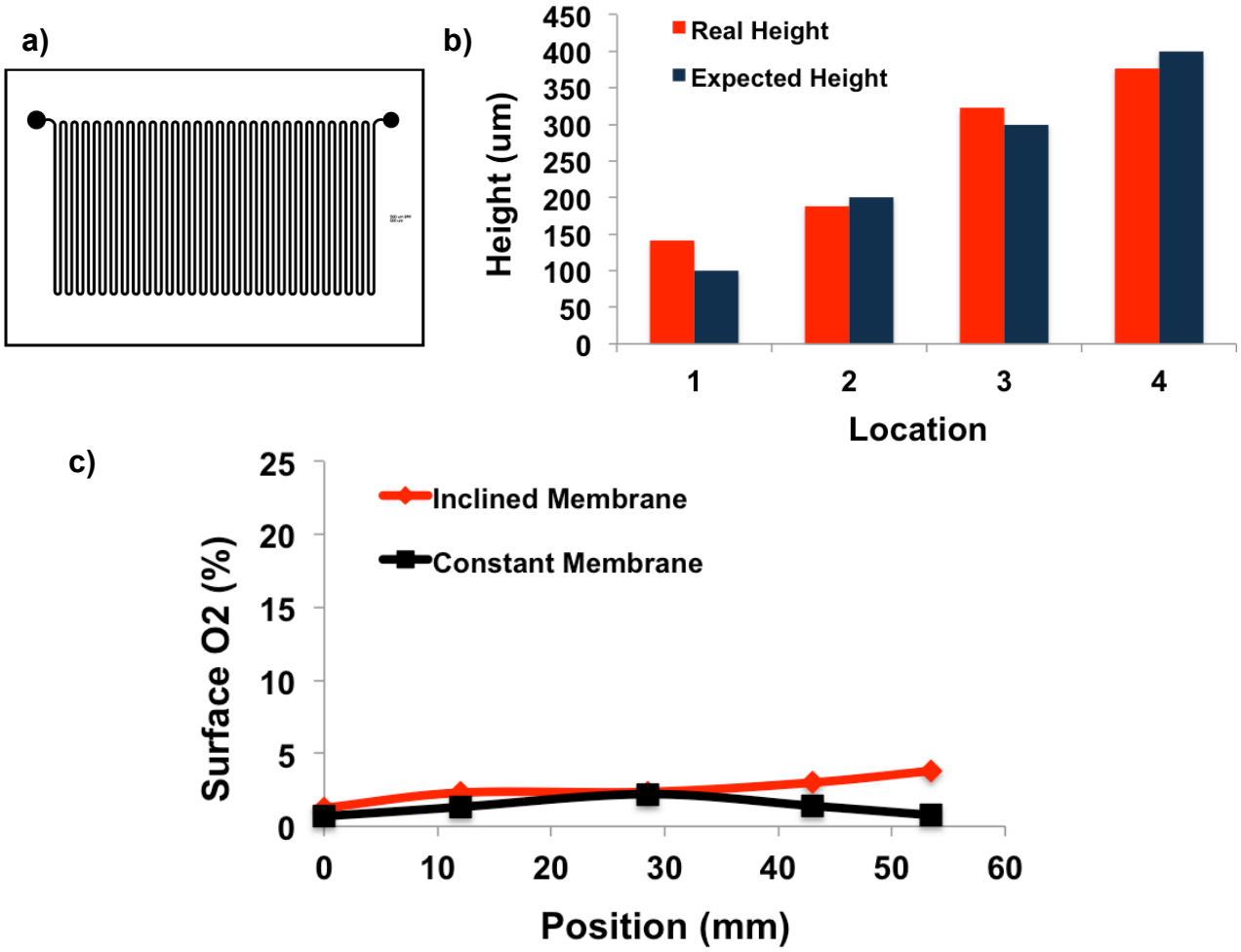


Figure 5. Inclined membrane oxygen validation. A) Photomask showing the design for a single input device where the oxygen gradient is created by the PDMS membrane thickness. B) Thickness measurements of the inclined membrane compared to the expected results. C) Oxygen profile as a function of position. As the thickness of the PDMS membrane increases, the oxygen diffusing across the membrane decreases.

### 2.3.3. Multiple Input Design Oxygen Characterization

Multiple oxygen compositions were injected into 2 design devices in an attempt to create a linear gradient. Figure 6A shows how oxygen mixtures of 0%, 5%, 10%, and 21% $O_2$ were used and measured by the hand-held oxygen sensor. Figure 6B shows the second design which used 0%, 5%, 10%, 15%, and 21% $O_2$ as the oxygen inputs. This was measured using the PtOEPK fluorescent sensor. In both cases, the different gas mixtures blend and perfuse the spaces separated by the PDMS walls to distribute a relatively linear gradient in the x-direction.

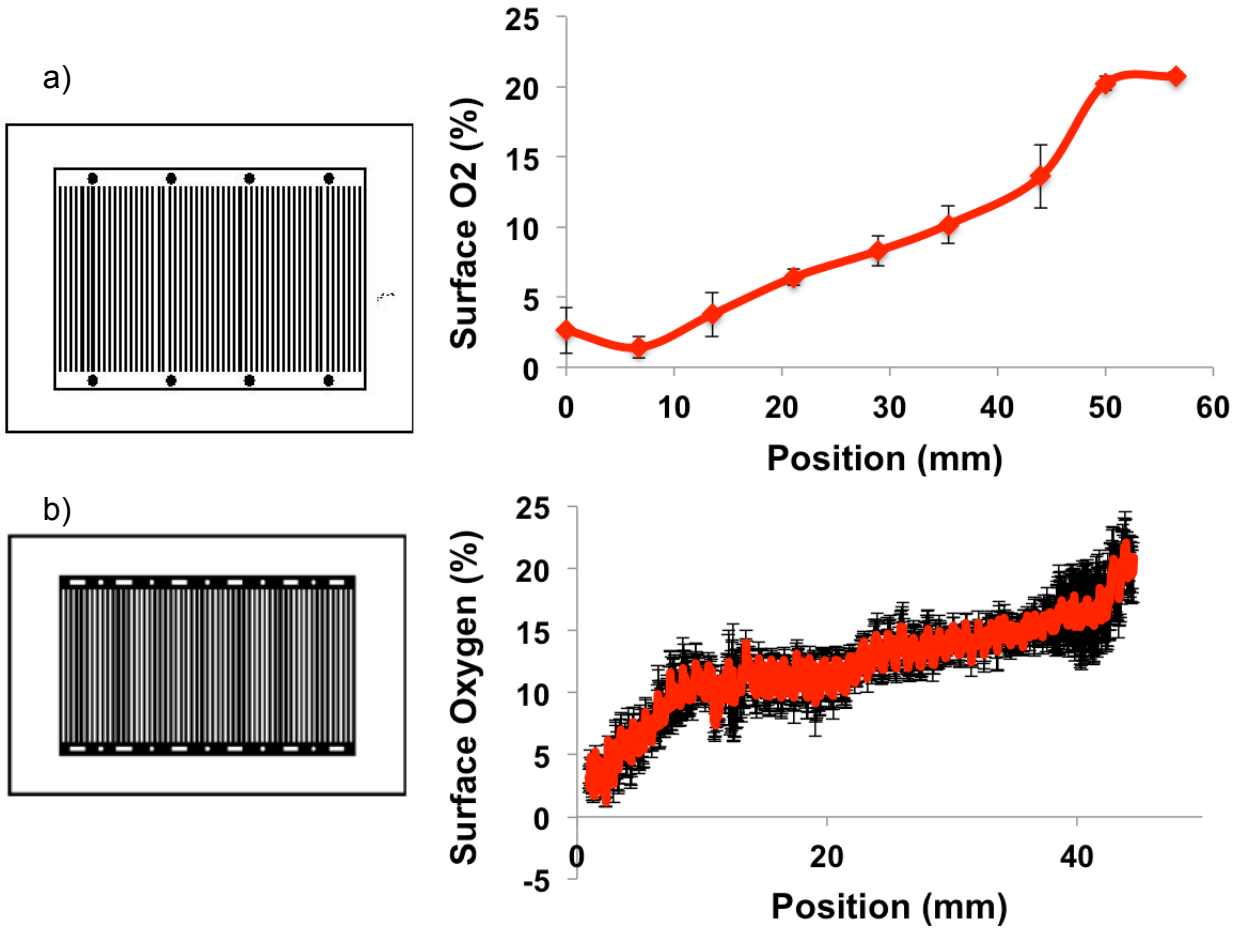


Figure 6. Active gradient devices. A) A four inlet device created in order to create a linear, stable oxygen gradient. B) A five inlet device that provides better mixing of the different oxygen gases. A PtOEPK sensor was used to measure the oxygen profile.

### 2.3.4. Characterization of 3D Printed Oxygen Mixer

2 distinct 3D printed oxygen mixers were designed and tested during this study. Using an oxygen sensitive probe, oxygen concentration was measured at the outlets of the first design. Figure 7 demonstrates the ability to create 22 different oxygen mixtures, ranging from 0-21% $O_2$. This technique can be replicated in individual devices, the error graph illustrates that the gradient skips several oxygen intervals and shows a jump from 15% to 21% $O_2$. In figure 8, the oxygen concentrations created by the second design are recorded and show 22 different oxygen mixtures, ranging from 0-21% $O_2$. When compared to existing techniques, this 3D oxygen mixer provides simplicity, accuracy within 1.5% $O_2$, and also allows the opportunity to create 22 distinct oxygen concentrations simultaneously with only two inputs.

### 2.3.5. Characterization of 3D Printed Oxygen Mixer as an oxygen supply

Using the PtOEPK oxygen sensor, the linear series created by the second version of the 3D printed oxygen mixer can be measured in a microfluidic device consisting of 22 parallel channels. Similarly to the case seen in figure 8, when the oxygen concentration was measured in the mixer, in figure 9 we see how a linear gradient ranging from 0-21% $O_2$ is created on the surface of the microfluidic device.

a)

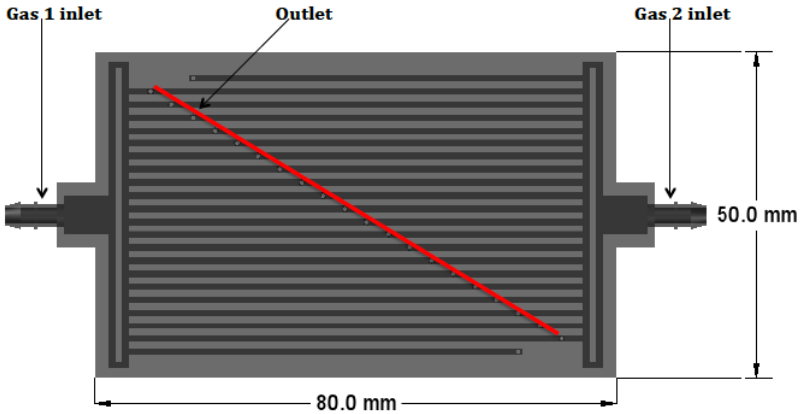


b)

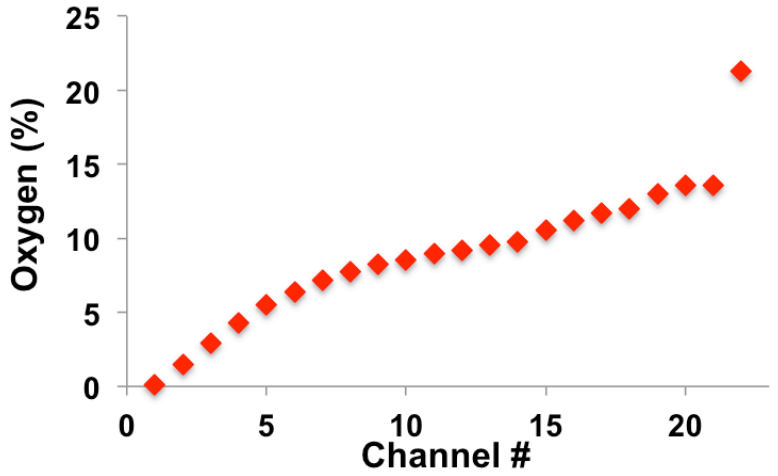


c)

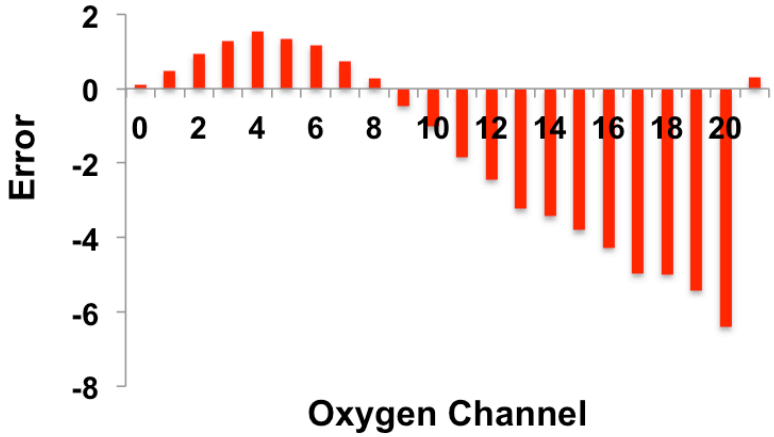


Figure 7. Oxygen mixer characterization version 1. A) 2 different input gases can mix to provide 22 different oxygen outputs. B) Using a hand-held oxygen sensor, the 22 outputs were measured and plotted as a function of the channel number. C) A gradient of oxygen concentrations was achieved, however, it did not provide the expected results, with several missing steps missing from the 0-21% expected gradient.

a)

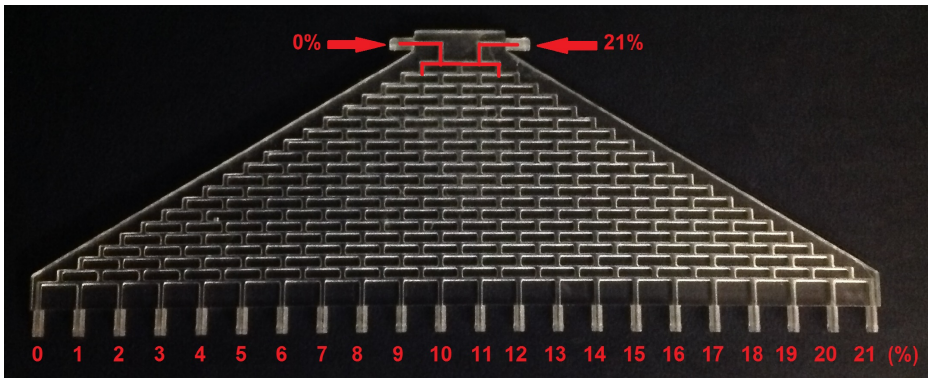


b)

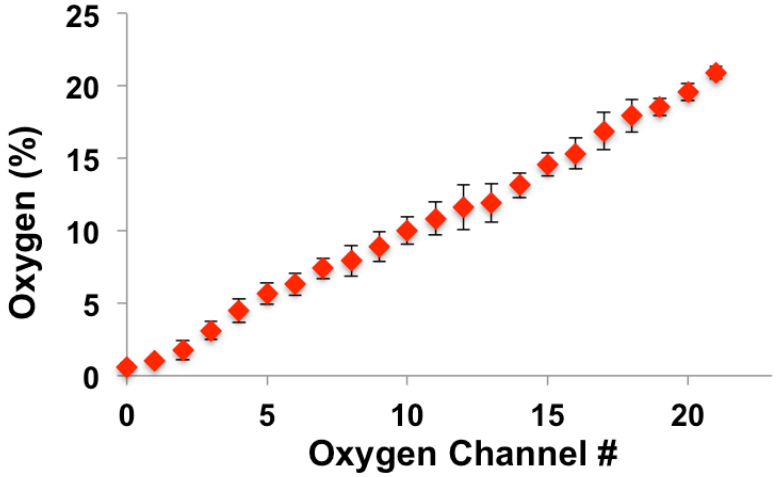


c)

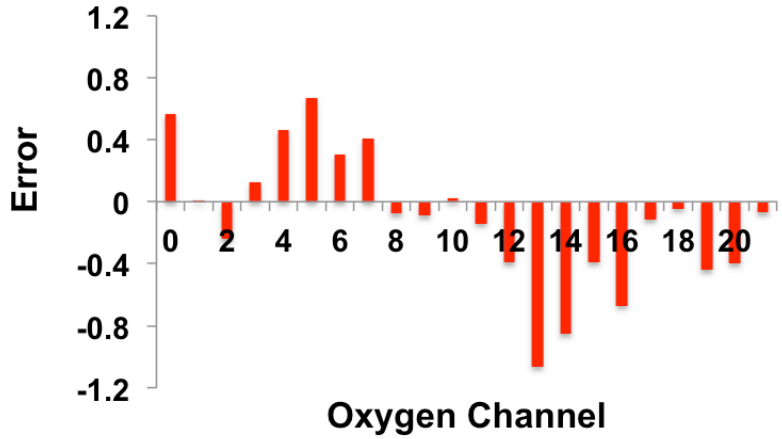


Figure 8. 3D Printed Oxygen Mixer Version 2. A) Photograph shows how the oxygen mixer can take two different oxygen concentrations as the inputs and deliver 22 different oxygen concentrations as the outputs. B) Using an hand-held oxygen sensor, the 22 outputs were measured and plotted as a function of the channel number. C) A gradient of oxygen concentrations was achieved as expected with all of the results within 1% $O_2$ from the expected gradient results.

a)

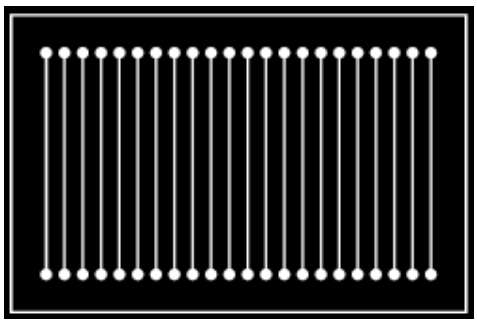

b)

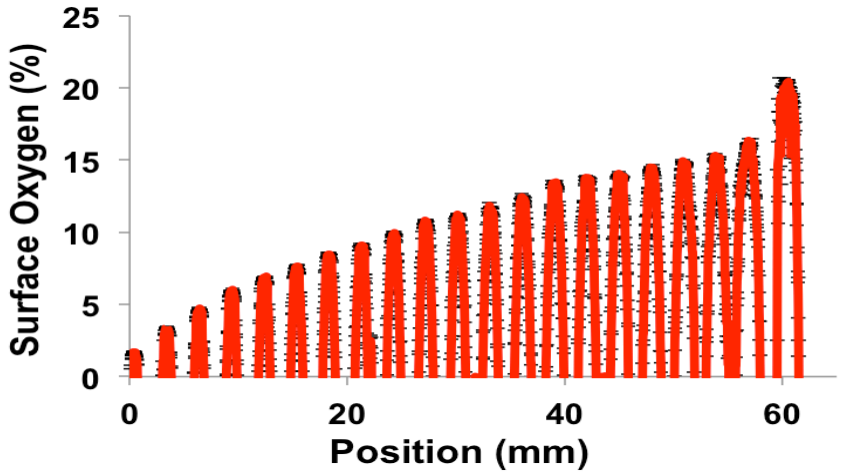


c)

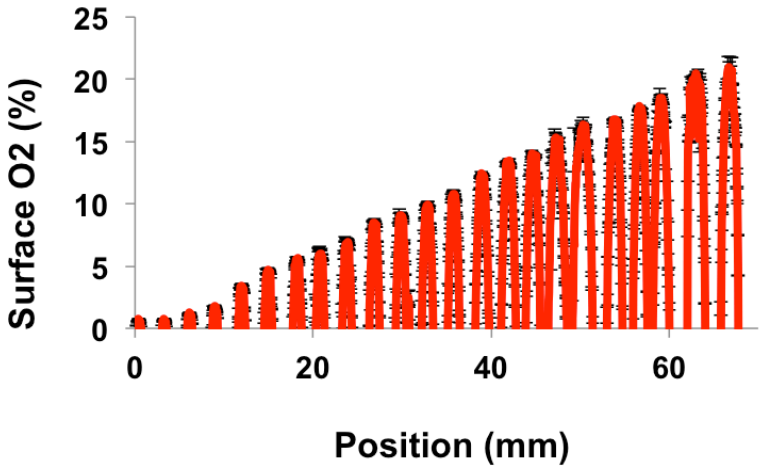


Figure 9. 3D Printed Oxygen Mixer for microfluidic devices. A) A 22 inlet microfluidic device was created to create a linear, stable oxygen gradient. B) Using the first version of the oxygen mixer as the oxygen supply, we measured a gradient of oxygen concentrations similar to the one measured in the mixer itself. C) The mixing tree design created a linear gradient in the microfluidic device ranging from 0-21% $O_2$.

### 2.3.6. 3D Printed Oxygen Switchboard

Figure 10 demonstrates that by utilizing the mixer as an oxygen switchboard, different oxygen concentrations can be quantified. During this experiments, the 3D printed oxygen mixer provided the gas input for the microfluidic devices. Figure 10A shows how individual gas outputs can be used to provide gas flow to the microfluidic device, in this case 0% and 7% oxygen are used in the microfluidic device. Figure 10B demonstrates how by changing the initial inputs (one input 95% $N_2$/5% $CO_2$, one input 10% $O_2$/5% $CO_2$), the 3D printed oxygen mixer can create an oxygen gradient much more focused to physiologically relevant oxygen conditions.

Additionally, figure 10C shows the photomask used to create a PDMS oxygen network which could create an oscillating stimulus device. Combining the microfluidic device with the oxygen mixer as an oxygen switchboard, numerous oxygen landscapes can be created by simply interchanging the oxygen concentrations as shown in figure 10D, where 0% oxygen and 6% oxygen create a hypoxic landscape. Figure 10E shows 0% oxygen and 16% oxygen can be used. Finally, 0% oxygen and 21% oxygen are used to create a hypoxic and normoxic environment (figure 10F).

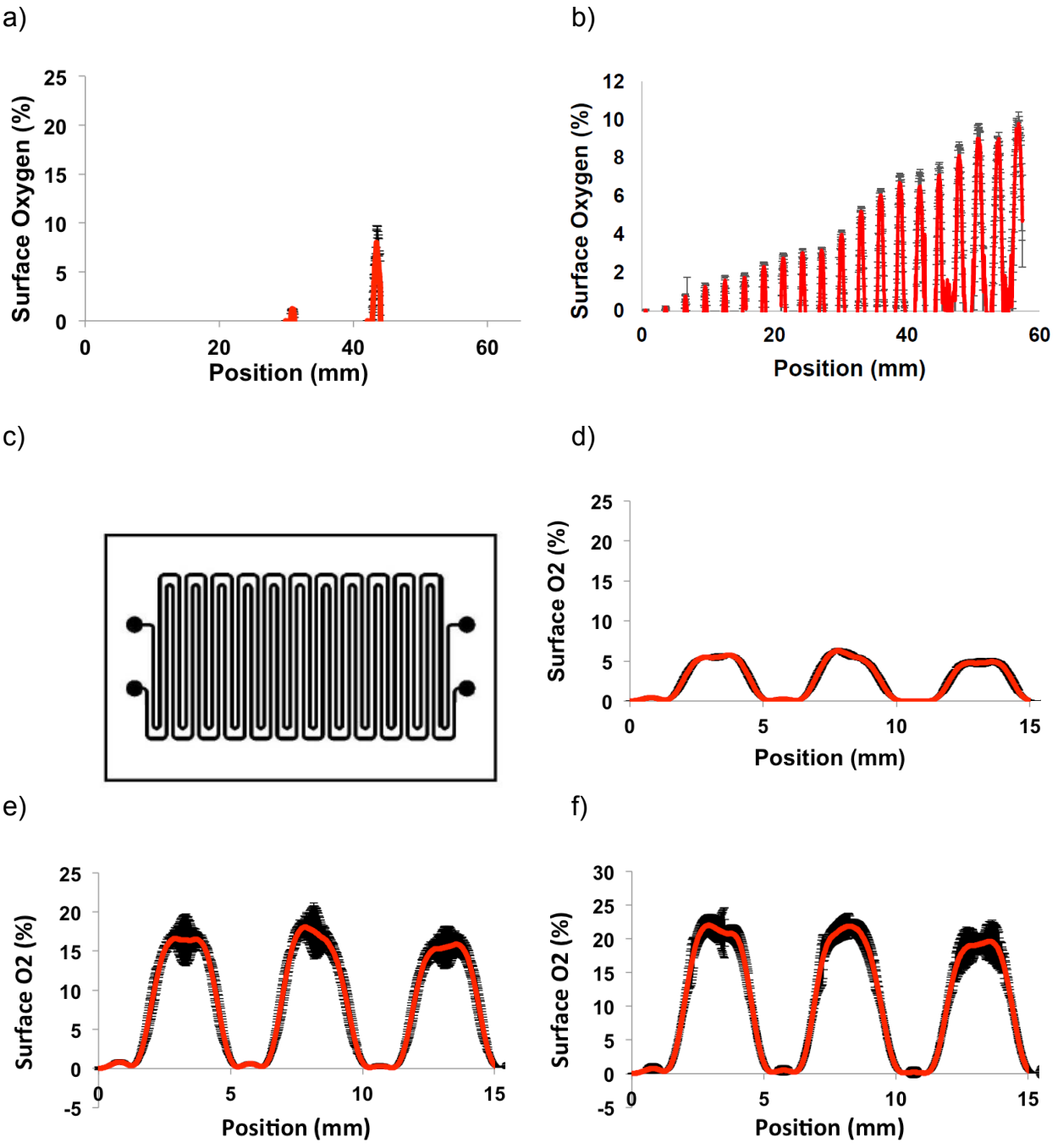


Figure 10. 3D Printed Oxygen Mixer as a universal oxygen supply. A) Individual outputs can be used in microfluidic devices; in this case 0% and 7% oxygen are being used. B) Alternatively, using 0% and 10% oxygen as the input gases, a different linear gradient can be achieved. C) An alternating oxygen profile can be achieved by using a different microfluidic device design and changing the input gases, with D) 0% and 6% oxygen, E) 0% and 16% oxygen, and F) 0% and 21% oxygen shown here.

## 2.4. Discussion

The previous chapter portrays how utilizing proper oxygenation can significantly increase the survival rate of living tissue, this allows tissue loading with a calcium indicator. Literature review emphasizes the importance of proper oxygenation for *in vitro* studies, yet, the oxygen environment is one of the most overlooked features of cell culture experiments. In most studies, a static oxygen environment is applied to the cell culture, however, realistically the cells are constantly exposed to a gradient of different oxygen concentrations. Current technology has not been practical in the creation of physiologically relevant oxygen gradients.

Oxygen gradients performed in microfluidic devices are performed on small-scale devices with dimensions of less than 4mm. Unfortunately, these dimensions are not large enough to perform biological assays such as western blots. Larger scale devices often have steep gradients, which may not be physiologically relevant. Previous studies attempted control of the oxygen gradient using patterned substrates, chemical and electrical reactions, and oxygen delivery using a sink-source approach. In a similar manner, this study strived to control the oxygen gradient with different degrees of success. The goal was to create a stable microfluidic device that would create a gradually increasing gradient, to avoid steepness. This would allow a large sample of biological material.

Figure 4, demonstrates initial attempts utilizing passive diffusion between 2 different gases (21% $O_2$ and 0% $O_2$). Both of these attempts create small linear gradients as well as plateau zones. The notion of utilizing an inclined membrane with different heights throughout the cell chamber was tested. It was theorized that flowing 0% $O_2$ into the

device, while exposing the chamber to ambient air would create an oxygen gradient across the cell culture chamber. As shown in figure 5, the oxygen concentration change is minimal from one side of the chamber to the other.

Once passive diffusion based approaches were eliminated, a microfluidic device was created to generate an oxygen gradient by active delivery of oxygen via multiple gas concentrations. As shown in figure 6, preliminary results using 4 and 5 different oxygen concentrations respectively, showed that a more linear gradient could be obtained using this more direct approach. However, this was not a practical approach due to the necessity of multiple gas canisters and gas flow regulators.

This problem was resolved by designing and fabricating a 3D printed microfluidic oxygen mixer that would allow 2 different oxygen concentrations as the input source, this in turn would create 22 different gas concentrations which could be utilized to create a stable, slowly increasing oxygen gradient in a microfluidic device.

Figure 8, demonstrates that this 3D printed microfluidic oxygen mixer was able to create 22 different gas concentrations that were within 1% of their expected value. The oxygen outputs can be used as a direct source of oxygen for other microfluidic devices, as shown in figure 9. If combined to a vacuum source the oxygen mixer can also be used as an oxygen switchboard, this will provide input to other microfluidic devices and create different oxygen landscapes as shown in figure 10.

## 2.5. Conclusion

To date, most studies that subject isolated cell culture to a hypoxic insult rely on hypoxia chambers or perfusion chambers in which the oxygen supply is carefully regulated by the investigator. Both of these types of chambers have the disadvantage of requiring relatively long equilibration times and providing only single oxygen levels. Using the 3D printed microfluidic mixer in conjunction with oxygen platforms with buried microfluidic gas networks, control over the spatiotemporal delivery of an oxygen gradient experienced by the cell culture is possible. Furthermore, utilizing the 3D printed microfluidic oxygen mixer as a switchboard simplifies oxygen delivery into the platforms. When compared to other existing techniques, this 3D oxygen mixer provides simplicity, accuracy, and low expense. The proposed method allows for a universal technique to be integrated into biological laboratories, more specifically, the model can be used in hypoxia research where the microenvironment must be greatly controlled due to the extreme sensitivity of cells to the oxygen levels.

## CITED LITERATURE


Acosta, M.A., Jiang, X., Huang, P.K., Cutler, K.B., Grant, C.S., Walker, G.M. & Gamcsik, M.P. 2014, "A microfluidic device to study cancer metastasis under chronic and intermittent hypoxia", *Biomicrofluidics,* vol. 8, no. 5, pp. 054117.

Adler, M., Erickstad, M., Gutierrez, E. & Groisman, A. 2012, "Studies of bacterial aerotaxis in a microfluidic device", *Lab on a chip,* vol. 12, no. 22, pp. 4835-4847.

Allen, J.W. & Bhatia, S.N. 2003, "Formation of steady-state oxygen gradients *in vitro*: application to liver zonation", *Biotechnology and bioengineering,* vol. 82, no. 3, pp. 253-262.

Allen, J.W., Khetani, S.R., Johnson, R.S. & Bhatia, S.N. 2006, "*In vitro* liver tissue model established from transgenic mice: role of HIF-1alpha on hypoxic gene expression", *Tissue engineering,* vol. 12, no. 11, pp. 3135-3147.

Au, A.K., Bhattacharjee, N., Horowitz, L.F., Chang, T.C. & Folch, A. 2015, "3D-printed microfluidic automation", *Lab on a chip,* vol. 15, no. 8, pp. 1934-1941.

Au, A.K., Huynh, W., Horowitz, L.F. & Folch, A. 2016, "3D-Printed Microfluidics", *Angewandte Chemie International Edition,* vol. 55, no. 12, pp. 3862-3881.

Brennan, M.D., Rexius-Hall, M. & Eddington, D.T. 2015, "A 3D-Printed Oxygen Control Insert for a 24-Well Plate", *PLoS ONE,* vol. 10, no. 9, pp. e0137631.

Byrne, M.B., Leslie, M.T., Gaskins, H.R. & Kenis, P.J. 2014, "Methods to study the tumor microenvironment under controlled oxygen conditions", *Trends in biotechnology,* vol. 32, no. 11, pp. 556-563.

Cairns, R.A., Kalliomaki, T. & Hill, R.P. 2001, "Acute (cyclic) hypoxia enhances spontaneous metastasis of KHT murine tumors", *Cancer research,* vol. 61, no. 24, pp. 8903-8908.

Carmeliet, P., Dor, Y., Herbert, J.M., Fukumura, D., Brusselmans, K., Dewerchin, M., Neeman, M., Bono, F., Abramovitch, R., Maxwell, P., Koch, C.J., Ratcliffe, P., Moons, L., Jain, R.K., Collen, D. & Keshert, E. 1998, "Role of HIF-1alpha in hypoxia-mediated apoptosis, cell proliferation and tumour angiogenesis", *Nature,* vol. 394, no. 6692, pp. 485-490.

Chen, Y.A., King, A.D., Shih, H.C., Peng, C.C., Wu, C.Y., Liao, W.H. & Tung, Y.C. 2011, "Generation of oxygen gradients in microfluidic devices for cell culture using spatially confined chemical reactions", *Lab on a chip,* vol. 11, no. 21, pp. 3626-3633.

Cheran, L.E., Benvenuto, P. & Thompson, M. 2008, "Coupling of neurons with biosensor devices for detection of the properties of neuronal populations", *Chemical Society Reviews,* vol. 37, no. 6, pp. 1229-1242.

Dunwoodie, S.L. 2009, "The role of hypoxia in development of the Mammalian embryo", *Developmental cell,* vol. 17, no. 6, pp. 755-773.

Espey, M.G. 2013, "Role of oxygen gradients in shaping redox relationships between the human intestine and its microbiota", *Free radical biology & medicine,* vol. 55, pp. 130-140.

Funamoto, K., Zervantonakis, I.K., Liu, Y., Ochs, C.J., Kim, C. & Kamm, R.D. 2012, "A novel microfluidic platform for high-resolution imaging of a three-dimensional cell culture under a controlled hypoxic environment", *Lab on a chip,* vol. 12, no. 22, pp. 4855-4863.

Grist, S.M., Schmok, J.C., Liu, M.C., Chrostowski, L. & Cheung, K.C. 2015, "Designing a Microfluidic Device with Integrated Ratiometric Oxygen Sensors for the Long-Term Control and Monitoring of Chronic and Cyclic Hypoxia", *Sensors (Basel, Switzerland),* vol. 15, no. 8, pp. 20030-20052.

Gross, B.C., Erkal, J.L., Lockwood, S.Y., Chen, C. & Spence, D.M. 2014, "Evaluation of 3D printing and its potential impact on biotechnology and the chemical sciences", *Analytical Chemistry,* vol. 86, no. 7, pp. 3240-3253.

Hajos, N., Ellender, T.J., Zemankovics, R., Mann, E.O., Exley, R., Cragg, S.J., Freund, T.F. & Paulsen, O. 2009, "Maintaining network activity in submerged hippocampal slices: importance of oxygen supply", *The European journal of neuroscience,* vol. 29, no. 2, pp. 319-327.

Hajos, N. & Mody, I. 2009, "Establishing a physiological environment for visualized *in vitro* brain slice recordings by increasing oxygen supply and modifying aCSF content", *Journal of neuroscience methods,* vol. 183, no. 2, pp. 107-113.

Khadka, S., Mauleon, G. & Eddington, D.T. 2014, "Fabrication of Oxygenation Microfluidic Devices for Cell Cultures", *Journal of Undergraduate Research,* vol. 7, no. 1, pp. 5-9.

Kofoed, H., Sjontoft, E., Siemssen, S.O. & Olesen, H.P. 1985, "Bone marrow circulation after osteotomy. Blood flow, pO2, pCO2, and pressure studied in dogs", *Acta Orthopaedica Scandinavica,* vol. 56, no. 5, pp. 400-403.

Lam, R.H., Kim, M.C. & Thorsen, T. 2009, "Culturing aerobic and anaerobic bacteria and mammalian cells with a microfluidic differential oxygenator", *Analytical Chemistry,* vol. 81, no. 14, pp. 5918-5924.

Lo, J.F., Sinkala, E. & Eddington, D.T. 2010, "Oxygen gradients for open well cellular cultures via microfluidic substrates", *Lab on a chip,* vol. 10, no. 18, pp. 2394-2401.

Lo, J.F., Wang, Y., Li, Z., Zhao, Z., Hu, D., Eddington, D.T. & Oberholzer, J. 2013, "Quantitative and temporal control of oxygen microenvironment at the single islet level", *Journal of visualized experiments : JoVE,* vol. (81):e50616. doi, no. 81, pp. e50616.

Mauleon, G., Fall, C.P. & Eddington, D.T. 2012, "Precise spatial and temporal control of oxygen within *in vitro* brain slices via microfluidic gas channels", *PloS one,* vol. 7, no. 8, pp. e43309.

Mehta, G., Mehta, K., Sud, D., Song, J.W., Bersano-Begey, T., Futai, N., Heo, Y.S., Mycek, M.A., Linderman, J.J. & Takayama, S. 2007, "Quantitative measurement and control of oxygen levels in microfluidic poly(dimethylsiloxane) bioreactors during cell culture", *Biomedical Microdevices,* vol. 9, no. 2, pp. 123-134.

Mohyeldin, A., Garzon-Muvdi, T. & Quinones-Hinojosa, A. 2010, "Oxygen in stem cell biology: a critical component of the stem cell niche", *Cell stem cell,* vol. 7, no. 2, pp. 150-161.

Oppegard, S.C., Nam, K.H., Carr, J.R., Skaalure, S.C. & Eddington, D.T. 2009, "Modulating temporal and spatial oxygenation over adherent cellular cultures", *PloS one,* vol. 4, no. 9, pp. e6891.

Park, J., Bansal, T., Pinelis, M. & Maharbiz, M.M. 2006, "A microsystem for sensing and patterning oxidative microgradients during cell culture", *Lab on a chip,* vol. 6, no. 5, pp. 611-622.

Paula-Lima, A.C., De Felice, F.G., Brito-Moreira, J. & Ferreira, S.T. 2005, "Activation of GABA(A) receptors by taurine and muscimol blocks the neurotoxicity of beta-amyloid in rat hippocampal and cortical neurons", *Neuropharmacology,* vol. 49, no. 8, pp. 1140-1148.

Polinkovsky, M., Gutierrez, E., Levchenko, A. & Groisman, A. 2009, "Fine temporal control of the medium gas content and acidity and on-chip generation of series of oxygen concentrations for cell cultures", *Lab on a chip,* vol. 9, no. 8, pp. 1073-1084.

Rexius-Hall, M.L., Mauleon, G., Malik, A.B., Rehman, J. & Eddington, D.T. 2014, "Microfluidic platform generates oxygen landscapes for localized hypoxic activation", *Lab on a chip,* vol. 14, no. 24, pp. 4688-4695.

Sinkala, E. & Eddington, D.T. 2010, "Oxygen sensitive microwells", *Lab on a chip,* vol. 10, no. 23, pp. 3291-3295.

Skolimowski, M., Nielsen, M.W., Emneus, J., Molin, S., Taboryski, R., Sternberg, C., Dufva, M. & Geschke, O. 2010, "Microfluidic dissolved oxygen gradient generator biochip as a useful tool in bacterial biofilm studies", *Lab on a chip,* vol. 10, no. 16, pp. 2162-2169.

Thomas, P.C., Raghavan, S.R. & Forry, S.P. 2011, "Regulating Oxygen Levels in a Microfluidic Device", *Analytical Chemistry,* vol. 83, no. 22, pp. 8821-8824.

Tsai, A.G., Friesenecker, B., Mazzoni, M.C., Kerger, H., Buerk, D.G., Johnson, P.C. & Intaglietta, M. 1998, "Microvascular and tissue oxygen gradients in the rat mesentery", *Proceedings of the National Academy of Sciences of the United States of America,* vol. 95, no. 12, pp. 6590-6595.

Wang, L., Liu, W., Wang, Y., Wang, J.C., Tu, Q., Liu, R. & Wang, J. 2013, "Construction of oxygen and chemical concentration gradients in a single microfluidic device for studying tumor cell-drug interactions in a dynamic hypoxia microenvironment", *Lab on a chip,* vol. 13, no. 4, pp. 695-705.

Wang, Z., Liu, Z., Li, L. & Liang, Q. 2015, "Investigation into the hypoxia-dependent cytotoxicity of anticancer drugs under oxygen gradient in a microfluidic device", *Microfluidics and Nanofluidics,* vol. 19, no. 6, pp. 1271-1279.

Xiao, W., Shinohara, M., Komori, K., Sakai, Y., Matsui, H. & Osada, T. 2014a, "The importance of physiological oxygen concentrations in the sandwich cultures of rat hepatocytes on gas-permeable membranes", *Biotechnology progress,* vol. 30, no. 6, pp. 1401-1410.

Xiao, W., Kodama, M., Komori, K. & Sakai, Y. 2014b, "Oxygen-permeable membrane-based direct oxygenation remarkably enhances functions and gene expressions of rat hepatocytes in both 3D and sandwich cultures", *Biochemical engineering journal,* vol. 91, pp. 99-109.

# 3. CHAPTER 3: 3D OXYGEN MICROFLUIDIC PLATFORM FOR *IN VITRO* HYPOXIC STUDIES

## 3.1. Introduction

### 3.1.1. Angiogenesis

Angiogenesis is the normal physiological process in which new blood vessels grow from preexisting vessels (Folkman, Haudenschild 1980). Chapter 1 examines the significant relationship between proper oxygen supply and healthy cellular function. In a similar fashion, chapter 2 analyses how various body tissues are consistently exposed to different oxygen gradients. This gradient difference can be caused by simple mechanisms, such as the distance of a blood capillary from the tissue. However, since blood vessels are created at a contstant rate most of the tissues in the human body have a relatively close source of oxygenated blood supply, usually no farther than a few hundred micrometers (Adair, Montani 2010).

The two main types of angiogenesis are sprouting and intussceptive. In intussceptive angiogenesis, the main vessel splits into two new separate vessels. This type of angiogenic process was first discovered 30 years ago in the postnatal rat lung, and as such, much is still unknown about this angiogenic mechanism (Burri, Tarek 1990). Conversely, sprouting angiogenesis was first observed more than 200 years ago and it is a well documented process (Adair, Montani 2010). Sprouting angiogenesis sends proliferating endothelial cells out from the main vessel acting as scouts trying to capture new areas for cell growth. This way, previously hypoxic areas can be supplied with proper oxygen levels. This angiogenic process starts with the enzymatic degradation of the basement membrane, the endothelial cells then start to reproduce at a faster rate

than normal. These endothelial cells start to migrate towards the hypoxic area and start to form tubular structures that can eventually become new vessels. Finally, pericytes wrap themselves around the endothelial cells, effectively creating a new basement membrane and stabilizing the vessel (Ribatti, Nico & Crivellato 2015).

If a hypoxic zone is created by means of injury or increased metabolism, neighboring cells will release several chemicals that stimulate angiogenesis. One of the most important signal proteins is the vascular endothelial growth factor (VEGF) (Gerhardt 2008). Leading cells (tip cells) and trailing cells (stalk cells) are characteristic of sprouting angiogenesis. The tip cell at the forefront of the growing vessel possess a large quantity of VEGF receptors that enable it to sense the angiogenic factors released by the hypoxic cells. Using these receptors as a guidance system, the tip cell can locate the hypoxic zone. The stalk cells will then start to reproduce and commence the creation of the new blood vessel, to supply enough oxygenated blood to meet the demands of the tissue (Carmeliet et al. 2009). It has not been established whether oxygen levels regulate the differentiation of these endothelial subpopulations during sprouting, this is a key point (Qutub et al. 2009).

### 3.1.2. *In Vitro* Models for Angiogenesis

Since the development of the first *in vitro* angiogenesis model by Folkman and Haudenschild in 1980, various assays have tried to replicate the real *in vivo* microenvironment created during a hypoxic stimulus (Vailhe, Vittet & Feige 2001).

Several of the most studied angiogenesis models rely on two-dimensional approaches. In these models, cultures of endothelial cells are grown on the surface of plastic cell culture dishes, gels, filters, or flow chambers (Vailhe, Vittet & Feige 2001). In an

attempt to recapitulate as much of the natural microenvironment as possible, the gels used for seeding are usually Matrigel, collagen type I or IV, fibrin, or gelatin (Hasan et al. 2014). As a result of these experimental models, it is now known that diverse factors such as: extracellular matrix components, shear stress, and chemical variables (such as growth factors) can influence the creation of capillary-like structures on planar cell cultures (Vernon et al. ).

Due to the importance of the extracellular matrix on the angiogenesis process, three-dimensional models are emphasized in the future of angiogenic research. 3D models function on the theory that when endothelial cells are exposed to angiogenic factors, they can invade the extracellular matrix, similar to an *in vivo* situation. Similarly, in two-dimensional approaches the extracellular matrix is typically composed of Matrigel, collagen, fibrin, or gelatin (Hasan et al. 2014). In these 3D experiments, the cells are seeded in between two layers of polymerized gel, or occasionally embedded into the actual gel (Haycock 2011). While this type of angiogenic model is more realistic to the *in vivo* conditions experienced by the cell, missing components remain. For example, the cells remain seeded in a planar culture and there is no shear stress that cause cellular influence.

Conventional planar cultures and three-dimensional models have increased our knowledge of the vascular system, the lack of an extracellular matrix in the correct configuration prevents true physiological accuracy. In order to truely model the vascular network, the correct three-dimensional cellular microenvironment needs to be integrated. This will allow native cell to cell and cell to ECM interactions the opportunity

to be adequately studied (Baker et al. 2013). Microfluidics can make a substantial impact in this particular field of celluar studies.

### 3.1.3. Microfluidic Models for Angiogenesis

Microfluidic technology is a platform that is well suited for three-dimensional angiogenic hypoxic studies as it offers a high degree of control over the timing and spatial presentation of chemical and hypoxic stimulus. In the literature, the majority of microfluidic devices related to angiogenic or vascularized models focus on similar subjects; spatially controlled co-culturing of cells (Du et al. 2011), controlled fluid flow (Unger et al. 2000), spatiotemporal control of chemical gradients (Mosadegh et al. 2007) and better extracellular matrix (Vickerman et al. 2008).

Some of the earliest microfluidic models consist of vascularization of two-dimensional microfluidic channels which were created using standard photolithography and soft-lithography techniques (Hasan et al. 2014). However, as the significance of the extracellular matrix was emphasized, improved fabrication techniques allowed for the utilization of hydrogels during the manufacturing process. The extracellular matrix is typically made from hydrogels such as calcium alginate, collagen, fibrin, agarose, poly(ethylene glycol) diacrylate (PEGDA), or methacrylated gelatin (GelMa) (Hasan et al. 2014).

Some of the earliest protocols took advantage of subtractive methods to create the 3D platforms. These techniques designed a microfluidic channel encased by hydrogel by removing a predetermined sacrificial template. Examples include, utilizing a stainless steel pin to create a straight microchannel that could be endothelialized (Chrobak, Potter & Tien 2006), or using additional hydrogel that could later be dissolved and

flushed out of the system creating hollow networks (Golden, Tien 2007). These models allow for co-culturing of different types of cells, controlled media flow, as well as chemical gradient control.

Newer methods tend to involve the addition of multiple two-dimensional layers to create a three-dimensional perfusable endothelialized network. Using these techniques, different angiogenic properties can be studied, such as: vessel sprouting, interaction between different co-cultured cells, and response to chemical gradients (Zheng et al. 2012). In addition, the process known as bioprinting has emerged in recent years. In bioprinting, a computer controlled 3D printer can precisely seed cells into a 3D microfluidic platform. Several studies have demonstrated the advantages 3D printing can have on angiogenic models (Campbell, Weiss 2007), however, several issues are noted, such as, consistent cell density, cost, and specialized equipment. These problems must be resolved before this technology can be universally applied (Hasan et al. 2014).

There are numerous devices that precisely control soluble factors that may influence overlaying cells plated on three-dimensional surfaces. Yet, no known device exists that can distinguish cellular response between a chemical or hypoxic stimulus. This study, presents an innovative microfluidic device that allows closer examination of the hypoxic effects on the angiogenic process, independent of growth factors. This microfluidic device permits formation of a 3D microvasculature, complete oxygen control, and the ability to generate chemical gradients.

### 3.1.4. Research Purpose

In previous studies, oxygen platforms with buried microfluidic gas networks made out of polydimethylsiloxane were used to control the spatiotemporal delivery of hypoxic stimulus as well as improving oxygen delivery to tissues in culture (Mauleon, Fall & Eddington 2012). However, angiogenesis lacks a comparable *in vitro* platform where hypoxic research can be reliably performed. The ability to precisely control the spatiotemporal oxygen environment in a 3D platform gives superior insight into the relationship between oxygen and angiogenic function in the human body.

The primary focus of this study is to develop and use a 3D angiogenic platform where *in vitro* hypoxic studies can be dependably performed. This design will improve upon previous methods by developing a hybrid collagen/PDMS platform that mimics a 3D culture setting under hypoxic conditions. Using this oxygen platform, the separate effect that growth factors and hypoxia have on the angiogenic response will be examined. Once the 3D oxygen microfluidic platform is completed, the device consists of three independent parts: the glass slide for support, a microfluidic channel that delivers the oxygen, and a gasket that doubles as a structural support for the 3D ECM and as a thin membrane for oxygen diffusion. However, unlike most microfluidic devices, this 3D oxygen microfluidic platform does not rely on PDMS microchannels. Instead, a unique protocol was followed in which molded gelatin is utilized as a sacrificial element and the device is created in 2 separate steps (Baker et al. 2013). This microfluidic device allows formation of a 3D microvasculature as well as complete control of the oxygen microenvironment.

## 3.2. Materials and Methods

### 3.2.1. Design and Fabrication of 3D Oxygen Microfluidic Platform

#### 3.2.1.1. Design of 3D Oxygen Microfluidic Platform

The 3D oxygen microfluidic platform was developed to study the effect of a hypoxic insult on angiogenic cell culture with constant, uninterrupted oxygen flow. As shown in figure 1, once the 3D oxygen microfluidic platform is completed, the device consists of three independent parts: the glass slide for support, a PDMS gasket that doubles as a structural support for the 3D collagen extracellular matrix and as a thin membrane for oxygen diffusion, and a microfluidic gas network that delivers the oxygen gas to the cell culture.

The microfluidic channels where the cells are seeded will be completely encased by a collagen matrix and have an approximate surface area of 14.8 $mm^2$ and a volume of 0.6$mm^3$. These measurements can vary depending on the PDMS gelatin template used during fabrication of the device.

All layers have 2 independent sets of inlet/outlet ports so that the oxygen gas introduced into the gas network does not interfere with the media flow within the microfluidic channels. This design criteria allows complete independent control of the hypoxic stimulus from any chemical stimulus.

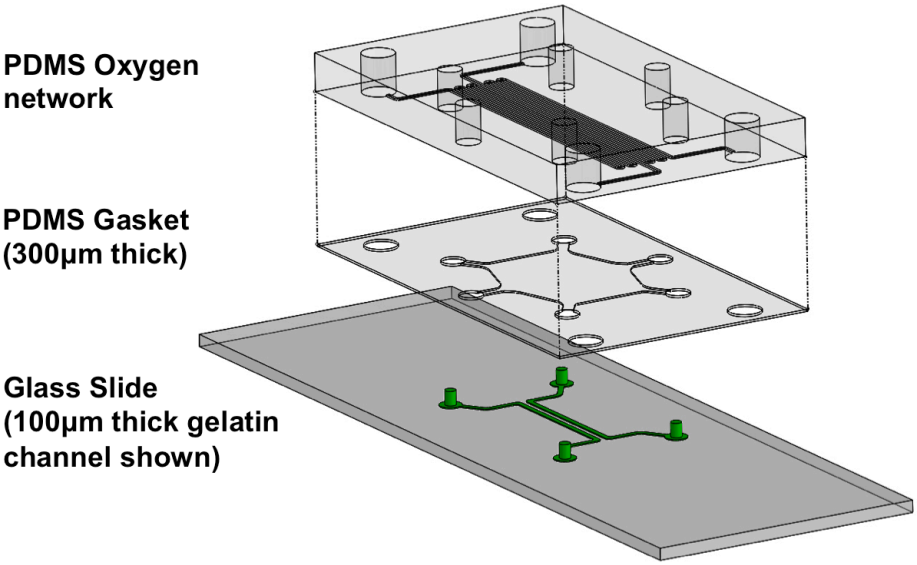


Figure 1. Schematic of the 3D oxygen microfluidic platform. Exploded view of the microfluidic device. As seen from the diagram, the device consists of 3 independent parts: the oxygen network that supplies the gas for the experiment. The PDMS gasket acts as an oxygen permeable membrane as well as a container for the collagen matrix. A glass slide that serves as a base for the device.

#### 3.2.1.2. Fabrication of 3D Oxygen Microfluidic Platform

Three different masters were used for the creation of the 3D oxygen microfluidic platform: the gelatin channel template, the gasket containing the collagen enclosure, and the oxygen network. Standard microfabrication techniques were universally applied. The PDMS gelatin template was made via casting of PDMS on a silicon wafer master possessing channels that are 500μm wide by 100μm tall. Conversely, the PDMS gasket was fabricated by spin coating PDMS on the gasket master to achieve a final thickness of 300μm thick. Finally, the microfluidic gas network was made via casting of PDMS on a silicon wafer master. Both, the PDMS gelatin template and the PDMS oxygen network were 0.5mm thick.

Once all PDMS devices were made, the microfluidic gas network and the gasket were exposed to oxygen plasma and bonded together, making sure that all inlet/outlet sets were in contact with each other. After this bonding step, the gasket assembly as well as the glass slides were then treated with consecutive two-hour incubations of 0.1mg/ml of poly-L-lysine and 5% v/v glutaraldehyde to help crosslink the collagen gel to the gasket walls. In a similar manner, the PDMS stamps were treated overnight with Sigmacote. In this experiment, siliconizing the PDMS gelatin template greatly aided with the removal process without disrupting the molded gelatin microchannel. After all of the appropriate incubation steps, all of the PDMS devices were punched with inlet/outlet ports.

Following these steps, the PDMS gelatin template was pressed to the glass slide and warmed 10% w/v gelatin solution was drawn through the channel template and allowed to solidify for 7 minutes prior to removal of the PDMS gelatin template. Then, the gasket assembly was pressed upon the gelatin channel structure making sure that inlets and

outlets were maintained. Once the gasket was firmly in place, a solution of bovine collagen type I solution was pipetted into the chamber and allowed to gel at room temperature for 7 minutes. Then, both inlets and outlets of the gelatin structure were filled with PBS prior to putting the devices in the incubator set to 37°C. As a result of the overnight incubation, the gelatin structure melted, allowing the PBS to flush it out of the collagen structure. The final result is microfluidic channels encased by a collagen extracellular matrix. The entire fabrication process can be seen in figure 2.

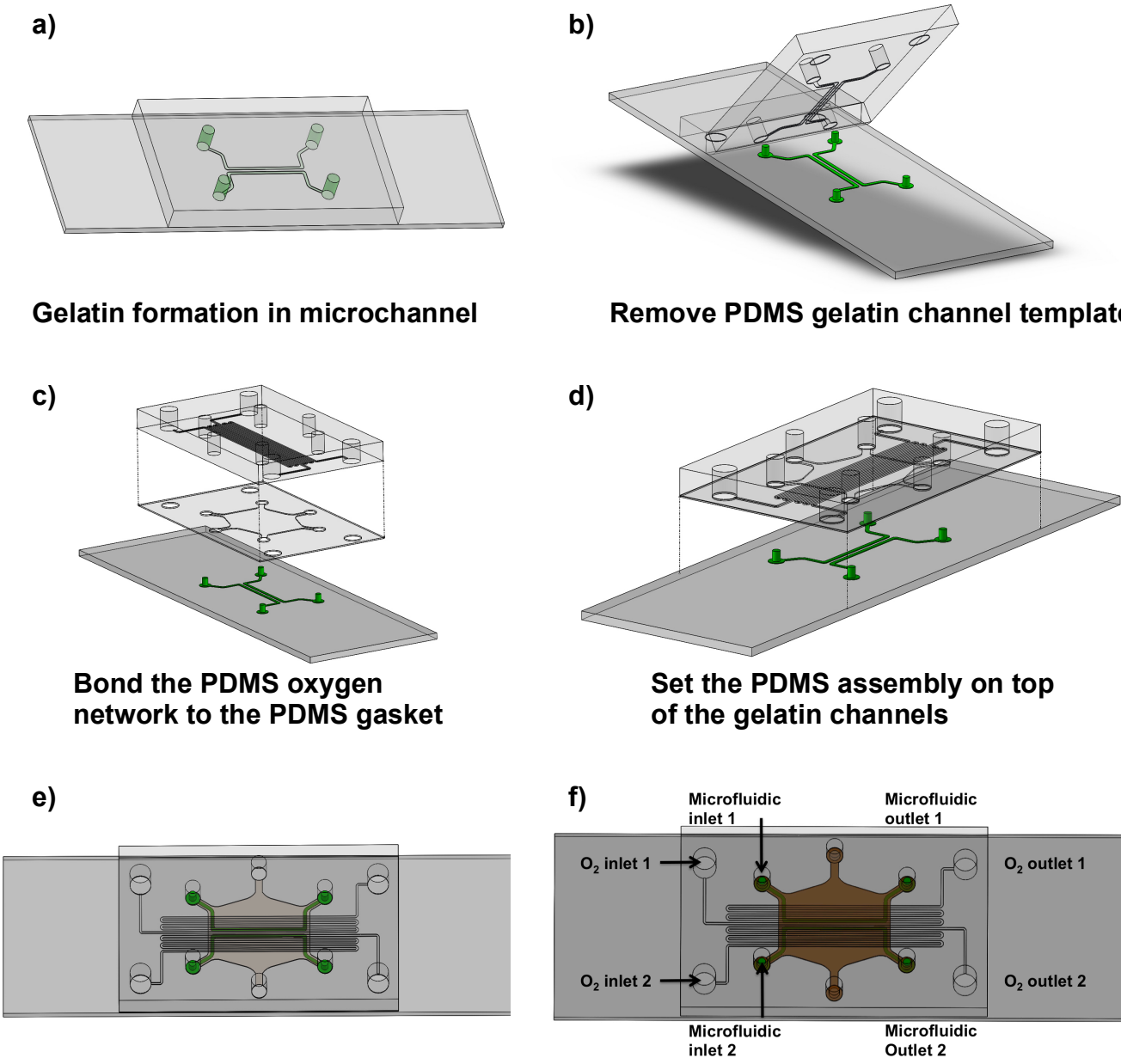


Figure 2. Fabrication process for the 3D oxygen microfluidic platform. A) Using a PDMS gelatin template, a gelatin structure is molded on top of a glass slide. B) After 7 minutes, template is removed leaving behind a gelatin structure. C) PDMS gas network and PDMS gasket are bonded together using oxygen plasma. D) PDMS assembly is registered on top of the gelatin structure. E) Collagen is injected into the PDMS structure encasing the gelatin. F) Device is incubated overnight setting the collagen and melting the gelatin. Finalized device has open channels with independent gas and fluid inputs.

### 3.2.2. Validation of 3D Oxygen Microfluidic Platform –Fluid Control

In order to demonstrate the ability to fabricate clear, stable fluidic channels within the collagen matrix, the opening of the channels using the fluorescent dye fluorescein isothiocyanate (FITC) is shown. The inlets of the microchannels were filled with a 100μM solution of FITC and PBS (phosphate buffered solution) , while the outlets were connected to a syringe pump set for withdrawal mode at 4μl/min. The resulting fluorescent scans were taken right after complete filling of the microchannels on a fluorescent inverted microscope (Olympus IX71) using the image acquisition and analysis software MetaMorph Imaging System (Universal Imaging Corp.); the pictures were acquired using the 4X objective.

### 3.2.3. Validation of 3D Oxygen Microfluidic Platform –Oxygen Control

In order to validate the oxygen gradient created by the 3D oxygen microfluidic platform, a thin film of PDMS-containing PtOEPK sensor was fabricated as described in chapter 2. In order to validate this specific platform, the PtOEPK sensor had to be included in the device itself. To do this, the oxygen sensor was placed on top of the glass slide at the beginning of the assembly process. The gelatin channels were molded on top of the sensor and finally encased by the collagen matrix itself. In the end, an oxygen sensor that covers the entire length of the 3D oxygen microfluidic platform remains.

Once fabricated, the inlet ports of the oxygen network were connected to gas tanks containing 5% $CO_2$, balanced nitrogen and 5% $CO_2$, balanced air. Then, using a fluorescent inverted microscope (Olympus IX71), computer controlled fluorescent scanning images were taken across the entire PtOEPK sensor and by solving the Stern-

Volmer equation, a relationship between PtOEPK intensity and oxygen concentration is obtained.

Once the oxygen gradient is validated, the necessary time for the gradient to equilibrate should be determinted. In order to do this, a time-lapse experiment was set up where images were taken every minute for the first 10 minutes right after the 0% oxygen gas was started in the device. Then, images were taken every 10 minutes for a total duration of 70 minutes. Images were analyzed in a similar fashion to the previous experiment.

One of the main problems that microfluidic gas network devices experience is the dehydration of the device itself. Specifically, this device was supplied with two different oxygen concentrations (5% $CO_2$, balanced nitrogen and 5% $CO_2$, balanced air) for a period of 24 hours and then measured the oxygen gradient using the PtOEPK sensor.

### 3.2.4. Cell Culture

Immortalized human brain endothelial cells (HCMED/D3) were expanded and passaged to 6-8 in EGM-2 MV (Lonza) prior to use in experiments. To endothelialize the channels, the outlet port was connected to a syringe pump set for withdrawal mode at 4µl/min while the inlet was filled with a concentrated solution of endothelial cells (2 x $10^6$ cells/ml). After 30 minutes of static incubation at 37°C, the device was covered with parafilm and carefully inverted in order to seed the top and the walls of the 3D platform. Following another 30-minute incubation period, the device was placed back into the original position and allowed to incubate for 3 hours finalizing the adhesion of the cells to all sides of the 3D platform. After this incubation period, the media was changed with EGM-2 MV, all cell pellets formed at the inlets and outlets were broken up, and the

device was incubated at 37°C. During the cell culture stage, cell media was changed every 6 hours.

### 3.2.5. Oxygen Induced Sprouting Imaging

In order to image the cell movement within the 3D oxygen microfluidic platform, the cells were labeled with cell tracker red-CMFDA according to the manufacturer's instructions (Life Technologies) prior to seeding into the devices.

Once the cells were seeded into the 3D device, the inlet ports of the oxygen network were connected to a 5% $CO_2$, balanced air gas tank. The cells were exposed to this 21% oxygen environment for 3 hours.

After this initial oxygen treatment, two different experiments were performed. In one case, the endothelialized microfluidic channel was kept under the 21% $O_2$ environment, while the other side of the device was exposed to a 0% $O_2$ environment. In the next experiment, the sides were switched and the endothelialized microfluidic channel was kept under the 0% $O_2$ environment. This oxygen gradient was kept for a minimum of 24 hours with some experiments running as long as 6 days. During the experimental stage, cell media was changed every 3 hours in order to avoid dehydration of the collagen and the cell culture. Fluorescent images using a fluorescent inverted microscope (Olympus IX71) were taken with both 4X and 20X magnifications every 24 hours to assess cell invasion into the collagen matrix.

### 3.2.6. Statistical Analysis

Experiments were performed a minimum of three independent times, and data is expressed as the average ± standard deviation. A matlab code (Appendix C) was used to solve the Stern-Volmer equation. Graphs were created in Excel.

## 3.3. Results

### 3.3.1. Validation of 3D Oxygen Microfluidic Platform –Fluid Control

Four different microfluidic channel designs were fabricated and tested during the course of this study. The different designs have diverse channel geometries that can be customized depending on the experiment. In order to show open, leak-free microfluidic channels encased by the collagen matrix, a fluorescent dye was injected into the channels and imaged using a fluorescent inverted microscope. Figure 3, demonstrates how the 3D platform is able to maintain the dye within the channel with minimal diffusion into the matrix.

### 3.3.2. Validation of 3D Oxygen Microfluidic Platform –Oxygen Control

Using the PtOEPK oxygen sensor at the bottom of the oxygen platform, the oxygen gradient created by the oxygen network can be measured. The two different sides of the network were connected to either a 0% $O_2$ or a 21% $O_2$ gas tank. Figure 4, shows the results plotting the position versus the oxygen concentration measured. The 3D oxygen microfluidic network is able to create two completely different oxygen microenvironments in the areas where the microchannels are located; with one channel experiencing hypoxia while the other channel is exposed to ambient air.

In order to test the time it would take for the microfluidic platform to equilibrate to a hypoxic environment, a 0% oxygen input was applied to measure the oxygen concentration as a function of time. As can be seen in figure 5, the device goes down to 3% $O_2$ in less than 9 minutes and reaches 0% $O_2$ after 60 minutes.

The microfluidic platform was also tested for durability and stability as shown in figure 6. The microfluidic platform was connected to inputs of 0% $O_2$ and 21% $O_2$ and incubated

for 24 hours at 37°C. After the incubation period, the oxygen concentration across the microfluidic platform was remeasured and confirmed to maintain a stable oxygen gradient as well as microfluidic channels.

**a)** **b)**

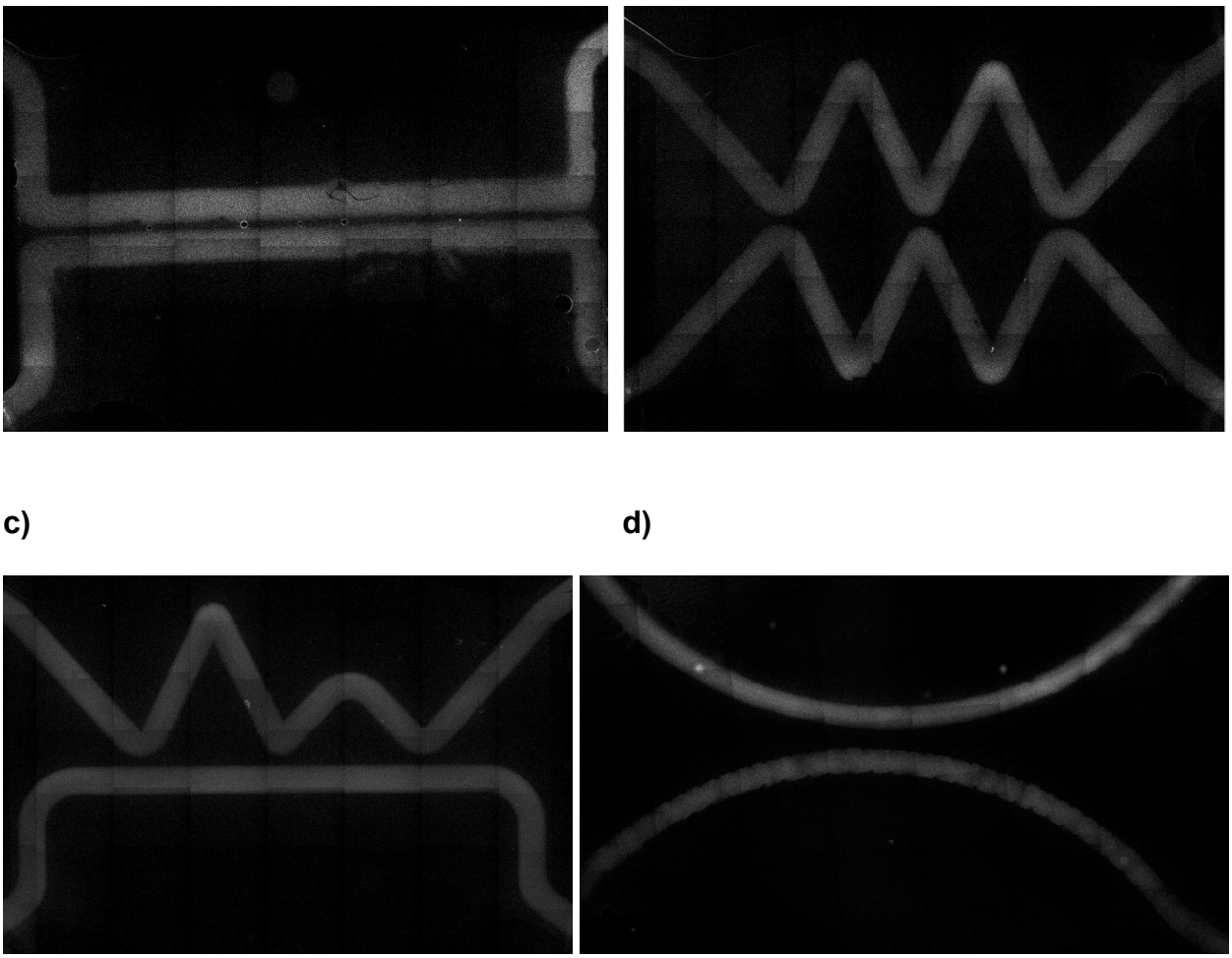

**c)** **d)**

Figure 3. Fluid control validation of the 3D oxygen microfluidic platform. FITC dye was drawn across the microfluidic channels using negative pressure created by a syringe pump. Four different designs are shown to be able to maintain the dye within the channel with minimal diffusion into the matrix.

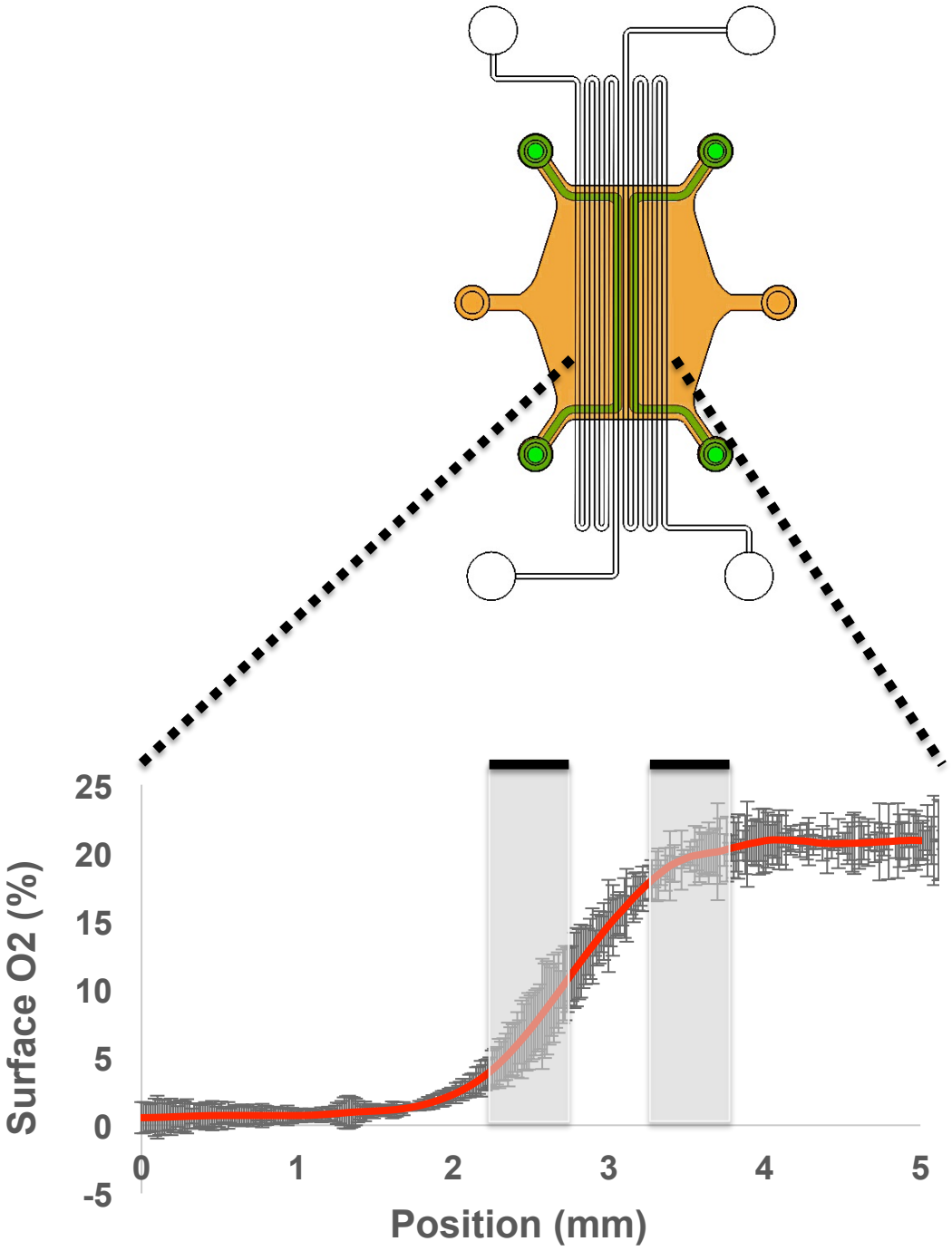


Figure 4. Gas control validation of the 3D oxygen microfluidic platform. Using a PtoEPK sensor embedded on a thin PDMS film, the different oxygen environments created by the platform can be measured. The two microfluidic channels are 500μm wide and are separated by a 500μm wide gap. The two channels are exposed to two different oxygen conditions.

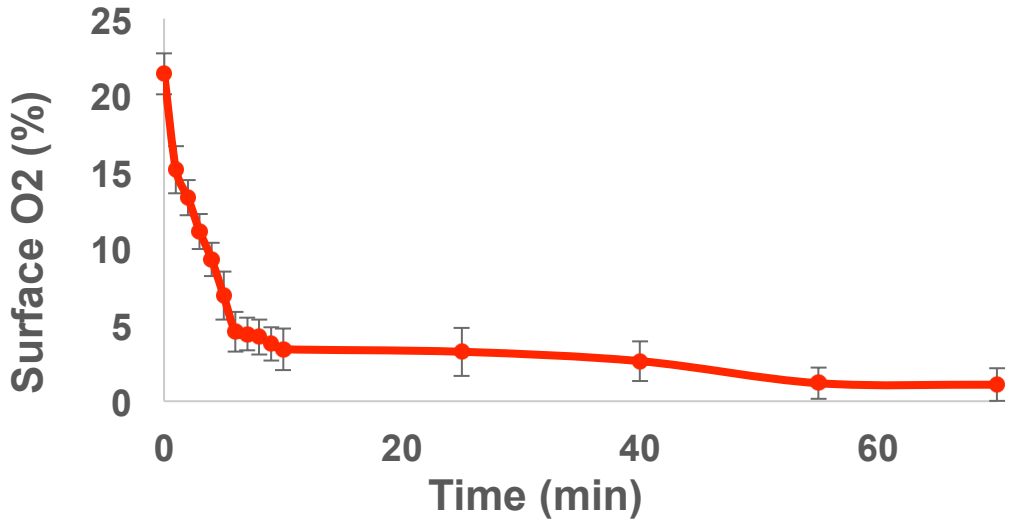


Figure 5. Hypoxia as a function of time. The oxygen profile measured over time shows that it takes close to one hour for the oxygen concentration in the microchannels to reach 0%.

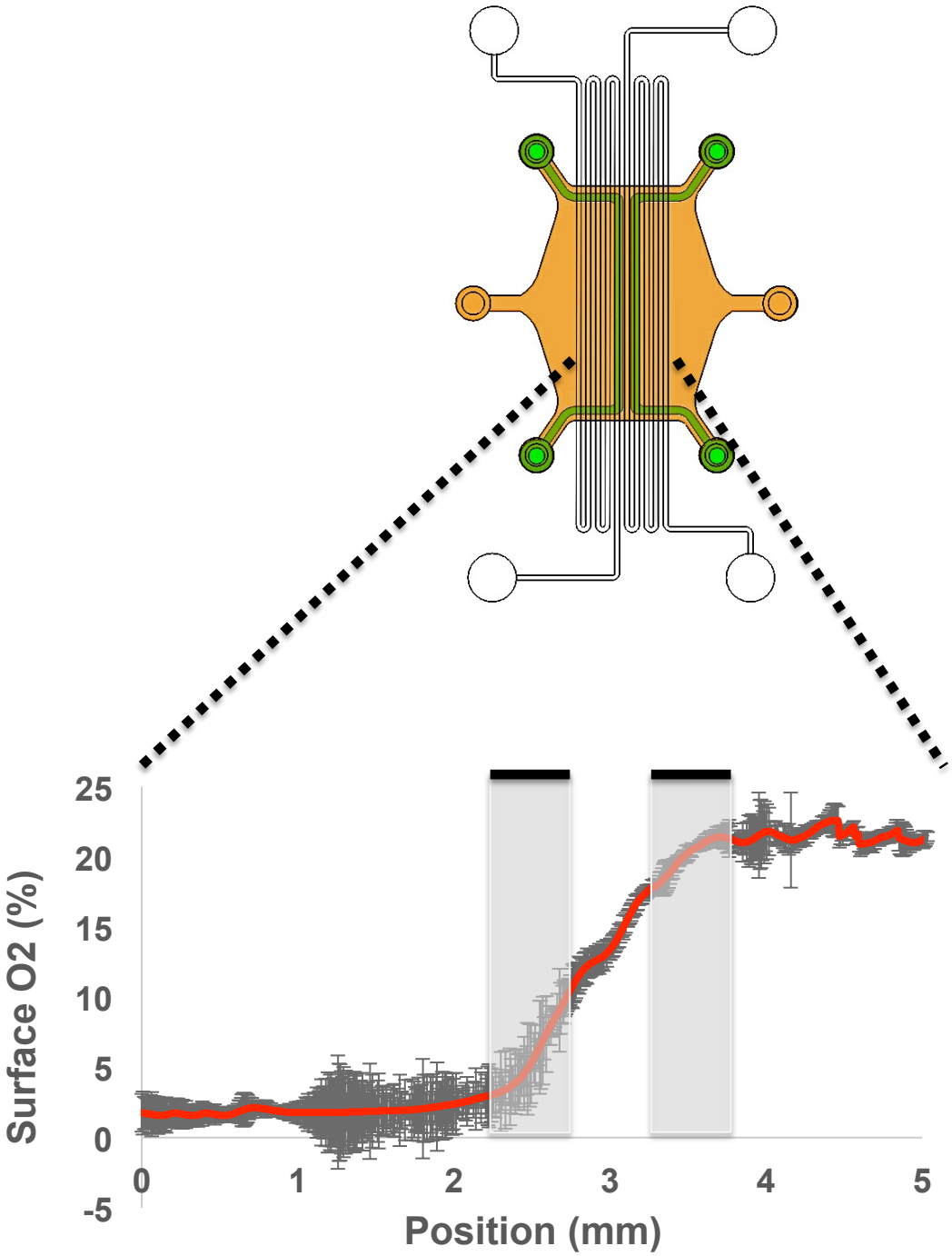


Figure 6. Long term hypoxic experiments. Gas flow was maintained for 24 hours in order to assure durability and stability. After the 24 hours, the oxygen gradient is maintained and the microchannels are still viable.

### 3.3.3. Cell Culture

In order to vascularize the microfluidic channels, endothelial cells labeled with cell tracker red-CMFDA were seeded at a concentration of 2 x $10^6$ cells/ml and incubated for 24 hours in an incubator set to 37°C. As shown in figure 7A, a confluent monolayer formed inside the microfluidic channel. The cells are completely enclosed by the collagen matrix and fresh media can be supplied every 6 hours. Figure 7B shows the boundary layer of the microchannels and some of the common defects observed during this study. Even though these defects occurred, the boundary of the microchannel is still strong enough to prevent cells or media from leaking into the matrix. Finally, figure 7C and 7D show how the 3D oxygen microfluidic platform can culture the cells in a three-dimensional setting. Some of the cells will be seeded on the bottom of the channel, while other groups of cells will be seeded on the walls or the top of the microchannel.

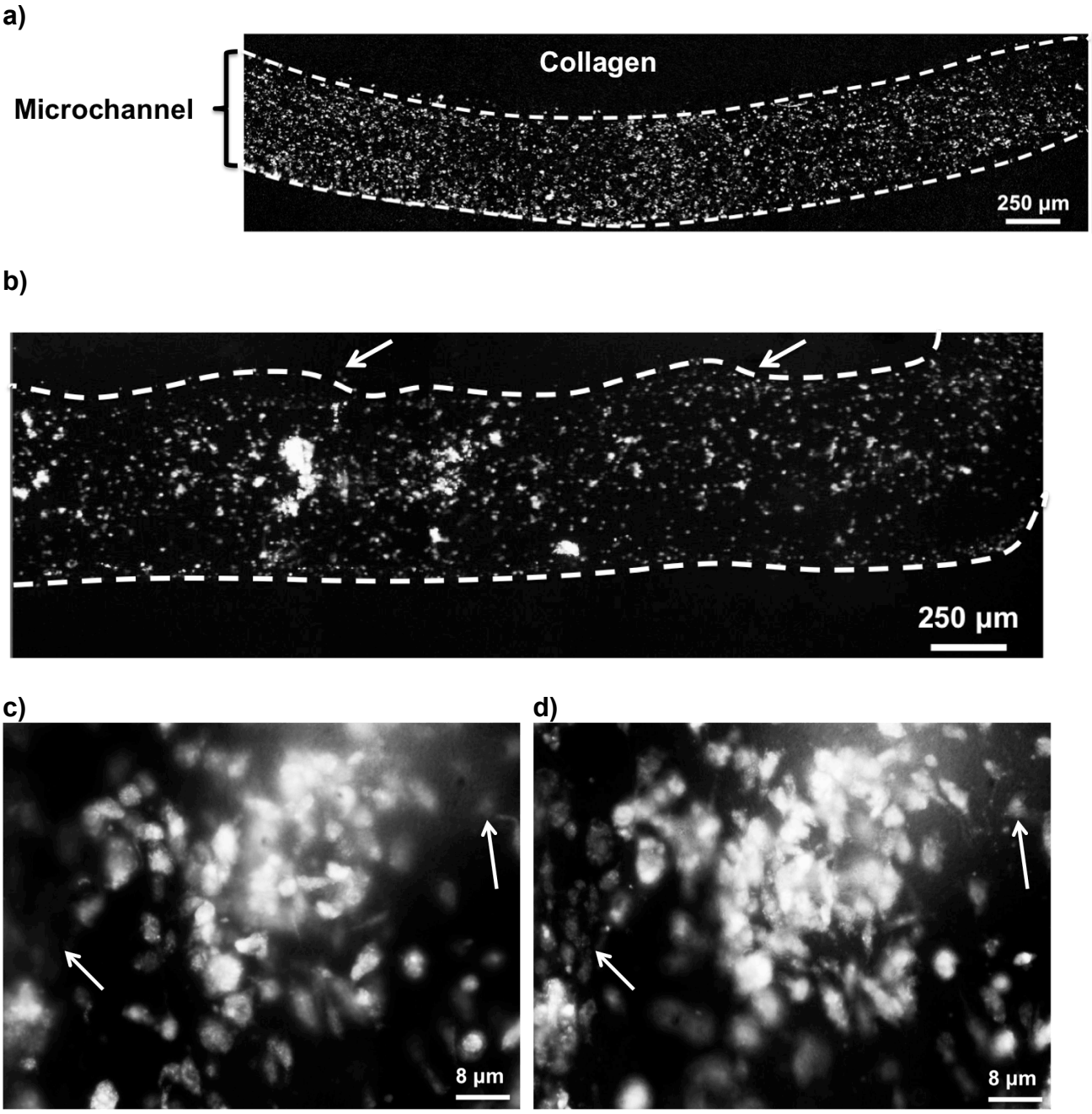


Figure 7. Vascularization of microfluidic channels. A) Cells labeled with a cell tracker are seeded and grown within the microfluidic channel. Channels are completely encased by the collagen matrix. B) Removal of a sacrificial gelatin structure is used to fabricate the microfluidic channels; therefore, some small defects can be seen in the boundaries of the microchannel. C) Cells are seeded in a 3-dimensional structure and as such, they are seeded at different levels within the channel. Some of them are on the bottom of the channels, while some of them are on the border and the top of the channel (D).

### 3.3.4. Oxygen Induced Sprouting Imaging

The 3D oxygen microfluidic platform is capable of creating two different oxygen environments within the device. When the cells are seeded in the microchannels, they are affected by only one of these oxygen environments. During the hypoxic stimulus experiments, 2 different experimental protocols were followed.

First, a microfluidic channel was endothelialized for 24 hours. Then, a baseline treatment of 21% $O_2$ (21% $O_2$ / 5% $CO_2$) was applied to the entire device for a period of 3 hours. After this baseline period, the endothelialized channel was exposed to a hypoxic stimulus (0% $O_2$ / 5% $CO_2$) for 8 hours. Figure 8 shows how the cells formed a confluent layer on the microchannel during the baseline treatment. However, after the hypoxic stimulus, the cells died off due to the lack of oxygen in the environment.

For the second set of experiments, the oxygen conditions were reversed. The microfluidic channel was endothelialized for 24 hours once again followed by the baseline 21% $O_2$ (21% $O_2$ / 5% $CO_2$) treatment. However, in this case, the endothelialized channel was kept under the 21% $O_2$ environment while the other side of the device was exposed to the hypoxic stimulus for the duration of the study. Figure 9 demonstrates how the cells can indeed survive for long periods of time. After 4 days of culture within the platform, the endothelial cells started to group together into tubular networks.

Some of the oxygen platforms (n=3) showed signs of angiogenesis towards the hypoxic environment two days after initial seeding when exposed to the oxygenation treatments. Figure 10 shows how small amounts of cells started to invade the collagen matrix on day 2. By day 4, more cells were moving towards the hypoxic stimulus and by the sixth

day, several groups of cells could be seen invading the collagen matrix. Figure 11 shows a zoomed in fluorescent photograph depicting the different levels of the invasion process: the boundary of the device, following cells, and leading cells. In order to view different cellular groups, the microscope focus needs to be adjusted.

The invading cells move toward the hypoxic stimulus at different rates. Figure 12A shows another example of an invading group of cells at day 4. Images like this can be measured for the total distance traveled. Figure 12B shows the results of plotting the distance travelled versus time. As can be seen, the rate of invasion is different for different devices.

a)

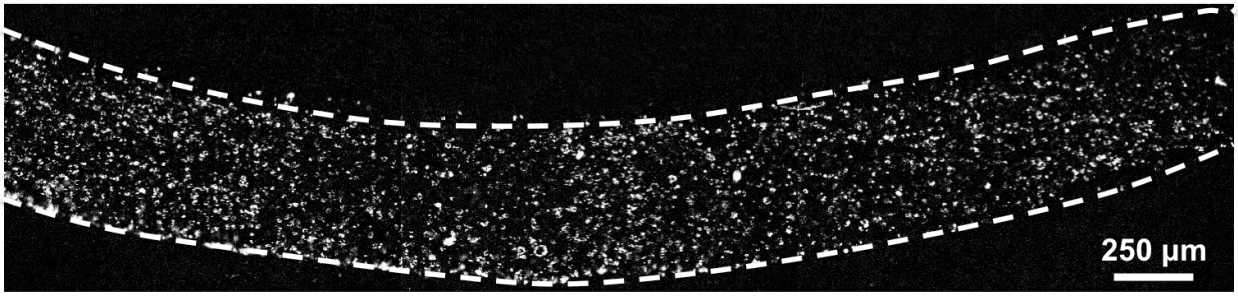


c)

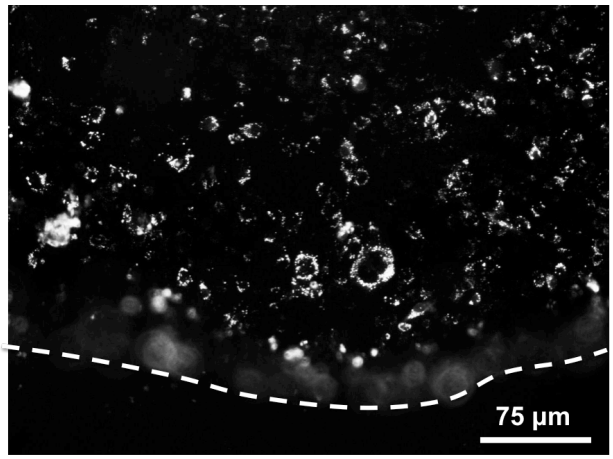


d)

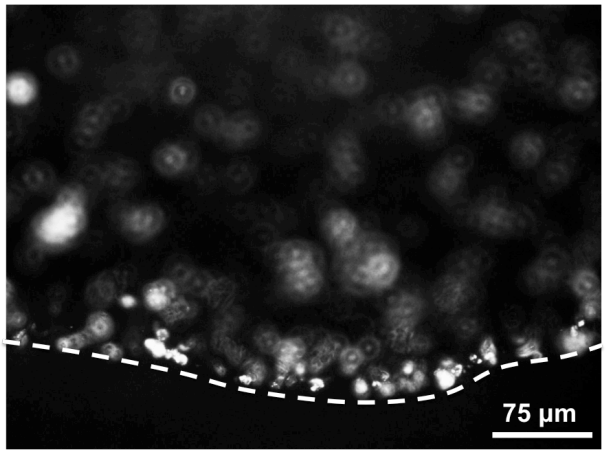


e)

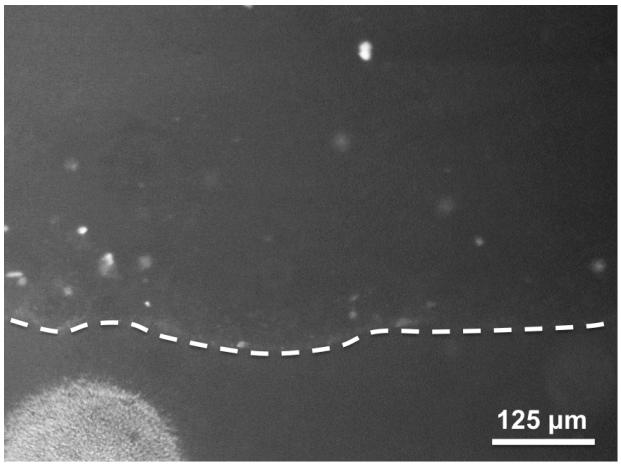


Figure 8. Hypoxic stimulus on endothelial cells. A) After 24 hours of culture within the platform, the cells cover the entirety of the microchannel. B, C) Cells grow on the bottom of the microchannels as well as on the walls of it. D) After exposing the cells to a hypoxic stimulus for 8 hours, most of the cells died off.

**a)**

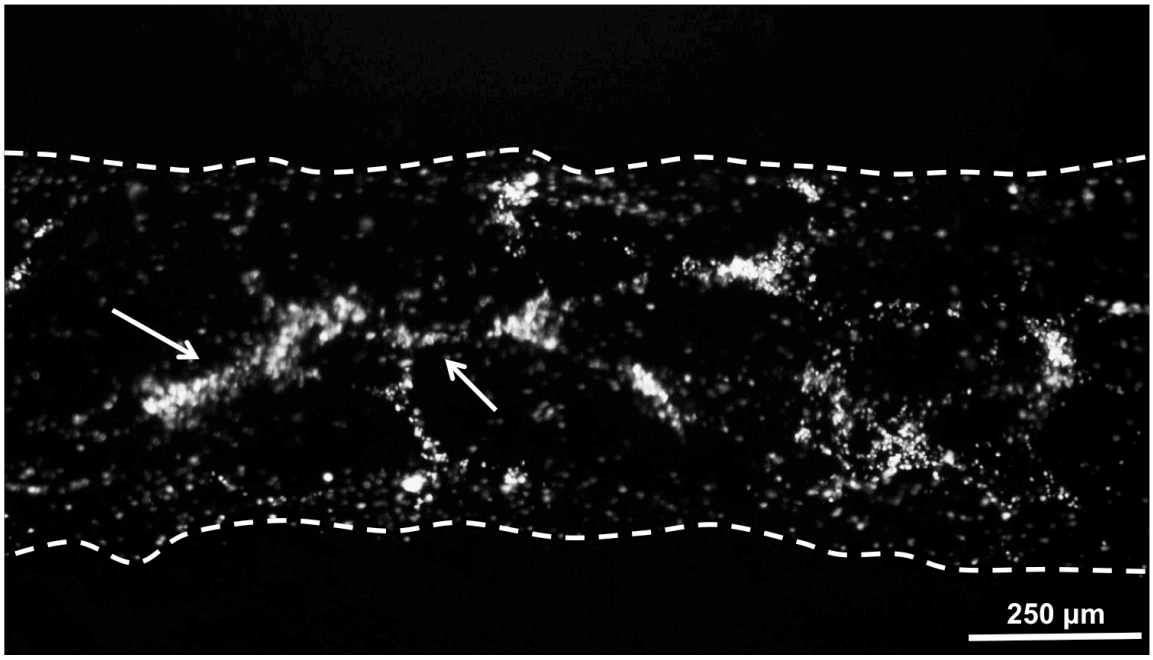


**b)**

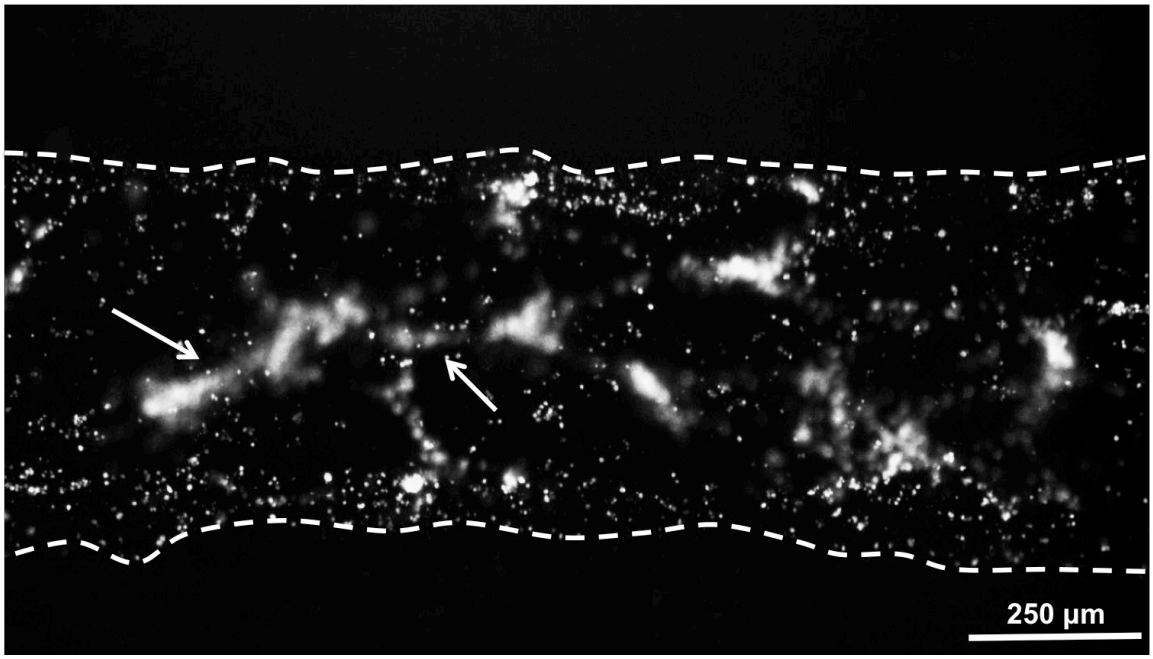


Figure 9. Network formation within the microchannels. A) After 4 days of constant oxygenation within the 3D oxygen platform, the endothelial cells were surviving on the platform. B) However, the cells on the top of the channel showed signs of tubular network formation.

a)

b)

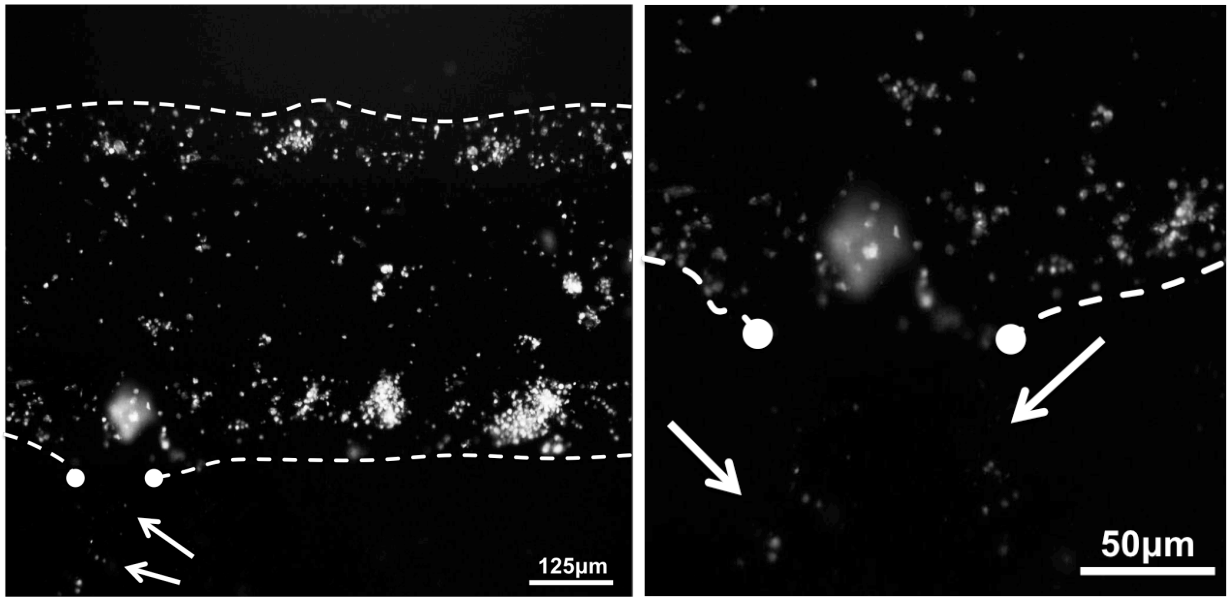


c)

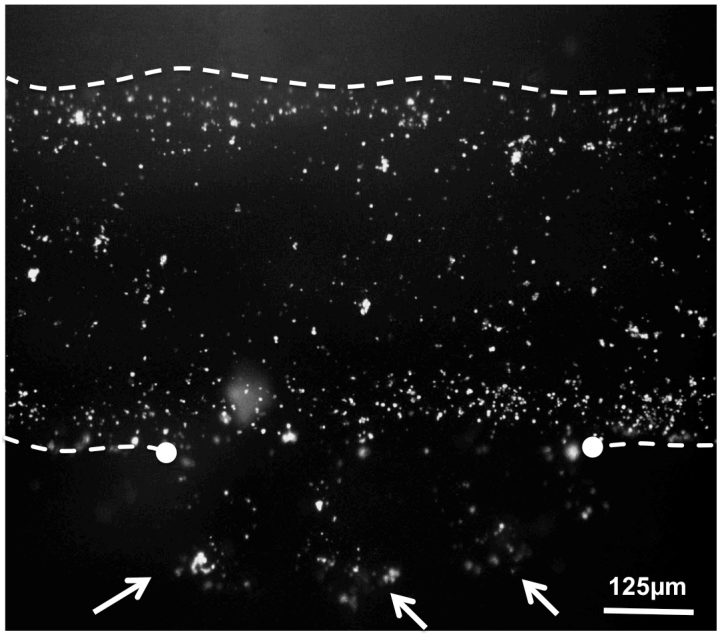


Figure 10. Collagen invasion. A) Small amount of cells start invading the collagen matrix two days after initial seeding. B) Two independent trails of cells are invading the matrix 4 days after seeding. C) Several groups of cells are actively invading the collagen matrix six days after seeding.

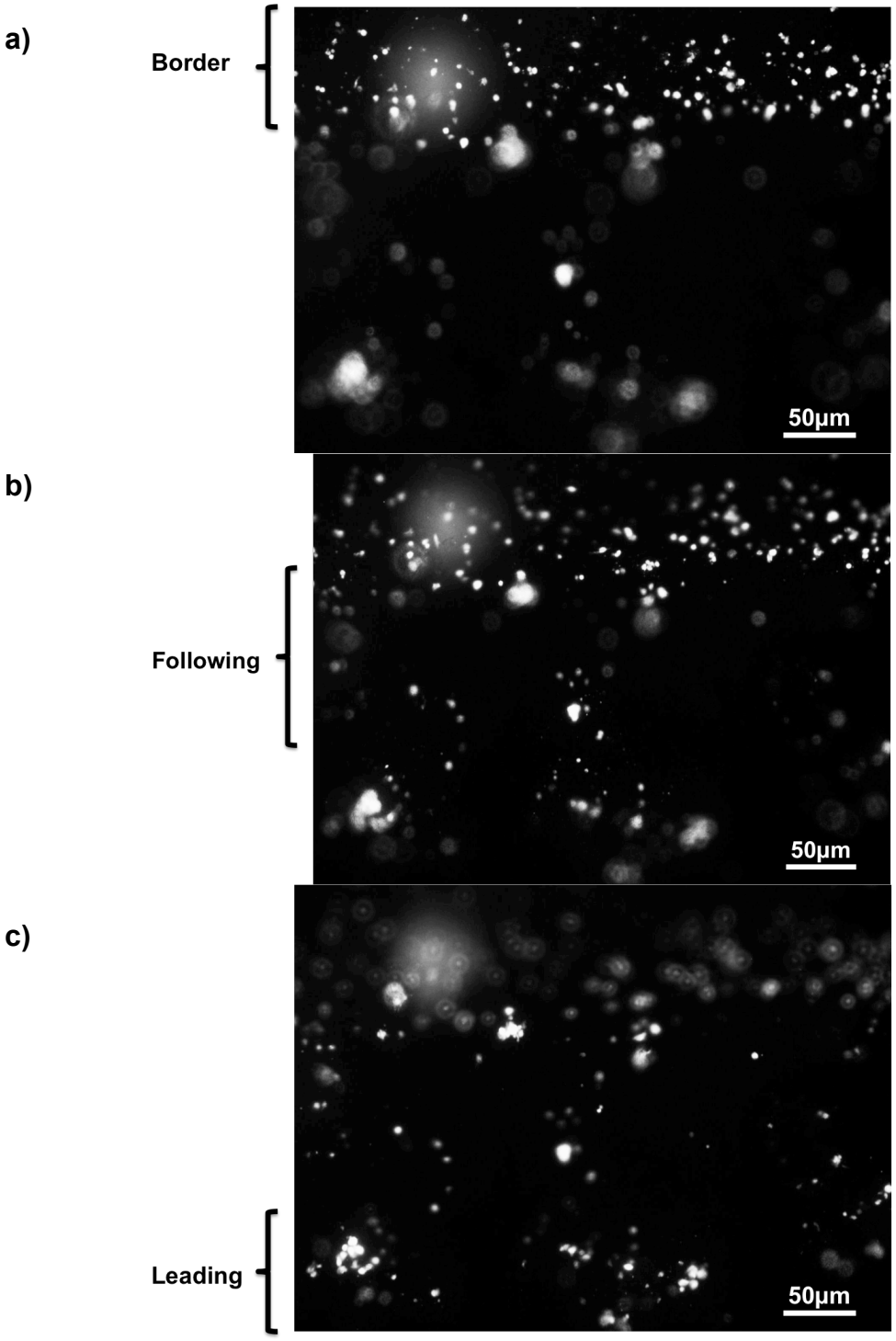


Figure 11. Groups of invading cells. Endothelial cells are seeded at different levels within the microfluidic platform. As such, when they invade, they can be visualized at different heights. A) Some cells can be seen in focus at the border of the channel. B) Some cells are following the leading cells and are remaining behind. C) The leading cells are looking for the hypoxic stimulus.

**a)**

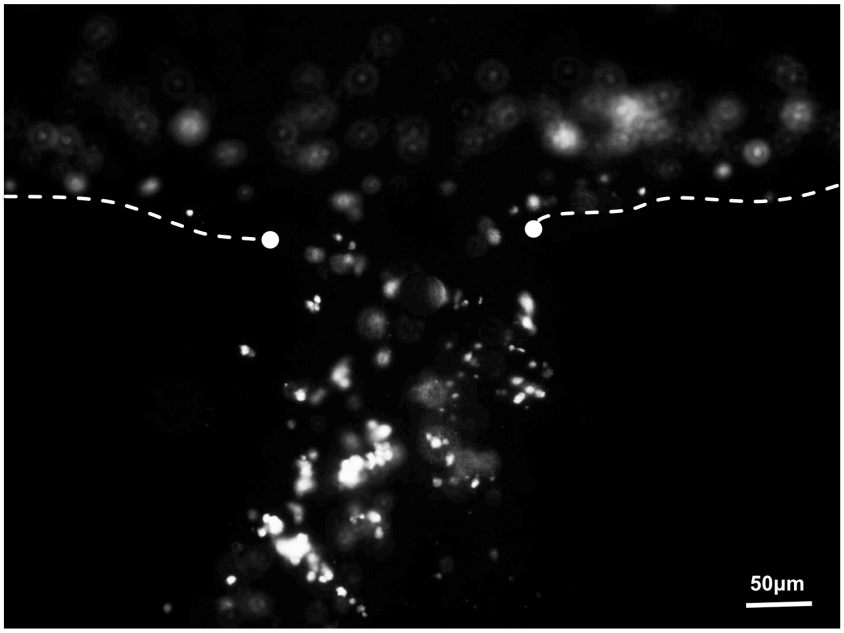


**b)**

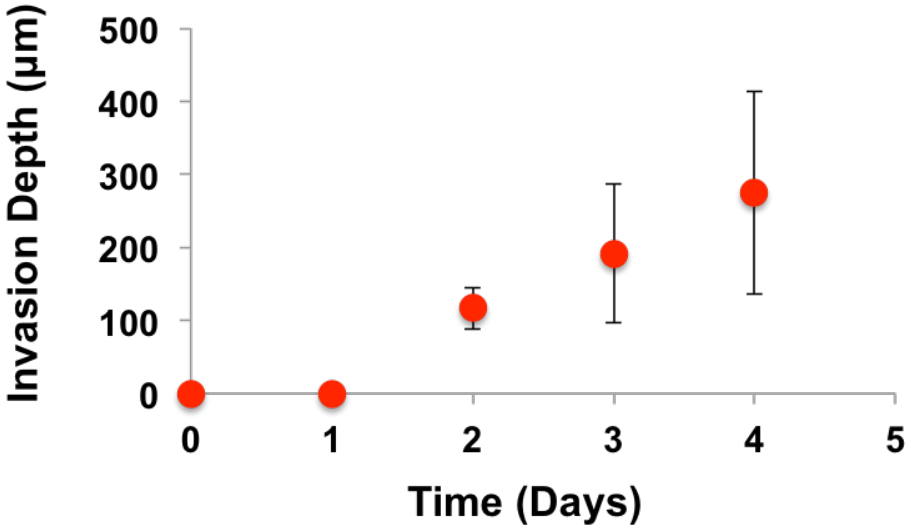


Figure 12. Invasion vs time. A) Cells seeded in the microfluidic platform started invading the collagen matrix by day 2. By day 4, a clear agglomeration of cells can be seen invading the collagen. B) By day 2, cells were within 100µm of the boundary channel. By the end of day 4, the endothelial cells were deep within the collagen with some cells moving as far as 400µm away.

## 2.6. Discussion

The mechanism by which cells and tissues respond to a hypoxic insult at the microscale level is a fundamental question in angiogenesis as well as in stroke research. The hippocampal acute brain slice preparation, with its defined cytoarchitecture, mechanical stability, and recognized sensitivity to oxygen variations, provides an *in vitro* model where the effect of oxygen deprivation on neuronal physiology can be studied in isolated detail (Medvedeva et al. 2009, Stork, Li 2009, Rambani et al. 2009). While neurogenesis possesses this three-dimensional platform for *in vitro* hypoxic studies, angiogenesis does not have a comparable *in vitro* platform where hypoxic research can be performed on a reliable basis. The ability to precisely control the spatiotemporal oxygen environment in a 3D platform, provides better insight into the relationship between oxygen and angiogenic function in the human body.

Oxygen microfluidic platforms have previously been used to control the spatiotemporal delivery of oxygen as well as improving oxygen delivery to tissues in culture (Mauleon, Fall & Eddington 2012). However, the 3D oxygen microfluidic platform used for this study is unique due to the fact that it does not rely on PDMS microchannels. As shown in figure 2, a subtractive method is employed where a sacrificial template is removed from the device; leaving behind open microchannels surrounded by a collagen matrix. The oxygen network is located on the top of the device and allows for quick and precise oxygenation of the cell culture.

An advantage of the 3D oxygen microfluidic platform is its customizability in the oxygen landscape and the microchannels themselves. By changing the master geometry, the gelatin template shape as well as the gas network can be reconfigured. As shown in

figure 3, a 100μM concentration of fluorescein isothiocyanate was delivered through each of the inlets of the microchannels. This image displays the delivery of FITC into the channels with four different geometries shown. The fluid is always driven via negative pressure by a syringe pump in order to avoid increased pressure within the platform.

In a similar manner, using the platinum based (PtOEPK) planar oxygen sensor, the oxygen landscape can be measured. As shown in figure 4, the two different oxygen microenvironments can be accurately measured and created by the 3D oxygen microfluidic platform. Each microchannel is completely exposed to only one oxygen stimulus, thereby making precise hypoxic studies possible.

Unlike previous oxygen platforms, the 3D oxygen microfluidic platform will not deliver the oxygen stimulus directly to the cultured cells. The oxygen will have to diffuse across a 300-micrometer collagen-filled chamber. Figure 5 shows how by using the platinum based oxygen sensor located at the bottom of the device, that it takes close to 60 minutes for the oxygen environment to equilibrate to 0% $O_2$. This result is longer than previous devices, but concurs with similar measurements taken with greater diffusion gaps (Oppegard et al. 2009).

This 3D oxygen microfluidic platform was developed to study the effect of a hypoxic insult on angiogenic culture. In order to show signs of angiogenesis, the cells must be exposed to a specific stimulus for extended periods of time. This study, exposes the cells to a hypoxic stimulus for a minimum of 24 hours. As shown in figure 6, even after this exposure time, the device shows stability and durability by producing the same oxygen gradient shown at the beginning of the experiment with no signs of drying.

The microfluidic device was endothelialized with endothelial cells by pipetting a

concentrated cell suspension into reservoirs and using negative pressure to draw the cells into the microfluidic channels. The device was then inverted onto parafilm in order to seed the top and the sides of the channels and placed in an incubator overnight. Figure 7 shows how the cells are indeed seeded in the device and can form a monolayer in the channels.

Oxygen alone is not known to be a highly proangiogenic factor. Utilizing a platform where only one of the microfluidic channels has been endothelialized, testing was conducted on whether a hypoxic stimulus was enough to show signs of sprouting. The first attempt involved exposing the cell culture to the hypoxic stimulus directly and figure 8 shows how most of the cells died during an 8 hours hypoxic stimulus.

For the next set of experiments, the endothelialized channel was exposed to a 21% $O_2$ environment, while the other side of the device was exposed to the hypoxic stimulus. This experimental protocol was successful in allowing the cells to survive for as long as six days within the oxygen platform. As shown in figure 9, by day 4, it is possible to see the endothelial cells start to agglomerate into tubular networks; a process that is expected in healthy endothelial culture. Furthermore, this experimental protocol was successful in showing signs of angiogenic behavior in the cell culture. Figure 12 shows how as early as 2 days after initial seeding, some signs of invasion into the collagen matrix can be observed. By day 4, some of the cells have moved as far as 400μm into the collagen matrix. However, this invasive movement is not uniform in the oxygen platforms. Some of the devices show a single group of cells invade the collagen (figure 12A), while some other devices originate with a small group of cells and eventually have as many as 4 different sets of invading cell clusters. An important factor to mention is

that while several groups of tip cells can be observed in this platform, the stalk cells that are expected from true angiogenic culture are not observed in this study. This can be explained by the lack of an angiogenic chemical factor, such as VEGF, in the microenvironment. It is possible that while the endothelial cells can respond to a hypoxic stimulus by becoming tip cells, the absence of a chemical factor prevents them from becoming a stalk cell. This is a key area of importance that should be expanded on in future studies.

## 2.7. Conclusion

Angiogenesis is the development of new capillary blood vessels that grow from preexisting vessels, this occurs as a normal body function for growth and healing but is also linked to pathological conditions (Folkman, Haudenschild 1980). Current *in vitro* studies of vascular physiology still rely on cultures of endothelial cells grown on centimeter scale plates, filters, and flow chambers (Vailhe, Vittet & Feige 2001). Additionally, hypoxic studies relied on the use of hypoxia and growth factors to stimulate sprouting angiogenesis (Folkman, Haudenschild 1980). However, current techniques offer no viable method of separating the angiogenic effects created by growth factors from those created by hypoxia. A microfluidic device was created that would allow analysis of hypoxic effect on the angiogenic process independent of growth factors. In this microfluidic device, we have a 3D microvasculature and complete oxygen control.

Using the 3D oxygen microfluidic platform it is possible to endothelialize microfluidic channels that are completely encased by a collagen matrix. The cells were grown in a 3D environment and exposed to a hypoxic stimulus for a period of 4 to 6 days. Results indicate that hypoxia alone is enough to start the sprouting process in an endothelialized channel. This is the first documented time that hypoxia is proven to be an angiogenic factor independently from other chemical factors. More studies should be conducted to expose what effect hypoxia has on cells at the genetic level and the main mechanisms involved. Nonetheless, this innovative and exciting model specifically illustrates the effect hypoxia has on angiogenic cell culture. The results of this study are paramount and demontrate a vital development in angiogenic research. Angiogenesis is a key component in numerous disease processess that greatly impact the human

population. This area needs to be further examined as it is a gateway to invaluable advancements in the biomedical field.

## CITED LITERATURE


Adair, T.H. & Montani, J.P. 2010, .

Baker, B.M., Trappmann, B., Stapleton, S.C., Toro, E. & Chen, C.S. 2013, "Microfluidics embedded within extracellular matrix to define vascular architectures and pattern diffusive gradients", *Lab on a chip,* vol. 13, no. 16, pp. 3246-3252.

Burri, P.H. & Tarek, M.R. 1990, "A novel mechanism of capillary growth in the rat pulmonary microcirculation", *The Anatomical Record,* vol. 228, no. 1, pp. 35-45.

Campbell, P.G. & Weiss, L.E. 2007, "Tissue engineering with the aid of inkjet printers", *Expert opinion on biological therapy,* vol. 7, no. 8, pp. 1123-1127.

Carmeliet, P., De Smet, F., Loges, S. & Mazzone, M. 2009, "Branching morphogenesis and antiangiogenesis candidates: tip cells lead the way", *Nature reviews.Clinical oncology,* vol. 6, no. 6, pp. 315-326.

Chrobak, K.M., Potter, D.R. & Tien, J. 2006, "Formation of perfused, functional microvascular tubes *in vitro*", *Microvascular research,* vol. 71, no. 3, pp. 185-196.

Du, Y., Ghodousi, M., Qi, H., Haas, N., Xiao, W. & Khademhosseini, A. 2011, "Sequential assembly of cell-laden hydrogel constructs to engineer vascular-like microchannels", *Biotechnology and bioengineering,* vol. 108, no. 7, pp. 1693-1703.

Folkman, J. & Haudenschild, C. 1980, "Angiogenesis *in vitro*", *Nature,* vol. 288, no. 5791, pp. 551-556.

Gerhardt, H. 2008, "VEGF and endothelial guidance in angiogenic sprouting", *Organogenesis,* vol. 4, no. 4, pp. 241-246.

Golden, A.P. & Tien, J. 2007, "Fabrication of microfluidic hydrogels using molded gelatin as a sacrificial element", *Lab on a chip,* vol. 7, no. 6, pp. 720-725.

Hasan, A., Paul, A., Vrana, N.E., Zhao, X., Memic, A., Hwang, Y.S., Dokmeci, M.R. & Khademhosseini, A. 2014, "Microfluidic techniques for development of 3D vascularized tissue", *Biomaterials,* vol. 35, no. 26, pp. 7308-7325.

Haycock, J.W. 2011, "3D cell culture: a review of current approaches and techniques", *Methods in molecular biology (Clifton, N.J.),* vol. 695, pp. 1-15.

Mauleon, G., Fall, C.P. & Eddington, D.T. 2012, "Precise Spatial and Temporal Control of Oxygen within *In Vitro* Brain Slices via Microfluidic Gas Channels", *PLoS ONE,* vol. 7, no. 8, pp. e43309.

Medvedeva, Y.V., Lin, B., Shuttleworth, C.W. & Weiss, J.H. 2009, "Intracellular Zn2+ accumulation contributes to synaptic failure, mitochondrial depolarization, and cell death in an acute slice oxygen-glucose deprivation model of ischemia", *The Journal of neuroscience : the official journal of the Society for Neuroscience,* vol. 29, no. 4, pp. 1105-1114.

Mosadegh, B., Huang, C., Park, J.W., Shin, H.S., Chung, B.G., Hwang, S.K., Lee, K.H., Kim, H.J., Brody, J. & Jeon, N.L. 2007, "Generation of stable complex gradients across two-dimensional surfaces and three-dimensional gels", *Langmuir : the ACS journal of surfaces and colloids,* vol. 23, no. 22, pp. 10910-10912.

Oppegard, S.C., Nam, K.H., Carr, J.R., Skaalure, S.C. & Eddington, D.T. 2009, "Modulating temporal and spatial oxygenation over adherent cellular cultures", *PloS one,* vol. 4, no. 9, pp. e6891.

Qutub, A.A., Liu, G., Vempati, P. & Popel, A.S. 2009, "Integration of angiogenesis modules at multiple scales: from molecular to tissue", *Pacific Symposium on Biocomputing.Pacific Symposium on Biocomputing,* , pp. 316-327.

Rambani, K., Vukasinovic, J., Glezer, A. & Potter, S.M. 2009, "Culturing thick brain slices: an interstitial 3D microperfusion system for enhanced viability", *Journal of neuroscience methods,* vol. 180, no. 2, pp. 243-254.

Ribatti, D., Nico, B. & Crivellato, E. 2015, "The development of the vascular system: a historical overview", *Methods in molecular biology (Clifton, N.J.),* vol. 1214, pp. 1-14.

Stork, C.J. & Li, Y.V. 2009, "Rising zinc: a significant cause of ischemic neuronal death in the CA1 region of rat hippocampus", *Journal of cerebral blood flow and metabolism : official journal of the International Society of Cerebral Blood Flow and Metabolism,* vol. 29, no. 8, pp. 1399-1408.

Unger, M.A., Chou, H.P., Thorsen, T., Scherer, A. & Quake, S.R. 2000, "Monolithic microfabricated valves and pumps by multilayer soft lithography", *Science (New York, N.Y.),* vol. 288, no. 5463, pp. 113-116.

Vailhe, B., Vittet, D. & Feige, J.J. 2001, "*In vitro* models of vasculogenesis and angiogenesis", *Laboratory investigation; a journal of technical methods and pathology,* vol. 81, no. 4, pp. 439-452.

Vernon, R.B., Lara, S.L., Drake, C.J., Iruela-Arispe, M.L., Angello, J.C., Little, C.D., Wight, T.N. & Sage, E.H. "Organized type I collagen influences endothelial patterns during ``spontaneous angiogenesis *in vitro*'': Planar cultures as models of vascular development", *In Vitro Cellular \& Developmental Biology - Animal,* vol. 31, no. 2, pp. 120-131.

Vickerman, V., Blundo, J., Chung, S. & Kamm, R. 2008, "Design, fabrication and implementation of a novel multi-parameter control microfluidic platform for three-dimensional cell culture and real-time imaging", *Lab on a chip,* vol. 8, no. 9, pp. 1468-1477.

Zheng, Y., Chen, J., Craven, M., Choi, N.W., Totorica, S., Diaz-Santana, A., Kermani, P., Hempstead, B., Fischbach-Teschl, C., Lopez, J.A. & Stroock, A.D. 2012, "*In vitro* microvessels for the study of angiogenesis and thrombosis", *Proceedings of the National Academy of Sciences of the United States of America,* vol. 109, no. 24, pp. 9342-9347.

# APPENDIX A

## HYPOXIA TOLERANCE OF THE MAMMALIAN NERVOUS SYSTEM UNDER SPATIALLY CONTROLLED OXYGEN CONDITIONS

### Introduction

The brain slice preparation is an excellent model for studying neuronal specialization in the brains of mammals, especially tolerance of neurons to extreme oxygen deprivation. Interface type chambers are commonly used in electrophysiology studies to determine the effect of hypoxia on the brain tissue. In these chambers, the brain slice is kept at the interface between the liquid and the gas. Placing of electrodes is facilitated by the open nature of the design. However, inverted microscopes cannot be used with this method and these types of chambers provide no spatial control for the hypoxic stimulus; therefore recreating a localized response is not possible.

Using microfluidic/microfabrication techniques, an open well microfluidic device was fabricated, characterized, and optimized. The microfluidic device can be categorized as a submerged type chamber in which the brain slice is completely submerged by the aCSF. The open nature of the device allows for easy placement of electrodes as well as imaging. The slice is in direct contact with a gas-permeable membrane making oxygen diffusion more efficient. A microchannel enables rapid and efficient control of oxygen and can be modified to allow a different region of the slice to experience different oxygen conditions, something that is not easily obtainable with current techniques. Marrying this technology with electrophysiological and imaging techniques, the biological mechanisms that allow hypoxia tolerance in the nervous system will be investigated.

**Materials and Methods**

As shown in figure A1, experiments were performed on interface type chambers as well as in the microfluidic device. The microfluidic device consists of a glass slide for support, a microfluidic channel delivering oxygen, a 100μm thick membrane, and a custom-made perfusion chamber where the slices are placed and submerged under artificial cerebral spinal fluid (aCSF).

Experiments were carried out on male and female wild type C57BL/6 mice at 2-3 months of age. 400μm thick hippocampal slices were used. Stimulation electrodes were placed in the CA1 and population recordings of extracellular synaptic fields potentials were made with micropipettes also in the CA1.

Oxygenated and deoxygenated aCSF was used as the stimulus for the interface type chamber experiments. Baseline oxygenated conditioned (95% $O_2$/ 5% $CO_2$) data was taken for at least 10 minutes before a hypoxic (95% $N_2$/ 5% $CO_2$) stimulus was applied. Hypoxia was maintained until fiber volleys evoked were eliminated, a condition called anoxic depolarization.

Data recorded shows the average of the signals as well as the amplitude of the field excitatory postsynaptic potentials (fEPSP).

**Results**

As can be seen in figure A2, the microfluidic device allows complete temporal and spatial control over the hypoxic insult. Figure A3 shows the placement of the electrodes on the hippocampal brain slice. Figure A4 shows the data recorded during field potential experiments. During 4 minutes of hypoxia, the device creates the hypoxic environment that leads to a decrease in the amplitude of the synaptic field potentials recording as expected. After 4 minutes of hypoxia, the device reverts back to its initial settings, however, the effects of the hypoxia lead to cell death in this example.

**Discussion/Conclusion**

Interface type chambers are commonly used in hypoxia-based electrophysiology studies. These chambers use flowing humidified oxygen gas over the brain slice and oxygenated artificial cerebrospinal fluid (aCSF) to control the oxygen environment. However, the chambers are unable to provide spatial control for the hypoxic stimulus. Microfluidic technology has provided neuroscience with the tools necessary to perform powerful yet elegant brain slice experiments. Using the microfluidic device, it is possible to control the oxygen environment inside the perfusion chamber, thus allowing the studies of hypoxia effects on mammalian brain tissue.

During this study, field excitatory postsynaptic potentials (fEPSP) were measured during a period of hypoxia. An EPSP is a small depolarization of the postsynaptic membrane potential. This is caused by the flow of positive ions into the neuronal body. The stimulating electrodes cause this flow to occur. Meanwhile, the percent change in the fEPSP amplitude at the end of the stimulus is taken as the acute response of the cells to hypoxia.

Figure 4 shows how during hypoxia, synaptic transmission is blocked as the field EPSP responses decreased to nearly 0%. The change in the signal demonstrates that the device is able to produce a reliable hypoxic episode. The microfluidic device is able to replicate results obtained from interface type chambers. Compared to current slice chambers ideal for electrophysiology and imaging access, the device improves control of oxygen within the brain slice to the microscale precision

As was previously mentioned, localized deoxygenation during electrophysiology experiments was not possible to do in a reliable manner. Hypoxia research, which uses

population recordings of synaptic fields potentials to assess the effects of hypoxia on neuronal cells, is a prime candidate to take advantage of this technology.

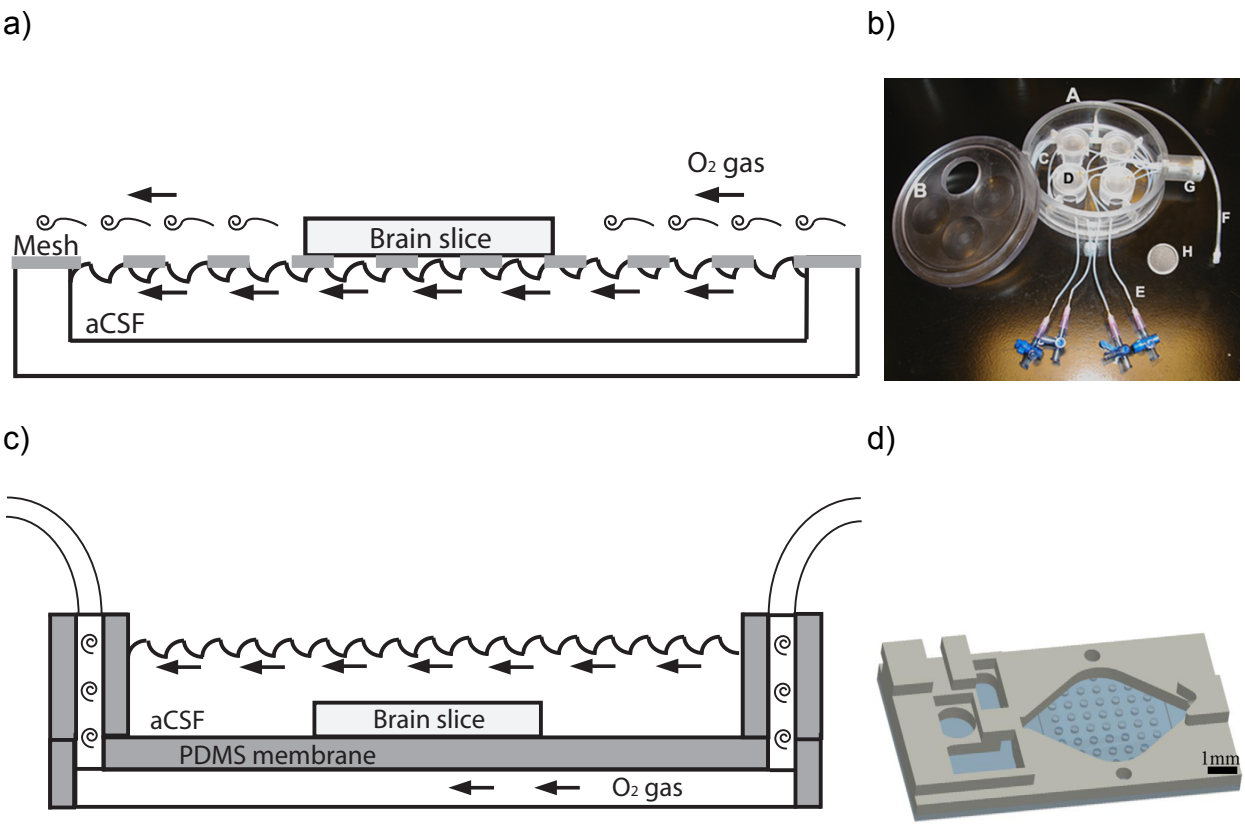


Figure A1. Electrophysiology chambers. A) Schematic of the interface type chamber where the brain slice is kept at the interface between the liquid and the gas. Placing electrodes is facilitated by the open nature of the design. However, inverted microscopes cannot be used with this method. B) Picture showing a standard interface type chamber. C) The PDMS microfluidic device allows rapid and efficient diffusion of oxygen to the brain slice. Due to its open well structure, electrodes and fluorescent microscopy are possible. D) 3D model showing the PDMS microfluidic device.

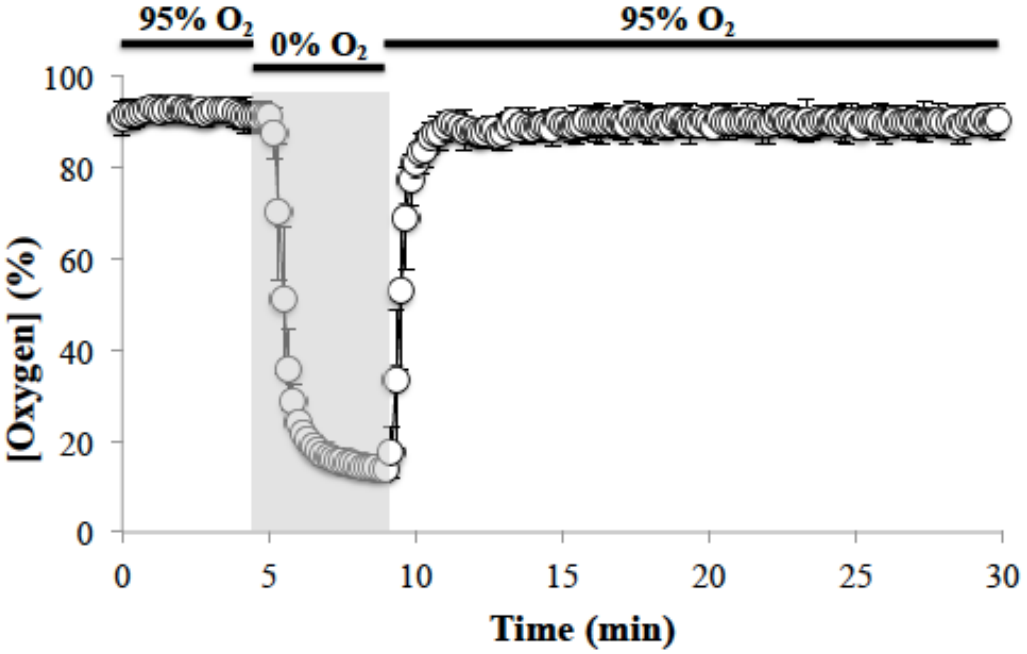


Figure A2. Precise oxygen control. The oxygen concentration was measured in the aCSF. The microfluidic device can create a hypoxic stimulus for a predetermined time period.

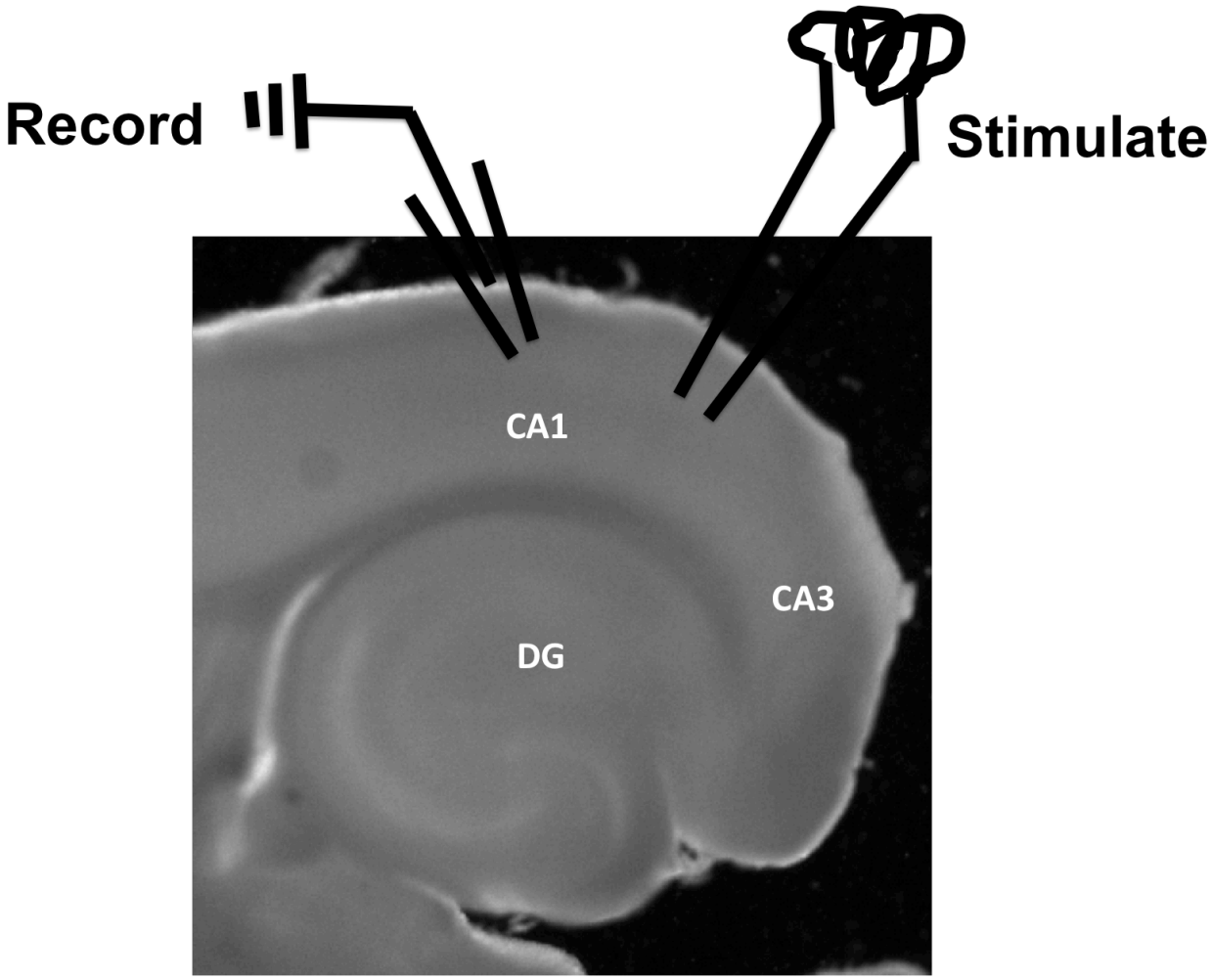


Figure A3. Electrode placement. Recordings were made in hippocampal brain slices. Stimulation electrodes were placed in the CA1. Population recordings of field excitatory postsynaptic potentials (fEPSP) were made with micropipettes also in the CA1.

a)

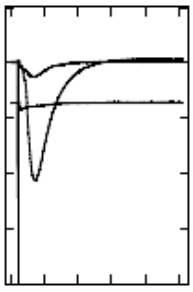

**Interface type chamber**

b)

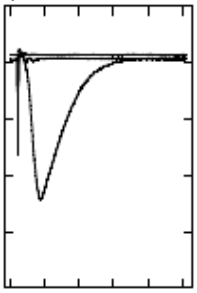

**Microfluidic device**

c)

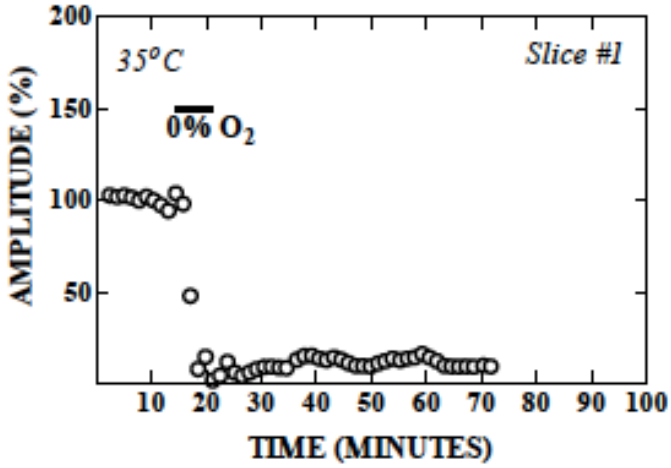


d)

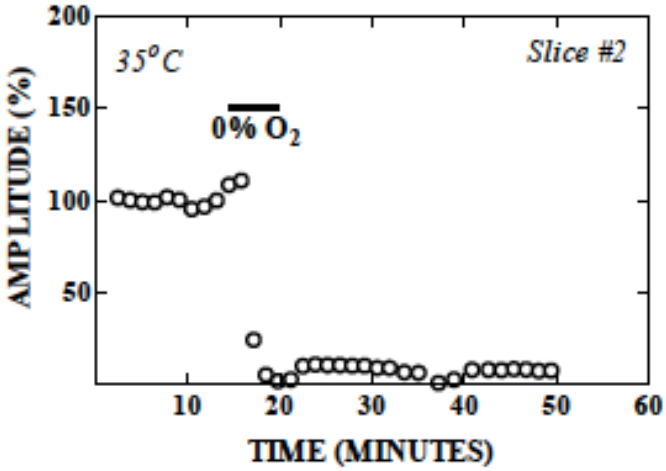


Figure A4. Effect of hypoxia on a brain slice. A,B) A series of responses (each trace is an average of four consecutive recordings) to an electrical stimulus at constant current in a slice placed in an interface type chamber and the microfluidic device. C) Graph of field EPSP amplitdue as a function of time. Perfusion of deoxygenated aCSF provided the hypoxic stimulus. D) The microfluidic device is able to replicate the responses obtained by the interface type chambers.

## APPENDIX B

### Oxygen sensor characterization

The oxygen concentration created by the microfluidic devices can be characterized using the fluorophore PtOEPK (platinum (II) octaethylporphine ketone). The fluorescence of PtOEPK is quenched in the presence of oxygen, as such, calibration of the sensor can be done using 5% $CO_2$, balanced nitrogen and 5% $CO_2$, balanced air prior to the experiment. Fluorescent intensities of the computer controlled scanning images can be converted to oxygen values by solving the Stern-Volmer equation.

The Stern-Volmer equation determines how a chemical species decays in the presence of another chemical species.

$$Eq.3 \qquad A^* + Q \rightarrow Q + A$$

where $A^*$ is a chemical species in the excited state, Q is the quencher, and A is the chemical species in the resting state. For these studies, Q will be the oxygen molecules, while $A^*$ will be the PtOEPK sensor during hypoxia. In order to obtain the oxygen measurements, the kinetics of the quenching of the oxygen sensor must be solved.

$$Eq.4 \qquad \frac{I_f^0}{I_f} = 1 + k_q \tau_0 * [Q]$$

where $I_f^0$ is the intensity of the sensor in hypoxic conditions, $I_f$ is the intensity of the sensor during normoxic conditions, $k_q$ is the quencher rate coefficient, $\tau_0$ is the fluorescence lifetime of the PtOEPK sensor, and Q is the oxygen concentration in the environment.

Figure B1 shows a typical fluorescent image scan obtained with the PtOEPK sensor. From these images, a Matlab code can be used to obtain the oxygen concentration generated by the devices. In figure B2, the fluorescent image is shown to correlate with the oxygen values shown in the graph.

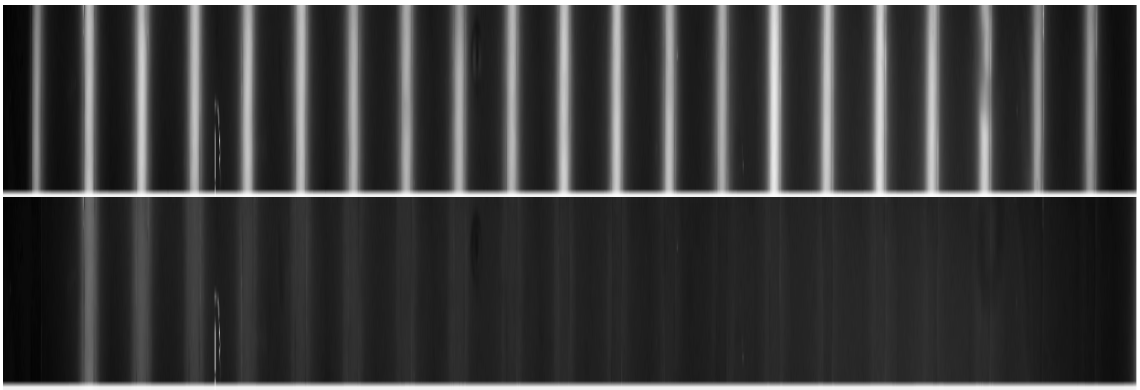

Figure B1. Fluorescent image scans showing 0% oxygen in all top channels. The bottom image shows the gradients formed when the 3D printed oxygen mixer is used.

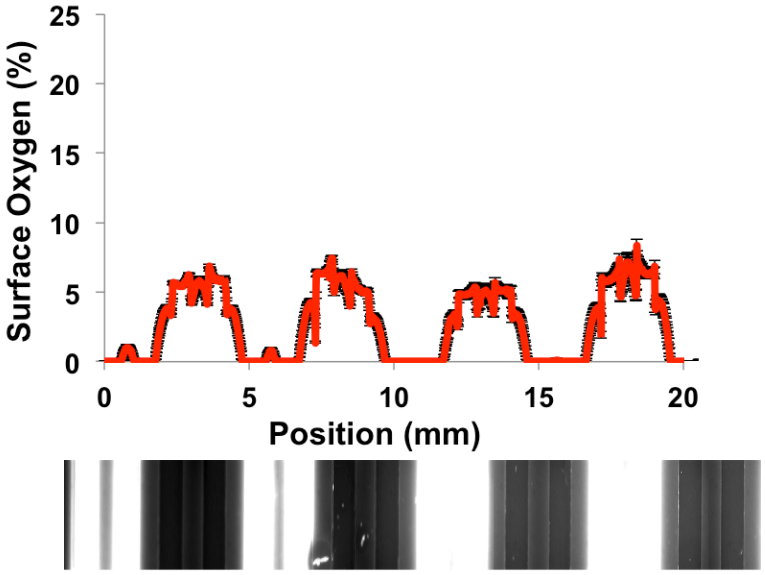


Figure B2. Surface oxygen graph correlates to the fluorescent scanning image shown below. Bright areas indicate hypoxic zones, while dark areas indicate high oxygen zones.

Megan Rexius created the following Matlab code. It takes 0% and 21% fluorescent intensities baselines, as well as the experimental data as inputs. The output of the code is the actual oxygen percentages correlated to the fluorescent data.

Command Window will need the following data:

```
zeropercent=xlsread(File location);                    % 0% oxygen
twentyonepercent=xlsread(File location);               % 21% oxygen
INT=xlsread(File location);                            % Experimental data
sternvolmer030513                                      % m. file
```

The m. file:

```
r= size(twentyonepercent, 1);
for i= 1:size(twentyonepercent,1)
    I1(i,1)= twentyonepercent(i,3);

    X1 = 21;
    I2(i,1)= zeropercent(i,3);
    X2=0;

    kt(i,1)= (I2(i,1)-I1(i,1))/((X1*I1(i,1))-(X2*I2(i,1)));
    I0(i,1)= (1+kt(i,1)*X1)*I1(i,1);

    x1 = 0:1:22;
    y1(i,:)= I0(i,1)./(1+kt(i,1)*x1);
    oxygenpercent(i,:) = ((I0(i,1)./INT(i,3))-1)/kt(i,1);
    hold on
end

plot(INT(:,2), oxygenpercent)
% axis([-10 30 0 7000])
```

## APPENDIX C

### Oxygen sensor characterization with smoothing component

The oxygen data obtained during the 3D oxygen microfluidic platform studies showed that the addition of a collagen matrix created some noise in the oxygen measurements. In order to account for this extra noise, a new Matlab code was used that had a smoothing component added to it.

Esther Shin created the following Matlab code. It takes 0% and 21% fluorescent intensities baselines, as well as the experimental data as inputs. The output of the code is the actual oxygen percentages correlated to the fluorescent data.

The m. file:

```
clear; clc; close all

font_size = 12; font_axes = 12;

%% load a data file
data = xlsread(File location);

signal = data(:,1); %setting data as a column matrix
N = length(signal); %size of data
sample_index = (1:N); %indexing through values for x-axis
idx = find(isnan(signal)==1); %finds values that are "NAN"
if ~isempty(idx),
   signal(idx) = []; sample_index(idx) = []; %sets NAN cells to empty and index values to
an empty cell
   signal = interp1(sample_index, signal, (1:N), 'linear'); %fills in empty cells to linear
interpolation values
end

figure(1), clf; plot(signal, 'linewidth', 2); grid; %figure 1 plots original signal with outliers
replaced by interpolation values
   title('data', 'fontsize', font_size); ylabel('noisy data samples', 'fontsize', font_size);
   xlabel('samples', 'fontsize', font_size); set(gca, 'fontsize', font_axes);
   set(gca, 'xlim', [0, N]); drawnow %sets x-axis to size of signal

%% apply a triangular window to smooth the data: low-pass filter to suppress noise
figure(2), clf;
for kk=1:4,
```

```
   if kk==1,
      Wlng = 21; % length of the triangular window to examine best triangle window
value
   elseif kk==2,
      Wlng = 41;
   elseif kk==3,
      Wlng = 61;
   elseif kk==4,
      Wlng = 81;
   end

   sm_signal = function_triangle_window(signal, Wlng); %plot for different triangle
window values to compare
   figure(2), subplot(4,1,kk), plot(sm_signal, 'linewidth', 2); grid;
      if kk==1,
         title('smoothed data', 'fontsize', font_size);
      elseif kk==4,
         xlabel('samples', 'fontsize', font_size);
      end
      ylabel(['L_{window} = ', num2str(Wlng)], 'fontsize', font_size);
    set(gca, 'fontsize', font_axes); set(gca, 'xlim', [0, N]);
    set(gca, 'ylim', [-5 25]); drawnow
end

%% decide the window length based on Figure 2 and estimate the slope
Wlng = 81; %setting window length
sm_signal = function_triangle_window(signal, Wlng); %setting signal to the smoothed
signal
% hist_bins = (0:1:25); Nhist_bins = length(hist_bins); %creates range for histogram
% Nhist = hist(sm_signal, hist_bins); %plots histogram based on previous values
figure(3), %subplot(211),
      plot(sm_signal, 'linewidth', 2); grid; %plots filtered signal
      title(['smoothed data with L_{window} = ', num2str(Wlng)], 'fontsize', font_size);
      xlabel('samples', 'fontsize', font_size);
      set(gca, 'fontsize', font_axes); set(gca, 'xlim', [0, N]); drawnow

return
```

The smoothing function file:

```
function sm_signal = function_triangle_window(signal, Wlng)

signal = signal(:); %makes signal into a column vector

if rem(Wlng, 2)==0, Wlng = Wlng + 1; end %making window an odd number
Wlng2f = floor(Wlng/2);
tri1d = triang(Wlng);

row = size(signal, 1); %setting size to the same as column vector size

temp1 = zeros(row, 1); %creates a vector of zeros
inx_column = find(signal~=0);
if ~isempty(inx_column), temp1(inx_column(1):inx_column(end)) = 1; end

temp = zeros(row+2*Wlng2f, 1);
temp(Wlng2f+1:Wlng2f+row,1) = temp1;

data = zeros(size(temp));
data(Wlng2f+1:Wlng2f+row,1) = signal; %inserts 0s in the front and back of data

sm_signal = zeros(size(data)); %resolving memory
inx_column = find(data~=0); %finds indexes where data is not 0
for k1=inx_column(1):inx_column(end), %looping through data to find weighted sum
   windowed_data = data(k1-Wlng2f:k1+Wlng2f,1);
   windowed_temp = temp(k1-Wlng2f:k1+Wlng2f,1);
   weighted_data = windowed_data .* tri1d;
   weights = windowed_temp .* tri1d;
   sm_signal(k1,1) = sum(weighted_data) / sum(weights);
end

sm_signal = sm_signal(Wlng2f+1:Wlng2f+row); %smoothed data points

return
```

## APPENDIX D

**Permission to use previously published material: Journal of Neuroscience Methods, PLOS ONE, Lab on a Chip, and the Journal of Undergraduate Research at UIC allow me to use the work in my dissertation.**

## Journal of Neuroscience Methods

Do I need to request permission to text mine Elsevier content? +

Can I post my article on ResearchGate without violating copyright? +

Can I post on ArXiv? +

Can I include/use my article in my thesis/dissertation? +

Yes. Authors can include their articles in full or in part in a thesis or dissertation for non-commercial purposes.

Which uses of a work does Elsevier view as a form of 'prior publication'? +

Can I include/use my article in my thesis/dissertation?
Yes. Authors can include their articles in full or in part in a thesis or dissertation for non-commercial purposes.

## PLOS ONE

PLOS applies the Creative Commons Attribution (CC BY) license to works we publish. This license was developed to facilitate open access – namely, free immediate access to, and unrestricted reuse of, original works of all types.

Under this license, authors agree to make articles legally available for reuse, without permission or fees, for virtually any purpose. Anyone may copy, distribute or reuse these articles, as long as the author and original source are properly cited.

### Using PLOS Content

No permission is required from the authors or the publishers to reuse or repurpose PLOS content provided the original article is cited. In most cases, appropriate attribution can be provided by simply citing the original article.

Using PLOS Content
No permission is required from the authors or the publishers to reuse or repurpose PLOS content provided the original article is cited. In most cases, appropriate attribution can be provided by simply citing the original article.

## Lab on a Chip

As scientific research is becoming more open and discoverable, the Royal Society of Chemistry supports our community of chemical scientists in sharing new research findings before and after publication through a variety of methods.

Authors publishing in our journals may present their research ahead of publication in the following ways.

- Through the deposition of a preprint version of the article in non-commercial repositories (eg ArXiv), institutional repositories or authors' individual websites - a preprint is defined here as an un-refereed author version of the article; a non-commercial repository is defined here as any platform or archiving service that makes digital content free to deposit and access
- At scientific conferences; this includes recorded presentations, poster presentations and abstracts that are made openly available online
- In commercial or non-commercial databases (data without interpretation, discussion, conclusions or context with a wider experimental project)
- In an open electronic lab notebook
- In blogs, wikis, tweets, and other informal communication channels
- As a thesis or dissertation published as part of an academic or professional qualification, in print and online
- In any digital medium which is operated by the Royal Society of Chemistry, excluding journals, books and magazines

Authors publishing in our journals may present their research ahead of publication in the following ways.
• As a thesis or dissertation published as part of an academic or professional qualification, in print and online

## Journal of Undergraduate Research at UIC



This publication is copyrighted by the University of Illinois at Chicago.

# Gerardo Mauleon

## EDUCATION

**Doctor of Philosophy, Bioengineering**
University of Illinois at Chicago, Chicago, IL — Expected June 2016
Advisor: David Eddington, PhD
Dissertation: 3D Oxygen Microfluidic Platform for In Vitro Hypoxic Studies

**Master of Science, Bioengineering**
University of Illinois at Chicago, Chicago, IL — 2011
Overall GPA: 4.00/4.00
Advisor: David Eddington, PhD
Thesis: Stroke on a Chip: Spatial and Temporal Control of Oxygen for In Vitro Brain Slices

**Bachelor of Science, Bioengineering**
University of Illinois at Chicago, Chicago, IL — 2009
Overall GPA: 3.81/4.00
Advisor: G Ali Mansoori, PhD
Project: Melanoma Prevention Through Nanotechnology

**Associates Degree, Engineering**
William Rainey Harper College, Palatine, IL — 2007
Overall GPA: 3.85/4.00

## RESEARCH EXPERIENCE

**Biological Microsystems Laboratory**
David Eddington, PhD
University of Illinois at Chicago, Department of Bioengineering — July 2009- Present

- Design and construct micro-scale devices using lithography methods
- Direct multiple collaborative projects that implement my microfluidic devices in areas as diverse as neuroscience, psychiatry, and pharmacology
- Perform image analysis on brain tissue slices and angiogenic cell cultures
- Successfully completed animal surgery training courses and protocols
- Supervised and trained students in the lab setting

**Thermodynamics Research Laboratory**
G Ali Mansoori, PhD
University of Illinois at Chicago, Department of Bioengineering — July 2008- June 2009

- Used computational methods to predict the formation of self-assembling monolayers on the upper layer of the skin in an effort to block UV-light

**Pulmonary, Critical Care, Sleep and Allergy Laboratory**
Irena Levitan, PhD
University of Illinois at Chicago, College of Medicine — August 2008- May 2009

- Created hybrid scaffolds using Polydimethylsiloxane (PDMS) and collagen
- Cultured and maintained human Embryonic Stem Cells

**Dermatology Department**
Claudia Hernandez, MD
University of Illinois at Chicago, College of Medicine — April 2008- May 2009

- Developed melanoma education and prevention program for Spanish-speaking healthworkers
- Acquisition, analysis and interpretation of data

## TEACHING/ MENTORING EXPERIENCE

**Teaching Assistant**
University of Illinois at Chicago, Department of Bioengineering Spring 2015
Professor: Terry Layton, PhD
Course: BioE 410: FDA and ISO Requirements for the Development and Manufacturing of Medical Devices

- Tutored and assisted students with assignments and course concepts
- Served as guest lecturer and graded presentations

**Guest Lecturer**
University of Illinois at Chicago, Department of Bioengineering Spring 2015
Professor: Daniela Valdez-Jasso, PhD
Course: BioE 102: Bioengineering Freshman Seminar

- Created a lecture showcasing the work done at the Biological Microsystems Laboratory

**Mentor**
University of Illinois at Chicago, Department of Bioengineering August 2013- Present
Student: Felix Morales
Course: HON 225: Undergraduate Research Assistant Program

- Trained student to develop, manufacture, and test microfluidic devices with the goal of manipulating the oxygen conditions experienced by cells.
- Tutored student in bioengineer undergraduate courses
- Gained experience in becoming a great communicator with mentee
- Mentees early research has been published in the UIC Bioengineering Student Journal with the latest research in preparation to be published in a major scientific journal

**Mentor**
University of Illinois at Chicago, Department of Bioengineering May 2013- Present
Student: Shauharda Khadka
Course: Summer Undergraduate Internship

- Trained student to fabricate, characterize, and apply microfluidic oxygenation devices to cells
- Research culminated with publication into the Journal of Undergraduate Research

## PUBLICATIONS

Rexius ML, **Mauleon G**, Malik AB, Rehman J, Eddington DT (2014). "Microfluidic Platform Generates Oxygen Landscapes for Localized Hypoxic Activation," Lab on a Chip, 14(24): 4688-4695

Khadka S, **Mauleon G**, Eddington DT (2014). "Fabrication of Oxygenation Microfluidic Devices for Cell Cultures," Journal of Undergraduate Research, 7(1): 5-9

Hernandez C, Kim H, **Mauleon G**, Ruiz A, Robinson JK, Mermelstein RJ (2013). "A Pilot Program in Collaboration with Community Centers to Increase Awareness and Participation in Skin Cancer Screening Among Latinos in Chicago," Journal of Cancer Education, 28(2): 342-345

**Mauleon G**, Lo JF, Peterson BL, Fall CP, Eddington DT (2013). "Enhanced Loading of Fura-2/AM Calcium Indicator Dye in Adult Rodent Brain Slices Via a Microfluidic Oxygenator," J. Neuro. Methods, 216(2): 110-117

**Mauleon G**, Fall CP, Eddington DT (2012). "Precise Spatial and Temporal Control of Oxygen within In Vitro Brain Slices via Microfluidic Gas Channels," PLoS ONE 7(8): E43309. doi: 10.1371/journal.pone.0043309

## CONFERENCES

**Mauleon G**, Villafana L, Eddington DT. "3D Printed Microfluidic Oxygen Mixer", Biomedical Engineering Society, San Antonio, TX, October 2014

Eddington DT, **Mauleon G**, Brennan MD, Rexius ML. "Precise Oxygen Landscapes for Cells and Tissues in Culture", IDBR: Workshop on Successful Approaches for Development and Dissemination of Instrumentation for Biological Research, Rosslyn, VA, May 2014

**Mauleon G**, Larson J, Eddington DT. "Hypoxia Tolerance of the Mammalian Nervous System Under Spatially Controlled Oxygen Conditions", Biomedical Engineering Society, Seattle, WA, September 2013

**Mauleon G**, Lo JF, Fall CP, Eddington DT. "Enhanced Calcium Staining of Adult Rodent Brain Slices Via a Microfluidic Oxygenator", Biomedical Engineering Society, Atlanta, GA, October 2012

**Mauleon G**, Fall CP, Eddington DT "Stroke on a Chip: Spatial and Temporal Control of Oxygen for In Vitro Brain Slices", MicroTAS, Seattle, WA, October 2011

**Mauleon G**, Fall CP, Eddington DT "Stroke on a Chip: Spatial and Temporal Control of Oxygen for In Vitro Brain Slices", CBC Symposium, Chicago, IL, October 2011

Bharadwaj S, Dahli H, Hanif M, **Mauleon G** "Differentiation of Embryonic Stem Cells into Endothelial Cells by Varying Mechanical Stiffness of the Collagen Substrate", Engineering Expo, University of Illinois- Chicago, Chicago, IL, May 2009

## PATENTS

Eddinton DT, Mauleon G, Lo JF, Rexius ML, Rehman J (2013). " Microfluidic Device and Method for Modulating a Gas Environment of Cell Cultures and Tissues." US20130295551 A1, filed March 15, 2013, and issued November 7, 2013.

## LANGUAGES

Fluent Spanish

## CONSULTING EXPERIENCE

**Commercialization and Strategy Consultant**

University of Illinois at Chicago, EnterpriseWorks Chicago June 2014- May 2015

- Build commercialization roadmaps for several startup companies originating from UIC research laboratories
- Assisted with market and stakeholder analysis as well as short-term funding goals
- Acted as a liaison between the teams and leadership to ensure timely submission of deliverables

## PROFESSIONAL SOCIETIES

Society of Hispanic Professional Engineers- SHPE
National Biomedical Engineering Society- AEMB, BMES
Tau Beta Pi-Engineering Honor Society-- *Corresponding Secretary for TBP*
Tau Sigma Honor Society
Phi Theta Kappa

**HONORS**

Medical Technology Scholarship, Scientist Mentoring & Diversity Program, 2014
Biotechnology Scholarship, Scientist Mentoring & Diversity Program, 2014
Chancellor's Graduate Research Fellowship, UIC- 2013 and 2014
Graduate College Academic Travel Award, UIC- 2012 and 2014
UIC Department (Bioengineering) Award, UIC- 2009
Honor's College Award, UIC- 2009
Transfer Merit Scholarship, UIC- 2007
Presidential Award, UIC- 2007
Xerox Scholarship, UIC-2007
Square D-Engineering Scholarship, Harper College- 2006
Distinguished Scholar Scholarship, Harper College- 2005